Tiago Miguel da Fonseca Cunha

Master of Science in Engineering Physics

Negative Ion Formation in Potassium-Purine Molecules collisions

Thesis submitted in partial fulfillment
of the requirements for the degree of

Doctor of Philosophy in
Radiation Biology and Biophysics
Applied Atomic and Molecular Physics

Supervisor: Prof. Paulo Limão-Veira, Full Professor, Universidade Nova de Lisboa

Co-supervisor: Dr. Filipe Ferreira da Silva, Assistant Researcher, Universidade Nova de Lisboa

Examination Committee

Chairperson: Prof. Virgílio António Cruz Machado
Raporteurs: Prof. Janina Kopyra
Prof. Alice S. Pereira
Members: Prof. António Joaquim de Campos Varandas
Prof. António Aguilar Navarro
Prof. Gustavo Garcia Gómez-Tejedor
Dr. Samuel Peter Eden

FACULDADE DE CIÊNCIAS E TECNOLOGIA
UNIVERSIDADE NOVA DE LISBOA

April, 2018

Negative Ion Formation in
Potassium-Purine Molecules collisions

This document was created using the (pdf)LaTeX processor, based in the "novathesis" template[1], developed at the Dep. Informática of FCT-NOVA [2].
[1] https://github.com/joaomlourenco/novathesis [2] http://www.di.fct.unl.pt

"I celebrate myself, and sing myself,
And what I assume you shall assume,
For every atom belonging to me as good belongs to you."
- Walt Whitman

To my mother.

Acknowledgements

To Prof. Dr. Paulo Limão-Vieira and Dr. Filipe Ferreira da Silva for their supervision throughout the course of this work, as well as for the opportunity to visit other international groups and attend several scientific meetings.
To Prof. Dr. Gustavo García for so kindly providing the hemispherical analyser that is now being used for energy loss experiments, and Dr. Samuel Eden for receiving me in his research group and for his always friendly and available help.
To the Portuguese National Funding Agency FCT-MCTES through SFRH/BD/52538/2014.
To the NOVA University of Lisbon and to the Department of Physics for welcoming me as an assistant professor during this last year.
To all of the remaining members of the Molecular Physics and applications research group, particularly Dra Susana Sério, Juscelino Ferreira, Afonso Moutinho and Ana Cruz for for their support and advising throughout this thesis.
To Prof. Nunes dos Santos for his interesting classes and for the inspiring books that he so kindly provided.
On a more personal note, to my colleagues Alexandra Loupas, André Rebelo, Diogo Almeida, Guilherme Meneses, João Ameixa, Sara Pereira and Telma Silva for turning stressful moments into the funniest situations. I have no doubt our friendship will endure for many years to come.
To my dearest friends, Ana Palma, Diogo Miguel, Filipe Goncalves, Goncalo Tomas, Hugo Racoes, Jorge Barreto, Patrícia Pais and Pedro Farinha for the many great moments that have given me along the years. My big thanks for their support at all times, and for the geeky conversations that I so much appreciate.
To Mariana Sousa for her love, her care, her smile, and most of all her patience.
And finally to my parents for their unconditional love and support, and for motivating me to be more and better; and to my family. That we may always be together in harmony. Happiness is only real when shared. Thank you all.

"I was sitting at the table writing my compendium, but the work did not yield; my thoughts were elsewhere. I turned the chair over to the fireplace and began to doze. Again the atoms began to tumble in front of my eyes. This time the smaller groups were modestly at bay. My mind's eye, sharpened by repeated visions of this kind, could now distinguish larger structures with different conformations; long rows, sometimes aligned and close together; all twisting and turning in winding movements. But look! What is that? One of the snakes had threaded its own tail and the shape it swirled mockingly before my eyes. As if there had been lightning, I woke up ... I spent the rest of the night checking the consequences of the hypothesis. Let us learn to dream, sirs, for then perhaps we perceive the truth."

— Friedrich August Kekulé, *1865*

Abstract

The research described in this thesis focuses on the study of electron transfer mechanisms in purine molecules and derivatives (adenine, 9-methyl adenine, 6-dimethyl adenine and 2-D adenine), in potassium-molecule collisions. The studies were performed in a crossed beam experiment, comprising a neutral potassium beam and a biomolecular effusive beam with a time-of-flight mass spectrometer and a recently implemented hemispherical analyser, yielding an experimental arrangement capable of providing relevant information of the collision dynamics. From this comprehensive investigation, we report for the first time, collision induced site and bond selective breaking in purine molecules by alkali collisions. The influence of the K^+ ion in the vicinity of the temporary molecular anion was also investigated, indicating to partially suppress auto-detachment resulting in new or enhanced dissociation pathways.

Concerning the energy loss set-up, we present in the 0 to 15 eV energy range novel K^+ profiles in the forward direction ($\theta \approx 0°$) from fast potassium collisions with nitromethane and tetrachloromethane where new features are unravelled, and reported for the first time as far as akali collisions are concerned. Due to the current configuration, it restricts the use of this technique exclusively to samples with high vapour pressure. The potassium beam energy resolution was determined to be ~0.6 eV in the laboratory frame.

Keywords: Electron transfer, ion-pair formation, time-of-flight mass spectrometry, atom-molecules collisions, DNA nucleobases, energy loss spectroscopy.

Resumo

O trabalho realizado ao longo desta tese, e que é aqui descrito, teve como objectivo o estudo dos mecanismos de transferência de eletrão em moléculas pertencentes à classe das purinas (nomeadamente a adenina, 9-metil adenina, 6-dimetil adenina e 2-D adenina), por colisões átomo-molécula. Os estudos foram realizados num aparelho de feixes moleculares cruzados no laboratório de colisões atómicas e moleculares do CEFITEC (Centro de Física e Investigação Tecnológica), que se encontra na Faculdade de Ciências e Tecnologia da Universidade Nova de Lisboa. Este dispositivo experimental consiste num feixe de átomos de potássio neutro e um feixe efusivo biomolecular que se fazem cruzar ortogonalmente, um espectrómetro de massa do tipo tempo de voo e um analisador hemisférico recentemente implementado.

No âmbito desta tese, foi observado pela primeira vez, mecanismo seletivo quanto ao tipo de ligação e posição, na abstração de um átomo de hidrogénio em moléculas de purina por colisões com átomos de potássio, a baixas energias. A influência do ião K^+ na vizinhança do anião molecular também foi investigada, indicando suprimir parcialmente o processo de auto-libertação do eletrão, formando novos fragmentos aniónicos ou resultando numa maior produção de fragmentos já observados. No que diz respeito à configuração de perda de energia, apresentamos perfis de perda de energia dos iões K^+, de 0 a 15 eV, na direção principal ($\theta \approx 0°$) em colisões átomo-molécula com nitrometano e tetraclorometano, após transferência de eletrão. Devido à configuração atual, a utilizaąo desta técnica encontra-se restrita a amostras com tensões de vapor altas. A resolução em energia do feixe de potássio foi determinada em 0,6 eV no referencial do laboratório, o que nos permitiu observar novas contribuições nos espectros de perda de energia obtidos, comparativamente ao encontrado na literatura, e que serão devidamente abordados.

Palavras-chave: Transferência de eletrão, espectrometria de massa, colisões átomo-molécula, DNA, espectroscopia por perda de energia.

Contents

List of Figures

List of Tables

Acronyms

.
.

α	Experimental correction factor.
θ	Pencil angle.
ρ	Charge density.
π^*	π antibonding orbital.
σ^*	σ antibonding orbital.
$\Psi(r,R)$	Total wavefunction.
$\Delta E(I_{max})$	Energy loss at maximum intensity.
2-DAd	2-deuterated adenine.
5-FU	5-fluorouracil.
5-ClU	5-chlorouracil.
6-dimAd	6-dimethyl adenine.
9-mAd	9-methyl adenine.
a_0	Bohr radius.

Ad	Adenine.
b	Impact parameter.
BR	Branching Ratio.
c.m.	Centre of Mass.
CE	Charge Exchange.
CEC	Charge exchange chamber.
CT	Constant transmission.
DBS	Dipole Bound State.
DC	Direct Current.
DEA	Dissociative Electron Attachment.
DSB	Double Strand Break.
e^-	single electron.
E_0	Pass energy.
E_1;E_2	Adiabaitc potential curves.
E_{av}	Available energy.
E_{cm}	Kinetic energy in the centre of mass frame.
E_{lab}	Kinetic energy in the laboratory frame.
E_{thresh}	Threshold energy.
EA	Electron affinty.

EA_{ad}	Adiabatic electron affinity.
EA_{v}	Vertical electron affinity.
ETS	Electron Transmission Spectroscopy.
FFR	Free Field Region.
FIR	Finite Impulse Response.
FWHM	Full Width at Half Maximum.
H_0	Non-perturbed Hamiltonian.
H_{11};H_{22}	Diabatic potential curves.
H_{12}	Coupling factor.
$H_{12}{}^*$	Coupling factor in a reduced form.
HEA	Hemispherical Energy Analyser.
HOMO	Highest Occupied Molecular Orbital.
I	Ion current.
IE	Ionisation Energy.
j	Ion flux.
k	Boltzmann constant.
K°	Potassium atom.
K^+_{hyp}	Hyperthermal potassium ion.

K_0	Initial kinetic energy.
K_a	Kinetic energy acquired in the acceleration region.
K_e	Kinetic energy acquired in the extraction region.
K_{hyp}	Hyperthermal potassium atom.
K_t	Total kinetic energy.
K_{th}	Thermal potassium atom.
KE	Kinetic Energy.
L	Total flight tube's length.
LEE	Low Energy Electrons.
LT	Langmuir-Taylor.
M	Molecular target.
$M^{\#-}$	Vibrationally excited molecular anion.
M^-	Molecular anion.
m_K	mass of potassium in u units.
m_{target}	mass of the molecular target in u units.
MO	Molecular Orbital.
NB	Nucleobase.
p	Landau-Zener non-adiabatic transition probability.
PES	Potential Energy Surface.

PID Proportional Integral Derivative.

Pu Purine.

r electronic coordinates.

R Nuclear coordinates.

R_0 Analyser centreline radius.

R_1 Analyser inner radius.

R_2 Analyser outer radius.

R_c Crossing radius.

$R_c{}^*$ Reduced crossing radius.

R(t) Nuclei classical trajectory.

SFS Sector Field Sweep.

SSB Single Strand Break.

t Total flight time.

T Temperature.

t_0 Time required to form an ion.

t_a Flight time in the acceleration region.

t_{col} Collision duration.

t_d Time to decelerate an ion to zero velocity inside the ion mirror.

t_e Flight time in the extraction region.

t_L Flight time in the field free region.

t_r Time of fight inside the ion mirror.

t_{vib} Period of vibration.

TDC Time to Digital Converter.

THF Tetrahydrofuran.

TNI Temporary Negative Ion.

TOF Time Of Flight.

U Potential energy.

v Relative velocity.

V_0 Centreline potential.

V_1 Inner electrostatic potential.

V_2 Outer electrostatic potential.

V_{acc} Accelerating voltage.

V_{cov} Covalent potential curve.

v_i Initial velocity.

V_{ion} ionic potential curve.

V_p Voltage applied between analyser hemispheres.

v_r Radial velocity.

v^* Reduced velocity.

$w_{1,2}$ Slits width.

z Charge.

CHAPTER 1

INTRODUCTION

"Begin at the beginning – the King said gravely –, and go on till you come to the end: then stop."

Lewis Carroll,
Alice in Wonderland

1.1 Radiation effects at the molecular level of cellular DNA

Despite cancer continues to pose great challenges to medical science, many scientific, technological and medical advances have been made for the past decades to improve the way we detect, and treat this disease. During recent years, the international scientific community has focused its research at studying chemical modification of cellular DNA to determine at a molecular level, the actual role of ionising radiation as a genotoxic agent [1]. The findings led to the development of probabilisitic [2] and mechanistic models [3–5], accounting for ionising radiation, free radical- and low energy electron (LEE-) induced damage mechanisms, that helped to understand the nascent stages of these (mutagenic) effects. However, still note that some refinements are needed, since it is still unclear the exact mechanisms that are mainly involved in single- and double-strand breaks of DNA and to what extent they may be related to oncological diseases. It is now clear that both ionising (X-rays, gamma rays, alpha particles) and secondary species such as electrons, radicals and ions from other sources, are quite efficient agents at damaging DNA. Indeed, by direct impact of the primary high-energy radiation with the biological environment, many secondary species are formed, mostly products from water radiolysis, that may strongly interact with DNA helix inducing single and double strand breaks [6]. These processes occur in the initial instants of irradiation (10^{-6}s) which may lead in a longer

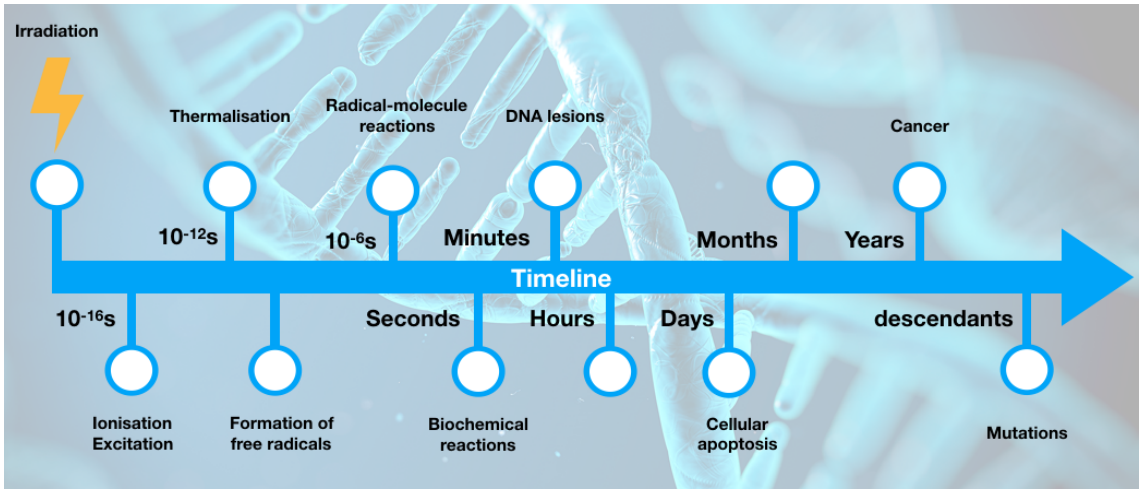

Figure 1.1: Chronological diagram of radiation-induced damage.

time scale to mutagenesis and eventually result in carcinogenesis (see figure 1.1). Such a molecular picture has been used to improve cancer irradiation treatments by developing radiosensitisers, radioprotectors or radiation mitigators [7, 8] to influence the effects of ionising radiation at a molecular level within the cell, i.e. to minimize injury to normal tissues and/or increase the sensitivity of tumour cells. At first, it was believed that free radicals produced from water radiolysis, were the main cause for such damage. They are highly reactive within the environment causing oxidative stress (cumulative damage to cause cell death, or eventually, cancer). However, recent studies on low-energy electron (LEE) interactions with plasmid DNA showed that at energies lower than the ionisation threshold (<10 eV), and even at sub-excitation energies (<3 eV), bond breaking in DNA sub-units shows a resonant behaviour [4]. From these findings, a model was proposed by Wang et al [9] where secondary pre-hydrated electrons may be the main cause for single strand breaks in this energy range, by the formation of short-lived anions through electron capture, as depicted in figure 1.2. Such mechanism, that is now known to cause DNA damage and promote cell death, was largely ignored and should now be considered with the purpose to transform these findings into therapeutic benefits for societal needs.

1.1.1 Indirect damage by free electron attachment and electron transfer processes

In living tissues, after irradiation, LEEs are the most abundant ($\sim 10^4$ per MeV of deposited energy) with an estimated energy distribution up to 20 eV [10]. These secondary electrons gradually lose their kinetic energy by a series of inelastic interactions with the surrouding until they reach near-zero energies (thermalisation) and become solvated [6]. Indeed, it is in this energy range where LEEs are accounted for the loss of helicity in DNA. They resonantly interact with DNA's constituents by dissociative electron attachment (DEA) processes that may initiate reactions leading to strand breaks [11]. The

electron is captured by resonant scattering forming a transient negative ion (TNI). The TNI formed in a metastable state has a short lifetime ($\sim 10^{-15}$s) and may decay through auto-detachment, fragmentation or radiative stabilisation into a stable TNI. The latter occurs in the microsecond timescale; thus, it is not able to compete with the other channels that occur on a femtosecond timescale [12].

Extensive studies on DEA to biomolecules have already been performed along the years, especially regarding the building blocks of DNA/RNA and aminoacids (see section 1.2). However, it may not show a complete picture of what occurs within the physiological environment since the lifetime of a free electron is very short, around the sub-picosecond scale. [6] To better understand the actual damage extent of processes induced by secondary electrons, cross section results concerning interactions of bound electrons are necessary, specially in slow collisions. Alkali atoms have very low ionisation energies and therefore are well suited to explore electron transfer processes by atom-molecule collision experiments. In the experimental set-up used in this thesis, the alkali atom of choice is potassium due to its low ionisation energy (IE(K°) = 4.34 eV). When colliding with a neutral target molecule, an electron may be ejected from this electron donor and accommodated into one of the target molecule's unoccupied orbitals. Generally, those orbitals are anti-bonding in character, hence the metastable TNI may decay by dissociation, auto-detachment or neutralisation. Following these processes, states with positive electron affinities can be achieved, in contrast to free electron experiments, and the role of vibrational excitation of the parent molecule can be studied in the collision dynamics [12]. Indeed, some of the excess internal energy can be transferred back to the K^+ ion. Furthermore, a stable parent anion can be observed in this type of collisions for molecules with positive electron affinity whose states involved are not accessible in the case of DEA [13]. Tipically, the TNI is unstable with respect to auto-detachment or dissociation. Thus, experimental results show that the presence of the K^+ cation near the TNI has a stabilisation effect suppressing auto-detachment, at least long enough for the parent anion to be detected [14]. This experimental observation is extremely relevant because the derived rationale can be generalised to interactions/collisions with other reactive species, namely, $OH^\bullet$ radicals. If the lifetime of the parent anion is longer than the fragmentation time, energy can be distributed along the available vibrational degrees of freedom, which may lead to new or enhanced fragmentation pathways [12].

Despite what was mentioned, surprisingly, many complex molecules have been found in the interstellar medium (IM). In fact, many meteorites that fell on Earth turned out to contain a variety of organic molecules, including purines and pyrimidines [15]. These findings raise important questions about the origin of life, being now accepted among the scientific community, that exogenous sources have also contributed and helped to provide the necessary precursor molecules for the evolution of life on Earth [16]. So far, a variety of molecules in the gas-phase has been detected in the IM such as alcohols, acids, and ethers, to name a few [17]. They can be found in interstellar clouds where they may be formed through ion-molecule reactions, dissociative recombination with electrons,

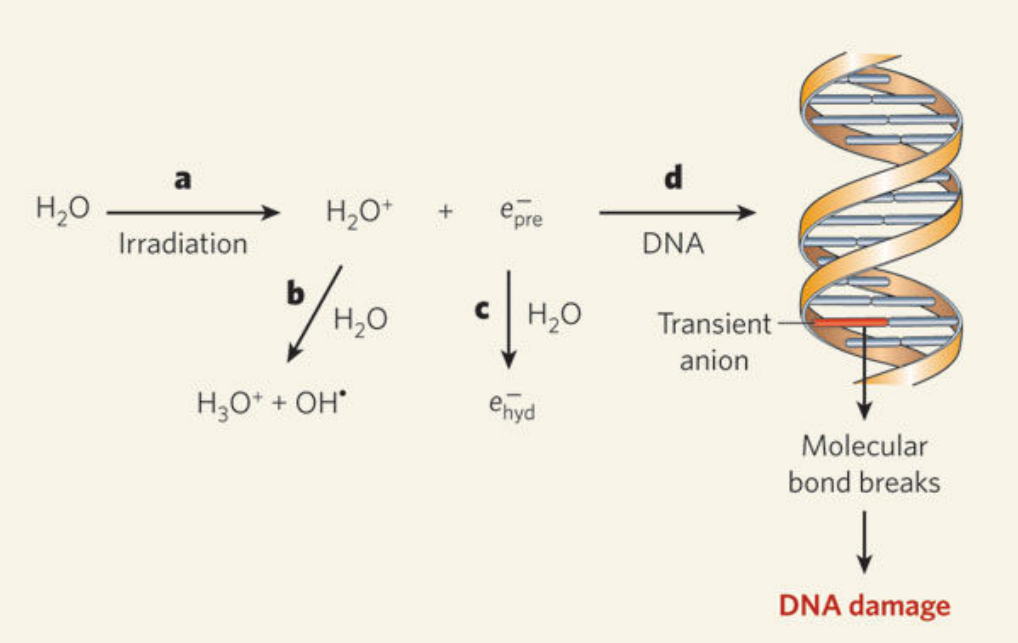

Figure 1.2: Representation of radical induced damage. From [5]

radiative association or radical-molecules reactions [18].

1.2 Experimental studies with DNA/RNA nucleobases

The nucleobases are of most relevance in several science fields since they bear the genetic information of all terrestrial life by forming base pairs and stacking one upon another resulting in DNA (see figure 1.3). It can also result in RNA which is in general a single-stranded molecule, altought in same cases it can form intrastrand double helises, as in tRN. They are divided in two classes: pyrimidines (thymine, cytosine and uracil), and purines (adenine and guanine). While the the first consist of one aromatic ring, the latter of two aromatic rings (pyrimidine + imidazole). In the DNA framework they are connected through a glycosidic bond to a five-carbon sugar unit (either ribose or deoxyribose) forming a nucleoside. The nucleotides are formed when phosphorilation takes place [19] and one or more phosphate groups are bound to the sugar's primary alcohol group of the nucleoside (see figure 1.3). Here we will focus our attention in the study of the effects induced by secondary species produced by ionising radiation, namely, the attachment of either pre-hydrated (free) electrons, or by electron transfer from reactive species, to one of these DNA building blocks. We will discuss few of the most relevant findings that were recently reported either in dissociative electron attachment (DEA) experiments or electron transfer studies by atom-molecule collisions in order to introduce the present work.

1.2.1 Free electron attachment experiments to biomolecules in the gas-phase

Exposure of cells to ionising radiation will cause the production of secondary electrons with energies up to 20 eV, being the most abundant of the secondary species produced. Such electrons were reported by Boudaiffa et al [4] to resonantly induce several single- and double-strand breaks in DNA sub-units that can eventually result in carcinogenesis as a consequence of diverse mutations that followed these events. Experimental results were obtained by irradiating plasmid dry DNA with a monochromatic low energy electron (LEE) beam for a specific time. Following these results, there have been numerous investigations concerning the effect of LEE's induced damage to DNA constituents in both gas phase, and dry DNA in vacuum (see ref [20] and references therein). Concerning gas phase studies, DEA experiments at sub-excitation energies (< 3 eV) yielded the dehydrogenated parent anion [21, 22], such reaction being schematically represented as:

$$e^- + \mathrm{NB} \longrightarrow \mathrm{NB}^{\#-} \longrightarrow (\mathrm{NB\text{-}H})^- + \mathrm{H}$$

where $\mathrm{NB}^{\#-}$ is the transient negative ion (TNI) formed with an excess of internal energy, and $(\mathrm{NB\text{-}H})^-$ the closed shell anion formed after H loss. As mentioned, this is a resonant process, i.e. the incoming electron occupies a previously unfilled orbital of the molecule which is defined by its specific energy [12] - resonant scattering. Due to the high electron affinity of the (NB-H) radical (typically > 3 eV), in DEA experiments this is one of the most intense fragment anions. Site- and bond-selective cleavage upon DEA has also been reported in both pyrimidines, i.e. thymine ($C_5H_6N_2O_2$) and uracil ($C_4H_4N_2O_2$) [23], purines like adenine ($C_5H_5N_5$) [24], and even for ribose sugar unit ($C_5H_{10}O_5$) [25]. This was achieved by tuning the electron energy and using partly methylated and/or deuterated compounds on specific sites. For instance, dehydrogenation of nucleobases can only arise from either C-H or N-H bond excision. Thus, by using partly deuterated thymine on carbon positions, Abdoul-Carime et al. [22] were able to show that this mechanism is bond selective in pyrimidines and arises exclusively from N-H bond excision at low collision energies since $(\mathrm{T\text{-}H})^-$ and $(\mathrm{T}_D\text{-}\mathrm{H})^-$ yield had similar behaviour (both showing an intense peak 1 eV), and $(\mathrm{T}_D\text{-}\mathrm{D})^-$ was only detected at energies up to 6 eV. Furthermore, Ptasinska et al. [23] concluded by studying the same fragment ion (in electron attachment experiments with deuterated and methylated pyrimidines), that H loss can further be made site selective by tuning the electron energy. They showed that H loss from N1 site is a consequence of resonant interaction with electrons of ∼1 eV, hence can either be switched to H loss from N3 site by properly tuning the electron energy to 1.8 eV or be completely blocked when a methyl group is added (N-CH_3). Similar mechanism was observed by Denifl et al. [24] in case of adenine where adenine analogues such as 9-methyl adenine (9-mAd) and 6-dimethyl adenine (6-dimAd) were used. Again, by properly tuning the electron energy, H radical excision was completely suppressed for 9-mAd – no $(\mathrm{M\text{-}H})^-$ was observed below ∼1.4 eV – whereas for adenine a sharp peak is present ∼ 1 eV.

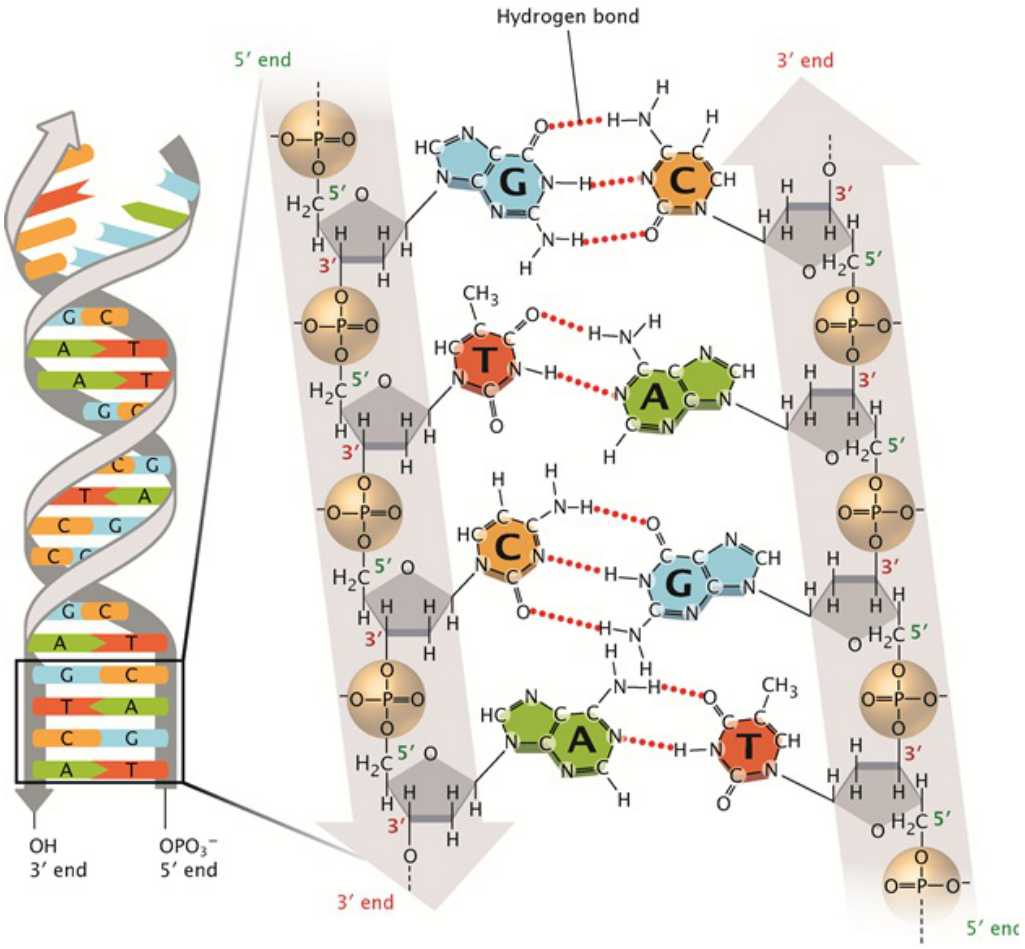

Figure 1.3: Chemical structure of DNA.The sugar-phosphate backbone of the double-stranded DNA is shown as two grey lines arranged in an anti-parallel manner that twist to form a double helix. Two grey vertical arrows, one pointing downwards, and one pointing upwards, demonstrate that the DNA consists of two anti-parallel strands. Phosphate groups are depicted within light brown spheres, and the bonds between the phosphate and oxygen atoms are shown. The sugars are represented by grey pentagons that show where oxygen atoms and hydrogen atoms are attached to the unmarked carbon atoms at the corners. An oxygen atom from each phosphate molecule is connected by a black line to a carbon atom from the sugar molecule. These black lines represent the covalent bonds between the sugars and phosphate groups. From ref [28].

In general, these results obtained in electron interactions with nucleobases clearly showed two distinct dissociation pathways that were discussed by Burrow et al. [26]. The sharp peaks observed $\leqslant 1$ eV are most likely attributed to the coupling of diffuse dipole-bound (DBS) and a valence state [27], while the broad features at higher energies are associated to shape π^* or σ^* resonances. Such states can then undergo auto-detachment or be transferred to a valence orbital. Owing to anti-bonding character of such orbital, if the auto-detachment lifetime is long enough, dissociation can occur. It is worth to point out the results reported by Ptasinska et al. [29] in DEA experiments with thymidine where they have shown that LEEs at sub-excitation energies (< 3 eV), leading mainly to H loss

(from N3 position) and to the rupture of the glicosidic bond (N1-C1 bond). Multi-photon ionisation (MPI) and electron impact ionisation (EII) mass spectrometry experiments on hydrated adenine clusters were performed by Barc et al [30] reporting an enhancement of the fragment $C_4H_4N_4^+$ (108u) intensity and the suppression of all sequential fragment ion pathways.

Several research groups have also extensively studied many halogenated compounds in DEA reactions [31–34] because of their electron scavenging properties. Hence, they can be used in cancer treatments in order to increase the radiosensitivity of hypoxic tumor cells. Fluoropyrimidines, thymidine and metronidazole analogues (such as, 5-fluoruracil (5-FU), bromodeoxyuridine, misonidazole, nimorazole and nitromimidazole), are just a few examples of radiosensitizers that have been found to be quite effective as anticancer agents [35]. However, such a picture of a free electron in a biological medium is not accurate. In fact, upon irradiation in the biological environment, the secondary electrons that were produced, are quickly thermalised (∼picosecond scale) and may become solvated. In this state, they are trapped in a deep potential well of ~ 3.2 eV [6]. Moreover, during inelastic collisions with the environment atomic/molecular constituents, they produce radicals, mostly being the result of interactions with water molecules, such as $OH^{\bullet}$, which have already shown to strongly interact with the DNA's building blocks and capable of inducing SSBs and DSBs [3]. Therefore, cross-section results of electron transfer processes are required in order to have a better and full understanding of the underlying mechanisms involved in damaging DNA.

1.2.2 Electron transfer to gas phase biomolecules in atom-molecule collisions

Here we discuss relevant research that has been performed at LCAM laboratory, Lisbon, in the crossed molecular beam apparatus where electron transfer processes on DNA bases have been studied by atom (potassium) - molecule collisions. The experiment represents a novel perspective spanning two traditionally independent research areas: electron attachment and electron harpooning studies of gas phase molecules. Of relevance electron transfer experimental studies have been reported on potential radiosensitizers such as 5-chlorouracil(5-ClU) and 5-FU [7, 36], the latter also termed by Adrucil, currently used to treat bowl cancer [37]. Antunes et al. [7] reported CNO^- as the most intense fragment from uracil and 5-FU followed by the dehydrogenated parent anion which is in contrast with DEA experiments performed by Denifl et al. [38]. Meaning, the electron donor species (which in this case is a potassium atom) plays an active role on stabilising the complex [K^++5-FU^-] suppressing auto-detachment long enough for a crossing of a π^* state with a σ^* state to occur – initially the electron is captured into a π^* state –, hence yielding enhanced ring breaking. Futhermore, by tuning the collision energy of the hyperthermal K^0 beam while studying methylated and partly deuterated pyrimidines, Almeida et al. [39] shown that the hydrogen radical excision may be turned site- and bond-selective,

in these type of collisions, as previously reported in DEA experiments [22]. Electron transfer studies on D-Ribose [40] and THF [41] sugar surrogates were also reported by Almeida et al. where remarkable differences regarding DEA have been observed. In fact, either in potassium collisions with d-ribose or THF, OH^- and O^- were the most intense fragments, respectively, which is in sharp contrast with electron attachment experiments. It is also worth noting the studies involving potassium collisions with uridine [42]. Here, similar to DEA results related to thymidine, the uridine fragmentation pattern showed evidences that the glycosidic bond seems to immediately dissociate after electron transfer with the excess charge localised either at the pyrimidine moiety or the furanosic ring.

One may conclude from both aforementioned experiments, that there is much more we need to know concerning these processes. It was demonstrated by both techniques, that the formation of the dehydrogenated parent anion, $(M\text{-}H)^-$, is a selective mechanism. Under biological conditions, such position is also blocked, and replaced by a glycosidic bond to sugar ring, hence such fragmentation channel may not be formed. Moreover, in atom-molecule collisions the presence of the electron donor greatly affects the fragmentation channels indicating to have a much more damaging effect than DEA. It is also worth noting the great abundance of O^- and OH^- in the anion yield for the sugar ring indicating that such functional groups may act as protective agents of the ring integrity – i.e. avoiding ring breaking. Therefore, comparison of cross section results from DEA experiments and atom-molecule collisions is crucial in order to develop a more complete and accurate model of electron induced damage in DNA. The work presented in this thesis follows the work carried out by Antunes [7] and Almeida [14] regarding the pyrimidines and their selective mechanisms involved in their fragmentation in atom-molecule collisions in order to ascertain if the same mechanisms also prevail in the purine molecules. Recently, in studies of this nature at low collision energies, it has been possible to demonstrate that in the case of purines the hydrogen loss process is also site-selective and proceeds exclusively from the N9 site for energy collisions $\leqslant 15$ eV, in the laboratory frame. Those results will be presented and discussed here. Other mechanisms, such as formation of CN^- and the release of one or more HCN molecules, will also be analysed in light of both experimental and theoretical methods.

1.3 Outline of the thesis

This thesis is organised in eight chapters, including the present one. The second chapter deals with the general principles involved in atom-atom collisions and atom-molecule collisions used in the interpretation of the results obtained. The third chapter provides the description of the experimental set-ups used throughout this thesis. Also, a full description of the implementation, optimisation and control of the hemispherical energy analyser is addressed in this chapter. In chapter 4 and 5 experimental results are presented for purine, adenine, 9-methyl-adenine, 6-dimethyl-adenine and 2-deuterated-adenine. Each of these chapters includes a review of relevant literature and the analysis of

the new data presented here. Chapter 6 is devoted to alkali energy loss spectroscopy that was implemented during this thesis, where results obtained for carbon tetrachloride and nitromethane are discussed. Chapter 7 presents the general conclusions and discusses further work that may be undertaken soon.

Chapter 2

General theoretical considerations

"Not only is the Universe
stranger than we think, it is
stranger than we can think."

Werner Heisenberg,
Across the Frontiers

In this chapter we will discuss theoretical aspects of potassium-molecule interactions in the gas phase (under single-collision conditions) starting with a simple model of atom-atom collision, followed by ion-pair formation probability given by the Landau-Zener formula, and extended to atom-molecule collisions. These models will serve as guidelines to predict the collision dynamics and to understand the underlying mechanisms involving ion-pair formation in such collisions for the present work.

2.1 Electron transfer processes

2.1.1 Introduction

Electron transfer processes have been widely investigated by recurring to neutral alkali beams in order to probe molecules and obtain key parameters as electron affinities, potential well-depths, as well as comprehensive studies on the dissociation dynamics [43]. Seminal studies date back to 1930's with the pioneering work of Polanyi [44] where rate constants for reactions of sodium atoms and halogen molecules have been measured. It was found the rate constants for some of these halogen compounds to be extremely large [45]. Such behaviour led to the proposal of the so-called "harpooning" model as a description of the mechanism, that was further developed by Magee [46] and Herschbach [47–49]. Later, additional studies were performed using crossed molecular beams [50–52] to study the reactions involved, either by using metastable noble gas atoms [53], Rydberg atoms [54–56] or alkaline earth atoms [57, 58]. Some halogens and simple halogen containing molecules, were investigated [59, 60] in order to develop models that were able to accurately describe electron transfer processes, followed by many diatomic molecules such as oxygen [61], and a few other more complex such as CCl_4, $SnCl_4$ and CH_3NO_2. From these experiments, the role of the initial molecular vibrational state as well as the effect of bond stretching during the collision were mainly addressed where for the latter, it was established a collision energy dependence. This effect was later demonstrated by Aten and Los [62]. Moutinho and co-workers [43] reported experimental studies , on Li, Cs and K collisions with F_2 (in the centre-of-mass energy range 10-100 eV), showing that bond stretching contributes negligibly for the ion-pair formation cross section with increasing collision velocities (typically above 60 eV in the centre-of-mass frame). In these conditions, the molecule can be assumed as "frozen" and the "electron jump" process from the projectile to the target can be described in terms of a Franck-Condon transition [43], similar to DEA [63] . Another interesting aspect pertains to pre-stretching of the molecular bond at low collision energies, which is not explained through semi-classical models such as the Landau-Zener scattering theory. Such is due to a clear violation of the Born-Openheimer principle, where it is assumed that the internuclear distance of the TNI is not influenced by the proximity of the fast incident particle. An adiabatic description must be considered. [64]. Such theoretical aspects that involve these type of collisions will be further discussed here.

2.1.2 Theory

In alkali-molecule collisions, electron transfer occurs when an electron is relocated from the alkali (electron donor) to the molecular target (electron acceptor). Such event can cause a perturbation in the interaction potential that, depending on the electron donor's velocity, can lead to unimolecular ion decomposition. Several reaction channels may occur from electron transfer, as briefly shown in table 2.1.

For electron transfer to occur the valence electron from the potassium atom must first be ejected to the continuum and then captured by the molecular target from which it results a K^+ ion and a transient negative ion (TNI). It will then decay through auto-detachment, leaving the molecular target vibrationally excited, or through one of the reaction channels mentioned in table 2.1. Thus, the collision-induced dissociation of the molecular anion formed, can also be described as a two-step process with a vibronic excitation followed by a unimolecular dissociation.

$$K^\circ + XY \longrightarrow K^+ + (XY)^{\#-} \longrightarrow K^+ + X^- + Y$$

The dissociation can be direct, when excitation occurs to a highly dissociative state, or indirect when excited to an intermediate state that decays eventually into dissociation by coupling with a highly dissociative state. The description of such a collision can be rather complex, only being achieved through approximations such as Born-Oppenheimer principle and Landau-Zener formalism. [59]

2.1.2.1 Born-Oppenheimer approximation

For simplicity, consider the interaction between two atoms brought together in a collision experiment. The system can then be described by the time-dependent Schrödinger equation [7, 14] as given:

$$\hat{H}\Psi(r,R) = i\hbar\left(\frac{d\Psi(r,R)}{dt}\right) \tag{2.1}$$

where $\hat{H}$ is the Hamiltonian operator and Ψ is the total wavefunction of the atom-atom isolated system. R represents the position of the nuclei and r the position of the electrons. The Hamiltonian is given as

$$\hat{H} = \hat{T}_n(R) + \hat{H}_{el}(r,R) \tag{2.2}$$

The $\hat{T}_n(R)$ operator is the kinetic energy of the nuclei and $\hat{H}_{el} = \hat{T}_e + \hat{V}$, is the electronic Hamiltonian. A special case of the Schrödinger equation is the situation when the potential energy term is not time-dependent, V(r,R,t) $\approx$ V(r,R). With V independent of time, the wavefunction can be written as the product of space and time variables which leads to the time-independent Schrödinger equation:

$$\hat{H}\psi(r,R) = E\psi(r,R) \tag{2.3}$$

Table 2.1: Types of collisional ionisation processes between atoms A and molecules BC. [59]

A + BC	$\longrightarrow$	$A^+ + BC^-$	Non-dissociative ionisation
	$\longrightarrow$	$A^+ + B^- + C$	Dissociative ionisation
	$\longrightarrow$	$A^+ + (B + C) + e^-$	
	$\longrightarrow$	$AB^+ + C + e^-$	
	$\longrightarrow$	$AB^+ + C^-$	Reactive chemical ionisation
	$\longrightarrow$	$A + B^+ + C^-$	Polar dissociation

Being the interaction potential $\hat{V}$ a sum of the potential between all particles in the system, the more complex (more particles involved) is, more difficult it becomes to determine the respective solution of the Hamiltonian, considering all possible interactions. However, approximations such as the Born-Oppenheimer approximation, can help to simplify the problem. This approximation is based on the large difference in mass of electrons and nuclei resulting in the electronic cloud moving much faster than the latter. Thus, we can treat the motion of the electrons and nuclei separately and expand the wavefunctions in a basis of adiabatic states ϕ_k (see equation 2.4):

$$\psi(r,R) = \sum_k \phi_k(r;R)\Omega_k(R) \tag{2.4}$$

where $\sum_k \Phi_k$ is total wavefunction of the electronic cloud, i.e. ϕ_k states are eigenfunctions of the electronic Hamiltonian and $\Omega_k(R)$ the wavefunction of the nuclei for a fixed internuclear distance R. This turns quite useful when studying the behaviour of the electrons since we can assume the nuclei to be "frozen" due to their higher mass, thus the effect of $\hat{T}_n$ is negligible and only the electronic Hamiltonian is taken into account as follows:

$$\hat{H}\phi_k(r;R) = \hat{H}_{el}\phi_k(r;R) = E_k\phi_k(r;R) \tag{2.5}$$

where E_k are the discrete eigenvalues of the Hamiltonian operator, i.e. the electronic energy levels of the corresponding electronic wavefunctions $\phi(r,R)$ at a given internuclear distance, R.

If we assume that the nuclei move slowly, the Born-Oppenheimer approximation is still valid due to the adiabatic theorem that states if the particle is initially in the n^{th} eigenstate of H_i, it will be carried, under the Schrödinger equation, into the n^{th} eigenstate of the H_f. In other words, as the nuclei coordinates change gradually over time, the electrons are allowed to adjust and reach their equilibrium positions. Furthermore, one can use a semiclassical approach in which the position vector R of the incident atom with respect to the system's centre-of-mass is assumed to follow classical straight line trajectories with constant velocity, v, and impact parameter, b: R = b + vt [43]. The electronic wavefunction $\Psi(r,R)$ is expanded in terms of a set of eigenfunctions $\phi(r;R)$ as given [14]

$$\Psi(r,R) = \sum_k a_k\phi_k(r,R)exp\left(-\frac{i}{\hbar}\int_0^t E_k(R)dt\right) \tag{2.6}$$

From equation 2.1 and 2.6, one can obtain a set of coupled equations for a_k [14]:

$$a_k = \sum_j a_j v_r \left\langle \phi_k \left| \frac{\partial}{\partial R} \right| \phi_j \right\rangle exp\left[-\frac{i}{\hbar}\int_0^t (E_j - E_k)dt\right] \tag{2.7}$$

From the equation above, a number of analytical results can be obtained for the Landau-Zener model [65].

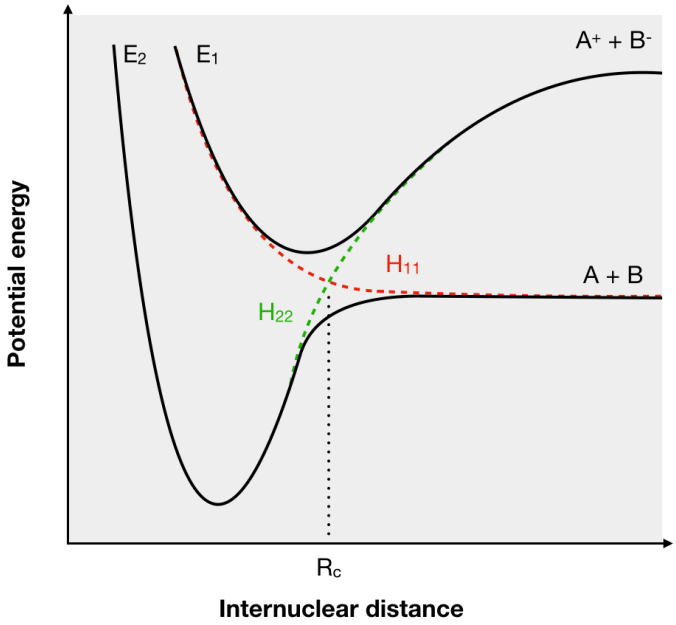

Figure 2.1: Representation of adiabatic and non-adiabatic states. Adiabatic potential curves, E_1 and E_2, are represented by full lines while non-adiabatic curves are represented by H_{11} and H_{22} in dashed lines. H_{11} represents a covalent curve whereas H_{22} is a ionic potential curve. Adapted from [7].

2.1.3 Landau-Zener formalism

In this topic the Landau-Zener non-adiabatic transition probability will be discussed in light of a "two-state" approximation in the crossing region(Figure 2.1). This probability of electron transfer between two states has been calculated by Landau, Zener and Stueckelberg by solving the time-dependent Schrödinger equation for simple one dimensional, two-state system. [66] This model is derived from a diabatic description and the Hamiltonian takes the form [14]

$$H_{el} = \begin{bmatrix} H_{11} & H_{12} \\ H_{21} & H_{22} \end{bmatrix} \tag{2.8}$$

where $H_{12} = H_{21}$. H_{11} and H_{22} represent the eigenvalues of the covalent and ionic diabatic states [43], and H_{12},H_{21} are the adiabatic coupling elements between these states(Figure 2.1). From the diagonalization of the coupling matrix in 2.8, the energy eigenvalues of this Hamiltonian are given by [14, 43]

$$E_{1,2}(R) = \frac{H_{11} + H_{22}}{2} \pm \frac{1}{2}\sqrt{(H_{11} - H_{22})^2 + 4H_{12}^2} \tag{2.9}$$

where $E_{1,2}$ are the adiabatic potentials. From this expression, one can see that when $H_{22} - H_{11} \gg H_{12}$ a diabatic transition occurs [7]. However, when $H_{11}(R_c) = H_{22}(R_c)$ the transition is dominantly adiabatic and the energy gap between the adiabatic states, due to an avoided-crossing, is equal to $2H_{12}(R_c)$. From the non-crossing rule, the adiabatic

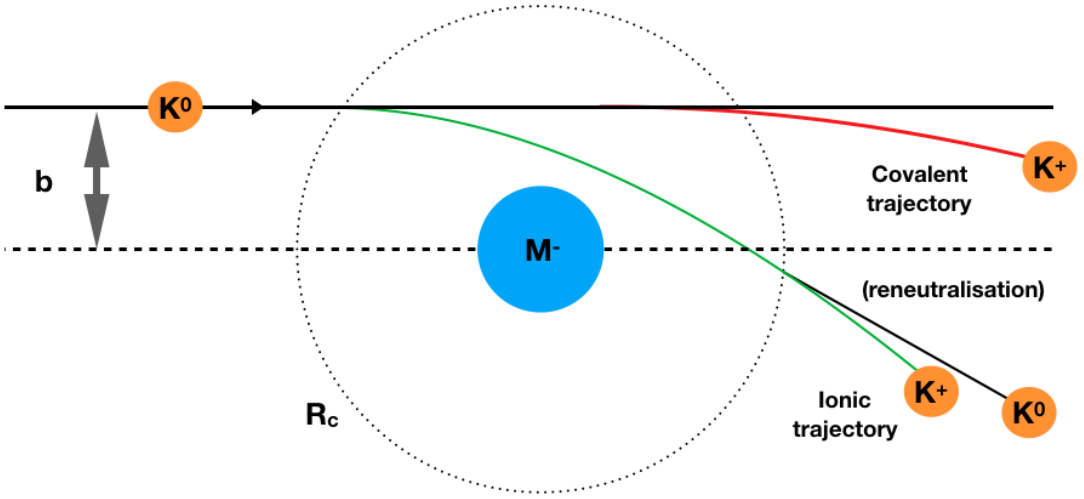

Figure 2.2: Representation of potassium-molecule collisions where 4 different trajectories can be discerned depending whether electron transfer occurs, at first or second crossing R_c (forming K^+ and a TNI, M^-), or not. Re-neutralisation can be also possible leaving the molecular target, M, in a vibrational excited state.

states can cross only if their respective wavefunctions show different symmetry and multiplicity. [14] From 2.8 and using time-dependent perturbation theory, it is possible to obtain the Landau-Zener non-adiabatic transition probability between the two diabatic states aforementioned. The model assumes that the transition only occurs in a strict region around the crossing radius, R_c, as shown in figure 2.2, where the radial velocity, $v_r = R(t)/t$ is constant (linear trajectory) and equivalent for both electronic states [43]. The Landau-Zener probability for making a single non-adiabatic transition can be calculated as [14]

$$p = exp\left(-\frac{v^*}{v_r}\right) = exp\left(-\frac{2\pi H_{12}^2(r=R_c)}{v_r|\frac{d}{dR}(H_{11}-H_{22}|_{r=R_c}}\right) = exp\left[-\frac{v^*}{v}\left(1-\frac{b^2}{R_c^2}\right)^{-1/2}\right] \tag{2.10}$$

where R_c is the crossing point between both ionic and covalent potential curves and v^* is the reduced velocity. The radial velocity v_r is given by [43]:

$$v_r = v\left(1-\frac{b^2}{R_c^2}\right)^{1/2} \tag{2.11}$$

where b is the impact parameter and v is the relative velocity. From equation 2.10 we can observe that the reduced velocity is given by:

$$v^*(r) = \frac{2\pi H_{12}^2(r=R_c)}{|\frac{d}{dR}(H_{11}-H_{22})|_{r=R_c}} \tag{2.12}$$

The coupling term H_{12} is therefore, dependent on the reduced velocity, hence it can be estimated empirically and used as a "measure" of the non-adiabatic transition probability.

If we approximate the covalent potential H_{11} to a constant and the ionic potential to roughly $H_{22} = -1/R$ [43], we obtain from equation 2.12, at $R = R_c$ [43]:

$$v^* = 2\pi H_{12}^2 R_c^2 \tag{2.13}$$

In collisions that lead to ion-pair formation, the transition probability between these two states will be [43]:

$$P = P_{cov} + P_{ion} = (1 - p_2)p_2 + p_1(1 - p_2) \tag{2.14}$$

where p_1 and p_2 are the non-adiabatic transition probabilities at the first and second crossing, respectively. In atom-atom collisions, $p_1 = p_2 = p$ because the distance of the second crossing is the same as the first. This leads to equation 2.15:

$$P = 2p(1 - p) \tag{2.15}$$

Thus, the transition is most probable when p is near 1/2. Furthermore, from equations 2.10 and 2.11, we see that $p = 0$ when $v = 0$ and $b = R_c$, meaning the probability of an adiabatic transition (electron transfer) is $1 - p = 1$, i.e. the crossing is adiabatic. In contrast when p reaches 1 (with rising velocity and for $b < R_c$), the crossing can be treated as diabatic. The factor of 2 appears in equation 2.15 due to the occurrence of two crossing regions for $b < R_c$, which can lead to four different trajectories (or transitions) during collision, as represented in figure 2.2.

In collisions where $b < R_c$, electron transfer can occur when approaching and when moving away from the molecular target. Depending on the electron transfer occurs at the first or second crossing, the trajectories are termed "ionic" or "covalent" type (see figure 2.2). In "ionic" trajectories, ion-pair formation occurs at the first crossing and there is no re-neutralisation at the second crossing while in a "covalent" trajectory, electron transfer only occurs at the second crossing. Both trajectories contribute to different scattering angles, due to different times of "exposure" to a Coulomb interaction. The corresponding total cross-sections, Q, for ion-pair formation will be of the order of πR_c^2 which is much larger than the corresponding gas kinetic cross sections. Such fact is what allows us to neglect vand der Waals and induction forces, thereby considering the interaction entirely Coulombic [12]. Such consideration leads to R_c being approximated by [14]:

$$R_c = \frac{e^2}{\Delta E} = \frac{14.41}{IE(K°) - EA(B)} \tag{2.16}$$

with R_c in Å, and ΔE in eV units. $IE(K°)$ is the ionisation of the potassium atom and EA(B) the target electron affinity. These simplifications provide the first tool available to describe these inelastic collisions [43] with more complex systems, and were used during this thesis work to make a careful qualitative analysis of the results obtained.

2.2 Atom-molecule collisions

In order to discuss these models applied to more complex atom-molecule collisions, a few other approximations must be taken, because even in collisions with diatomic molecules,

other processes such as vibrational and rotational excitations of the molecular target must be considered. In first approximation, this can be ignored if we consider the molecule a structureless target, similar to an atom. This is valid if we assume the molecule is "frozen" during collision. Or in other words, the period of a vibration is much larger than the collision time ($t_{col} << t_{vib}$) [43]. The electron affinity must also be independent of the molecule internal degrees of freedom which happens to be true for higher collision velocities. Indeed, in this regime bond stretching no longer occurs [43] and the electron transfer process can be described in terms of a vertical Franck-Condon transition, that may lead to vibrational excitation of the TNI.

It is important to note, since the electron transfer in atom-molecule system may be represented as in a three-body collision, if the available energy of the system in the centre-of-mass frame is high enough, all the energetically allowed anionic states may be accessible, in constrast to dissociative electron attachment where is only observed for specific energies of the electrons (resonance). This available energy is set in equation 2.19 [7] as the maximum kinetic energy, in the system's centre-of-mass frame, that a bound electron can have which is related to the energy carried by the electron donor. Thus, anionic states with energies above E_{av} are not accessible.

$$E_{cm} = \frac{m_{target}}{(m_{target} + m_K)} E_{lab} \tag{2.17}$$

$$E_{lab} = \alpha V_{acc} \tag{2.18}$$

$$E_{av} = E_{cm} - IE(K^{\circ}) = \frac{m_{target}}{(m_{target} + m_K)} \alpha V_{acc} - IE(K^{\circ}) \tag{2.19}$$

where V_{acc} is the acceleration voltage, E_{lab} is the kinetic energy in the laboratory frame, E_{cm} is the kinetic energy in the centre-of-mass frame, m_K is the mass of the potassium atom, m_{target} is the molecular target mass, $IE(K^{\circ}) = 4.34$ eV, is the potassium ionisation energy and α is an experimental correction factor of the incident beam energy. Concerning the latter parameter, some studies have been performed and recent charged particle trajectory simulations alongside with energy loss measurements determined this quantity. This value shows that the final kinetic energy of the hyperthermal alkali beam is appreciably smaller than the corresponding accelerating voltage and therefore cannot be neglected (see further discussion in Chapter 3). For simplicity, the molecular target velocity is negligible in comparison to the projectile beam's velocity.

Another important mechanism that has been shown to be critical to the way the reaction pathways decay after electron transfer, is the presence of the electron donor in the vicinity of the TNI. Experimental results clearly indicate that its presence can stabilize the complex or it can influence some dissociation pathways. Indeed, in potassium collisions with nitromethane the parent anion is formed suggesting a clear evidence of the TNI stabilisation due to the presence of the K^+ ion in the vicinity of the collision complex. As for purine derivatives studied in the course of this research work, enhanced fragmentation and new fragmentation pathways are observed, relative to DEA experiments (see Chapter

5). Such differences in the fragmentation pattern have been ascribed to a Coulombic interaction between the K^+ cation and the TNI, supressing auto-detachment [14].

Knowing the collision time is also extremelly relevant when vibrational excitation is taken into consideration. Indeed, some mechanisms relate with the ratio of collision time and the vibration period of the TNI. The collision time will strongly depend on the variation of R_c. When the TNI is formed the equilibrium internuclear distance of the respective bond that may lead to dissociation is always greater than the equilibrium distance of the neutral molecule. The TNI is formed in the repulsive part of the potential curve inducing the nuclei to move apart, increasing R, and from equation 2.16 [14], increasing the molecule's electron affinity. If electron transfer occurs at the first crossing, R_{c1}, the second crossing, R_{c2}, will in fact depend on the collision velocity (that relates with the collision time). Particularly, in the low velocities region where ion-pair formation thresholds are obtained ($t_{col} \geqslant t_{vib}$), the TNI may be allowed to "relax", achieving an equilibrium, due to the presence of the alkali cation. Therefore, the electron affinity will correspond to the difference between the ground state of the neutral and the ground state of the anion, i.e. the adiabatic electron affinity, EA_{ad}:

$$EA_{ad} = IE(K^{\circ}) - E_{thresh} \tag{2.20}$$

where E_{thresh} is the experimentally observed threshold energy for the TNI formation.

Chapter 3

Experimental Apparatus

"An experiment is a question which science poses to Nature, and a measurement is the recording of Nature's answer."

Max Planck, *The Meaning and Limits of Exact Science', Science (30 Sept 1949), 110, No. 2857, 325*

In this chapter a comprehensive description of the experimental set-up used throughout this work is presented as well as the phases of assembling, characterisation and optimisation of the implemented alkali energy loss technique to study electron transfer mechanisms in potassium-molecule collisions, with special focus on biologically relevant molecules. This chapter also describes both time-of-flight (TOF) mass spectrometers used throughout this thesis.This work was performed at the Atomic and Molecular Collisions Laboratory (Laboratório de Colisões Atómicas e Moleculares - LCAM, Universidade NOVA de Lisboa, Portugal).

3.1 Overview

The crossed molecular beam apparatus comprises two distinct high-vacuum chambers interconnected by a 4 x 8 mm gate valve and each differentially pumped independently by diffusion pumps, models Edwards E06 and Varian NRC 0184, reaching base pressures around 4×10^{-6} hPa and 7×10^{-7} hPa (with a two stage E2M18 Edwards and a Leroy Somer LS90S51 Alcatel rotary pumps as backing pumps), respectively. In the alkali chamber a hyperthermal neutral potassium beam from 7 to 900 eV collision energy (in the lab frame) is produced by resonant charge exchange of accelerated K^+ ions with vaporized potassium (K°). The experimental set up used for most of the (TOF) mass spectra recorded from electron transfer experiments is schematically represented in figure 3.1. Initially, K^+ ions (hyperthermal alkali ions) are generated by a commercial K^+ ion

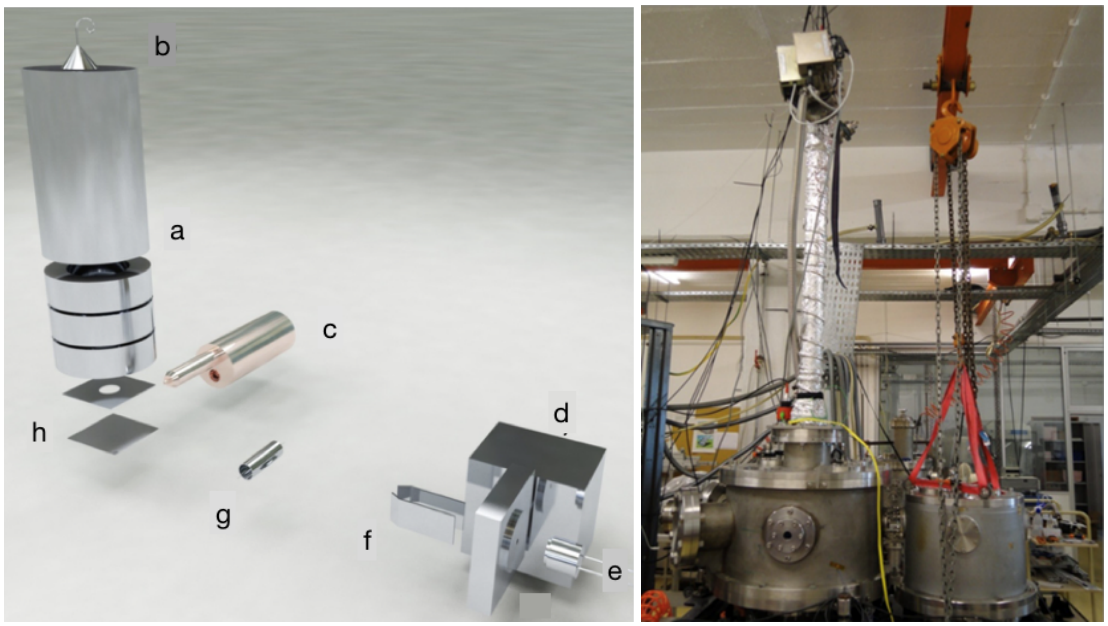

Figure 3.1: Schematic of the molecular crossed beam apparatus with: a channeltron type detector (a); the molecular target oven (b); the Langmuir-Taylor type detector (c); the potassium oven and CEC (d); the ion source (e); the deflecting plates (f); and the former TOF mass spectrometer (g). Picture in left from ref [7]

.

source (Heatwave Labs, model 1011139), and accelerated to a set kinetic energy towards the charge exchange chamber (CEC), where they resonantly charge exchange with thermal K° atoms. The potassium vapour produced by heating solid potassium in an oven at about 393 K is diffused to the CEC kept at 413 K to avoid condensation on the slits. Both oven and CEC are heated by a a pair of 200 W cartridge heaters controlled by independent PID (CAL3300) units. At the exit of the CEC, a pair of deflecting plates is located, deflecting the undesired K^+ ions that did not charge exchange (see figures 3.1 and 3.2). By connecting one of the plates to a positive voltage and the other to an electrometer it provides a current measurement that can be used to monitor both

the ion source and the charge exchange efficiency – which is estimated to be 20% at 100 eV lab frame collision energy by relating the K^+ current measured when electron transfer occurs (K oven at 393K), and the current measured when K^0 oven is at room temperature. The collision chamber comprises the molecular target oven, the surface ionisation detector, the TOF mass spectrometer, and a recently implemented electrostatic hemispherical analyser. A set of three 500 W halogen lamps is also installed to perform bake-out to the collision chamber inner walls favouring the desorption of molecular residues (mainly water). The molecular target oven is made of a sample container, an outer body and a capillary tip with 1 mm in diameter (all made of 316L stainless steel). It also allows liquid samples admission from an external sample holder to the collision region. The oven is heated by a 200 W halogen bulb, both lamp and oven are surrounded by cylindrical stainless-steel reflector used to increase heating efficiency. Both bake-out and sample heating systems are manually regulated by two Variac DC voltage supplies and the temperature is monitored by two K-thermocouples. In the previous set-up, the

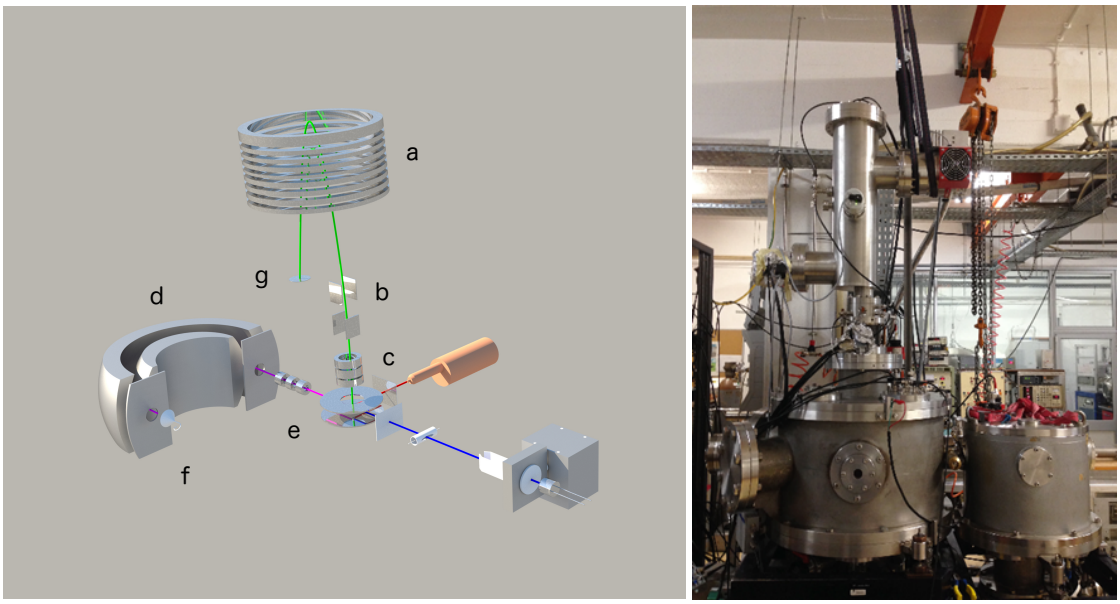

Figure 3.2: Current arrangement of the crossed molecular beam set-up with a new mass spectrometer and a hemispherical analyser (d) located in the forward direction of the potassium beam after an Einzel lens (e) placed at the analyser's entrance. The analyser uses a canneltron type detector (f) coupled to the exit slit. In the picture is also displayed the ion mirror (a); the deflecting plates (b); and the lens system (c). The spectrometer uses a micro channel plate detector (g).

negative ions formed upon electron transfer during collision were extracted by a dual stage Wiley-McLaren type home-made TOF mass spectrometer with a total length of 1.4 m and a drift tube 1 m long. The pulse triggering was applied by a HP 214B signal generator and both triggering and signal acquisition were controlled by a FasComtec P7888 Multiscale acquisition board. The acquisition board initiates each scan when the voltage pulse is applied to the extraction region repeller plate (start pulse), and the stop

input signals coming from the TOF detector are recorded in the time bin corresponding to their arrival time. Currently, the negative ions are analysed by a commercial dual stage Reflectron-TOF mass spectrometer (Kore Technology, UK) with an optical bench adjuster (± 20 mm,± 5 deg), and 70 mm diameter wide extraction plate, capable of mass resolution up to 3000. The pulse triggering is controlled by a time-to-digital converter (TDC) unit with 0.25 ns time resolution and the voltages are applied by high-voltage power supplies, both from Kore. The signal is collected by a microchannel plate and pre-amplified towards the TDC. TOF mass calibration can be accomplished using very well-known negative ion formation and fragmentation from nitromethane (CH_3NO_2) and/or carbon tetrachloride (CCl_4). Data recording is performed using a Kore software interface provided. During an electron transfer collisional process, ion-pair formation occurs, i.e a temporary negative ion from the target molecule and a K^+ ion. K^+ ions can now be energy analysed in a range up to 20 eV. They are focused into the entrance of a hemispherical analyser and the transmitted ions are collected by a channeltron type detector (model sjuts25, from Dr. Sjuts Optotechnik GmbH), as depicted in figure 3.2. The information obtained from these energy loss measurements, enables to asses the nature of the underlying molecular states involved in such electron transfer mechanisms. Here we will describe the operation principle of the energy loss experiments with the aid of complementary charge particle simulation using SIMION 8 © [67].

3.2 Langmuir-Taylor surface ionisation detector

To monitor the hyperthermal K° beam, a Langmuir-Taylor (LT) surface ionisation detector is used and it is located prior to the collision centre. The detector is made of a cylindrical collector connected to an electrometer and an iridium filament (0.125 mm thickness and 99% purity) that passes the collector longitudinally, as depicted in figure 3.3. The

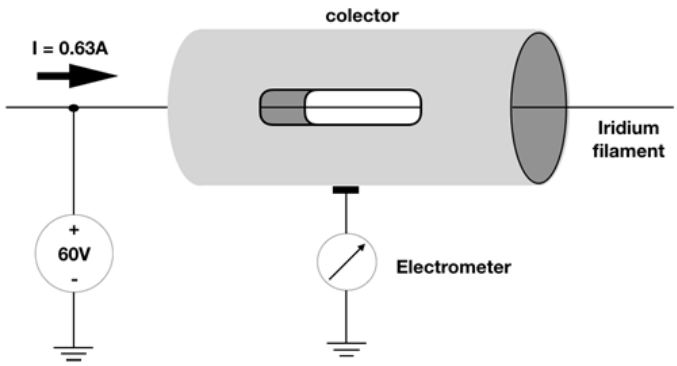

Figure 3.3: Schematic representation of the LT ionisation detector.

filament is +60 V biased relative to ground and a current typically around 0.63 A is applied reaching a temperature ~510 K. The neutral K° atoms that hit the filament are desorbed as positive ions, deflected towards the collector and measured as a current.

Iridium is used in detriment to tungsten because of its higher work function (around 5.7 eV [68]). It increases ionisation efficiency for potassium to higher values (close to 1) and avoids negative ionisation that may occur for elements with large electron affinity. [68, 69]

3.3 Projectile beam characterisation

The neutral potassium beam is produced in a resonant charge exchange process which consists of a potassium oven, a charge exchange chamber (CEC) and a K^+ ion source as schematically depicted in figure 3.4. A pair of deflecting plates deflects the hyperthermal alkali ions and extract them from the hyperthermal K° beam. The charge exchange process results from electron transfer from a thermal K° atom to a hyperthermal K^+ ion as a result from a short-range interaction between the two particles. The neutral hyperthermal potassium beam formation is schematically shown in figure 3.4. K^+ ions are produced and tuned up to a set kinetic energy. The hyperthermal K^+ beam that is emitted by a commercial ion source will then be accelerated towards the CEC where it resonantly charge exchanges with thermal potassium atoms K°, hence the system's kinetic energy is conserved. The result is a hyperthermal neutral beam. In the intermediate energy range

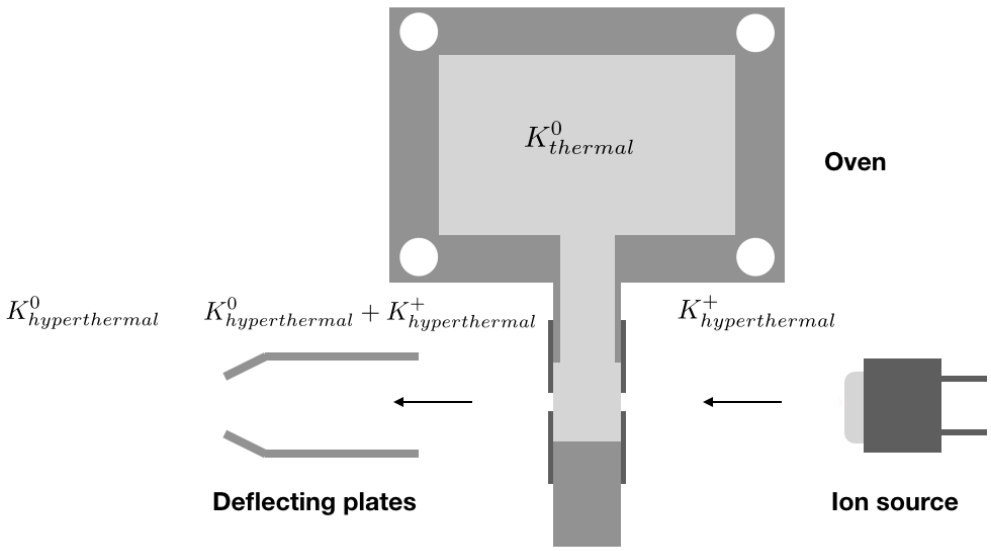

Figure 3.4: Schematic representation for the formation of a hyperthermal neutral potassium beam.

(30-100 eV), the deflecting plates when biased with a voltage roughly ~1.3-1.6 times the accelerating voltage, will extract both thermal and hyperthermal K^+ ions that did not charge exchange. An electrometer is connected to one of the plates to monitor the charge efficiency. Some experimental studies along with charged particle trajectory simulations were carried out to characterise the hyperthermal potassium beam, and they determined

that its effective kinetic energy is appreciably smaller than the voltage applied. This was explained by Aten and Los in terms of space charge affects [70]. They also demonstrated that its kinetic energy was dependent on the acceleration system geometry.

3.3.1 Child-Langmuir Law

In the low acceleration region, the ion flux will be limited by charge space effects, according to the Child-Langmuir law (see Figure 3.5). Consider in a region of space with charge density ρ (space charge), one can use Poisson's equation to obtain the equation that governs the potential V(x) between the electrodes that limit the acceleration region in the present set-up – being the anode the ion source holder and the cathode the CEC entrance slit.

$$\frac{d^2V}{dx^2} = 4\pi\rho \tag{3.1}$$

$$J = \rho v = I/A \tag{3.2}$$

$$\frac{1}{2}mv^2 = eV(x) \tag{3.3}$$

From equations 3.1, 3.2, 3.3 we obtain equation 3.4

$$\frac{d^2V}{dx^2} = C_1 V^{-1/2} \tag{3.4}$$

where C given by

$$C_1 = 4\pi\frac{I}{A}\sqrt{\frac{m}{e}} \tag{3.5}$$

The boundary conditions are given as follow:

$$V(d) = V_0 \tag{3.6}$$

$$\frac{dV}{dx}(0) = 0 \tag{3.7}$$

where d is the length of the acceleration region. Finally, by solving the differential equation we obtain Child-Langmuir law.

$$j = \frac{\sqrt{2}}{9\pi}\sqrt{\frac{e}{m}}\frac{V^{3/2}}{d^2} \tag{3.8}$$

Concerning a flux of ions, the Child-Langmuir law is expressed as[71]:

$$j = 5.44\times10^{-8}\frac{V^{3/2}}{d^2}\sqrt{\frac{Z}{A}} \tag{3.9}$$

where Z is the atomic number and A the mass number. The current system arrangement can be described as two planar electrodes placed apart by d = 2.5 mm, thus we can apply the Child-Langmuir law to determine the flux of K^+ ions in the current set-up. From figure 3.6, one can observe the Child-Langmuir law behaviour for accelerating voltages

<300 V, above which a “plateau” is formed. According to the Richardson-Dushmann law, the maximum flux of charged particles that is achieved is temperature dependent and given by:

$$j = C_2 T^2 \exp^{-W/kT} \tag{3.10}$$

where T is the temperature, W is the work function and k is the Boltzmann constant. The constant C_2 is known as the Richardson constant and is given by:

$$C_2 = \frac{4\pi m k^2 e}{h^3} \tag{3.11}$$

where m is the mass of potassium, e the particle’s charge and h the Planck constant. Thus, the observed "plateau"indicates that the flux reached its maximum, imposed by the temperature of the ion source.

Charged particle trajectory simulations performed with SIMION 8© [67] along with current measurements in the LT detector, allowed us to estimate, from equation 3.2, the flux of ions emitted by the ion source. The simulations indicated a low transmission coefficient of $K°$ along its optical path towards the collision region of 0.004%. Given that $T = \rho_0/\rho_i$ and using equation 3.2, we obtain a flux of 0.59 mA/cm^2 for an accelerating voltage V_{acc} = 100 V, which agrees quite well with the expected value according to equation 3.9 (j = 0.60 mA/cm^2). The ion source has an emitting surface area of 0.196 cm^2. The current measurements were performed with the K oven at room temperature (no CE is involved). When the oven is heated to 393 K the measured current is generally one order of magnitude lower. Such current drop is explained in terms of the charge exchange limiting the real value of the current. The ratio between these two regimes gives an estimation relating the CE efficiency ~ 20% (at V_{acc} = 100 V).

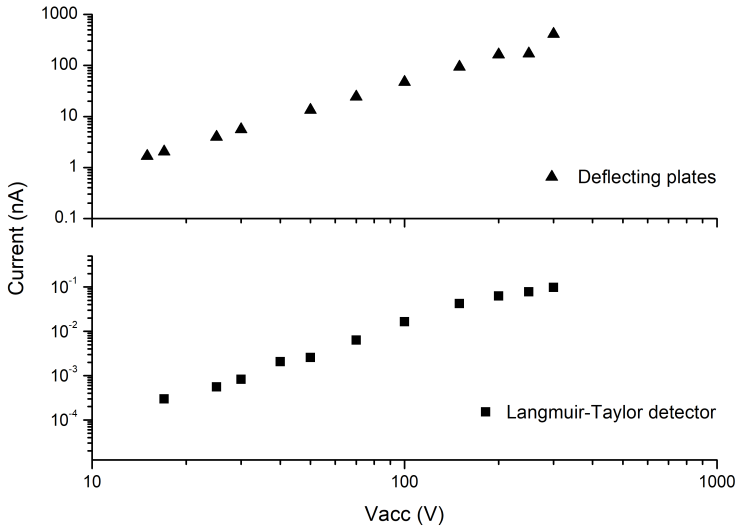

Figure 3.5: Current measured (nA) as a function of accelerating voltage (V), with the current being proportional to V$^{3/2}$.

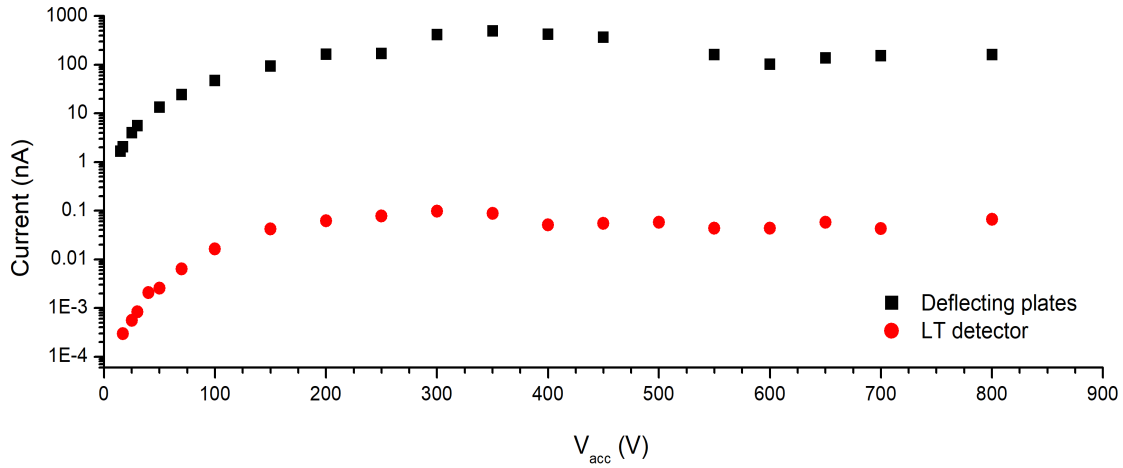

Figure 3.6: Current measured as a function of accelerating voltage between 15 V and 800 V in the lab frame. Above 100 V, a saturation region is reached.

3.3.2 Energy resolution and energy dependence

Information about the kinetic energy of the neutral alkali beam, formed upon a resonant charge exchange process, is of vital importance in atom-molecule collisions for determining electron affinities and to perform accurate threshold measurements [43]. To quantify the potassium primary beam energy resolution, a hemispherical analyser was used to determine the FWHM (full width at half maximum) of the hyperthermal K^+ ions. As mentioned, the process where it produces a neutral beam is resonant, hence there is energy conservation in the isolated system $[K^\circ + K^+]$. Thus, to determine the incident K° beam energy profile we studied the K^+ beam in the forward direction through the use of electrostatic energy analysers. Energy profiles obtained for different collision energies in the centre-of-mass frame, at 45, 61, 73 and 84 eV, show Gaussian distributions with FWHM of 0.4 eV (see Appendix D). Preliminary results using a home-made electrostatic linear energy retarder showed that the resultant beam has an energy deficit of roughly 15% (see figure 3.7). Indeed, the potential will increase from the edge to centre to the beam by ΔV as studied by Aten and Los [70]. The shielding effects by the ions on the outer layers can cause this decrease and owing to divergence of the beam, only the centre part is neutralised to form alkali atoms whose final kinetic energy will be smaller by the same amount. This experimental value for the correction factor, α, is in good agreement with the previously obtained through charged particle trajectory simulations [7, 72].

3.4 The implemented hemispherical energy analyser (HEA)

The analyser consists of two concentric hemispheres and by applying a potential difference between them it acts as a narrow energy filter for charged particles. Considering a K^+ ion travelling along the centre of the electrodes gap, its kinetic energy E_0/z – being z

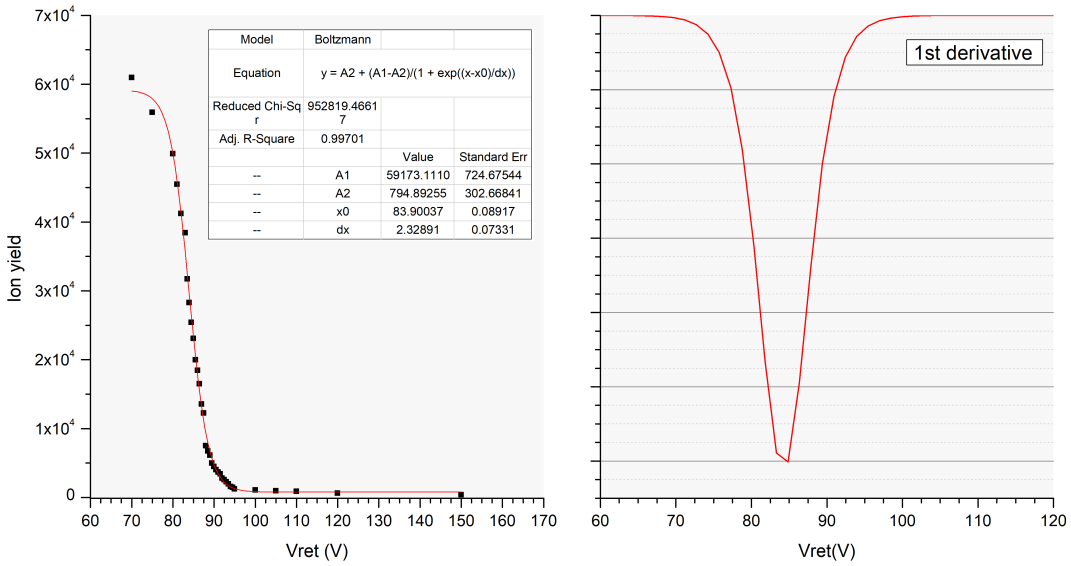

Figure 3.7: Experimental determination of the effective K beam kinetic energy

the ion's charge – can be expressed by the following equations [71]:

$$V_p = V_0\left(\frac{R_2}{R_1} - \frac{R_1}{R_2}\right) \Leftrightarrow V_p = \frac{E_0}{z}\left(\frac{R_2}{R_1} - \frac{R_1}{R_2}\right) \tag{3.12}$$

$$V_1 = \frac{E_0}{z}\left(2\frac{R_0}{R_2} - 1\right) \tag{3.13}$$

$$V_2 = \frac{E_0}{z}\left(2\frac{R_0}{R_1} - 1\right) \tag{3.14}$$

where V_1 and V_2 are the voltages applied to the inner and outer hemispheres respectively, and V_p is the voltage difference in the hemispheres. $R_1 = 73$ mm and $R_2 = 93$ mm correspond to their internal and external radius. Setting $R_0 = \frac{R_1+R_2}{2}$ as the mean radius, the voltages $V_{1,2}$ can be written as a function of the transmitted energy E_0/z and the analyser hemispheres' dimensions, according to equations 3.13 and 3.14. Thus, the transmitted energy is proportional to the potential V_p. The advantage of a set-up with a large electrode gap is the resolution enhancement and the acceptance of wider trajectories improving transmission. If the beam energy is very broad, the chances of ions striking the electrodes surface are very unlikely resulting in a lower background. However, this configuation imposes a disadvantage regarding fringing field effects that become more relevant and to reduce the spread of the beam caused by these unwanted effects, slits are used in a Herzog type configuration [73].

3.4.1 Control and Acquisition

With this type of analysers, it is possible to work in two energy scan modes: constant transmission (CT) and sector field sweep.(SFS). In the latter, a potential is scanned in one

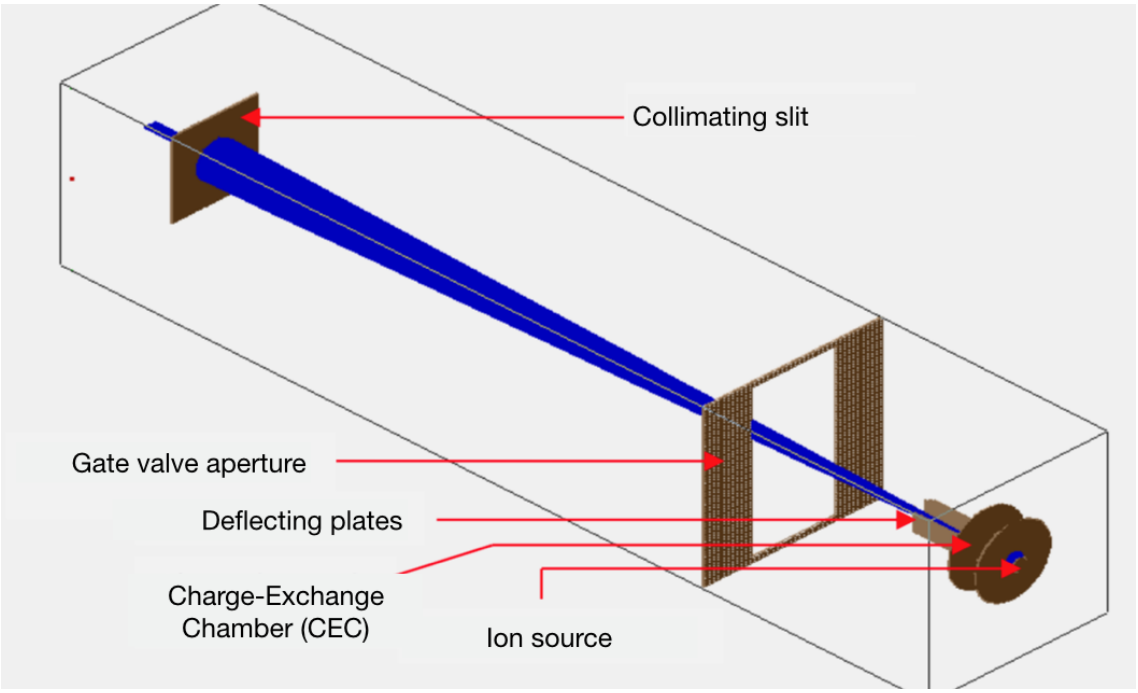

Figure 3.8: K beam simulation performed with SIMION 8© software. [67]

electrode while the other is kept constant. This sweeps the trajectory of the transmitted ion, while keeping the ratio $\Delta E/E_0$ constant. Therefore, ΔE will change with energy E_0 (being ΔE the baseline energy full width). A more convenient procedure is to maintain a constant potential, V_p, between the hemispheres and scan the centreline potential, V_0. This method keeps ΔE constant for the entire scan which allows a constant pass energy. To achieve such experimental arrangement a resistor bridge was used, as shown in figure 3.10. To allow the potential V_0 to scan independently of V_p, an external resistor was connected between the electrodes. The potentials applied are all schematically represented in figure 3.10. The analyser entrance slit stays in the beam's optical path. Both entrance and exit slits are adjustable in width, varying from 1 to 3 mm. At the entrance slit an Einzel lens is placed to focus the K^+ ions into the analyser without influencing its energy. It is formed by 3 similar electrodes where $V_1 = V_3$ and V_2 regulates the focusing power.

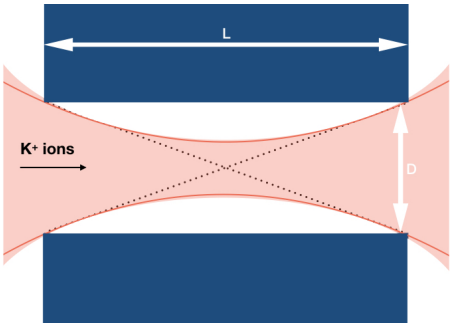

Figure 3.9: Schematic representation of the energy analyser entrance slit.

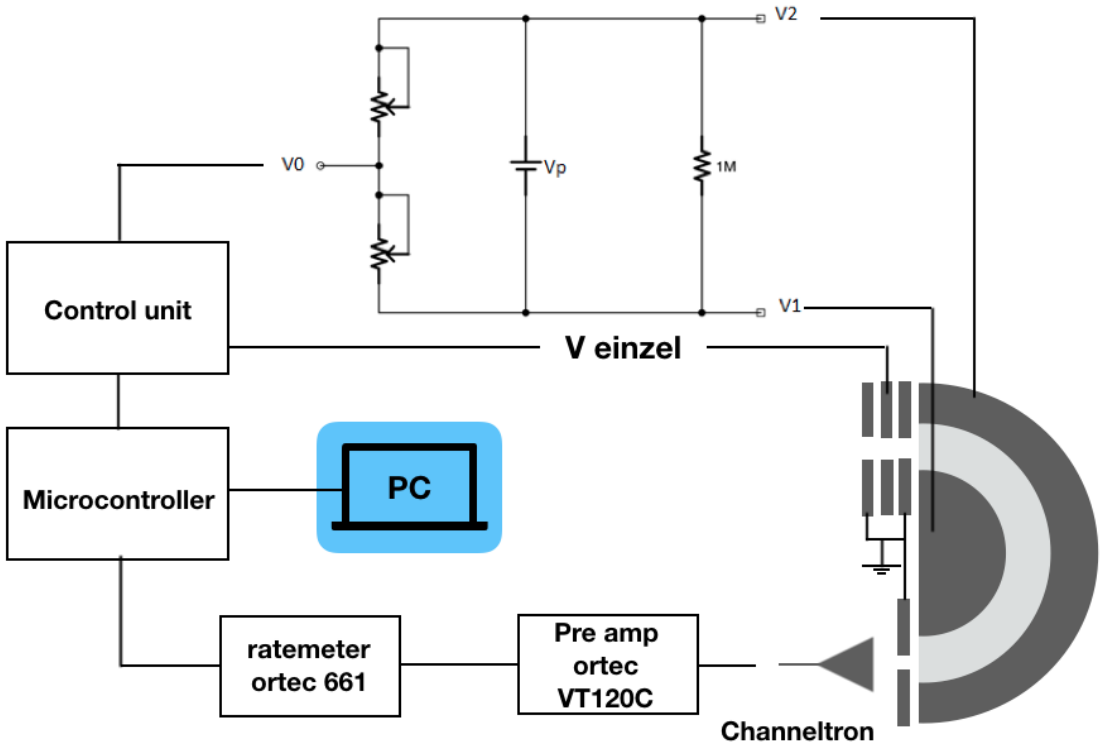

Figure 3.10: Schematic of the energy loss setup control and acquisition system.

These electrodes are cylindrical in shape with 3 mm of inner diameter, 7 mm outer diameter and 3 mm in length. They are placed 1 mm apart. To scan the pass energy in CT mode, the analyser was configured for $E_0 = 100$ eV with $V_p = 41$ V and the voltage V_0 mapped using an Arduino UNO R3 microcontroller. It is worth noting that no differential pumping is applied to the analyser. Potentials V_{Einzel} and V_0 were optimised for different beam energies until a signal with a maximum intensity was obtained, as a function of the accelerating voltage from where an energy calibration function (see figure 3.11), is determined. All voltages applied are controlled by a recently built voltage supply unit and varied with reference to potential V_0. Due to the analyser dimensions, the acceptance angle will be limited by the pencil angle $\theta = D/L$ (see Figure 3.9). The entrance slit has a cylindrical shape with length L = 8 mm and diameter D = 2.5 mm setting the pencil angle around 0.3°. Thus, from equation 3.15, one can state that the analyser energy resolution is merely dependent of its geometric properties. [71]

$$\frac{\Delta E}{E_0} = \frac{(w_1 + w_2)/2}{2R_0} + \frac{\theta^2}{4} \approx \frac{w_1 + w_2}{4R_0} \tag{3.15}$$

where w_1 and w_2 are the widths of the entrance and exist slits. They are not equal, thus it is commonly used the value $(w_1 + w_2)/2$ as an estimation. With the current configuration and for a potassium energy of 100 eV in the lab frame, $\Delta E \sim 1eV$ (FWHM ≈ 0.5).

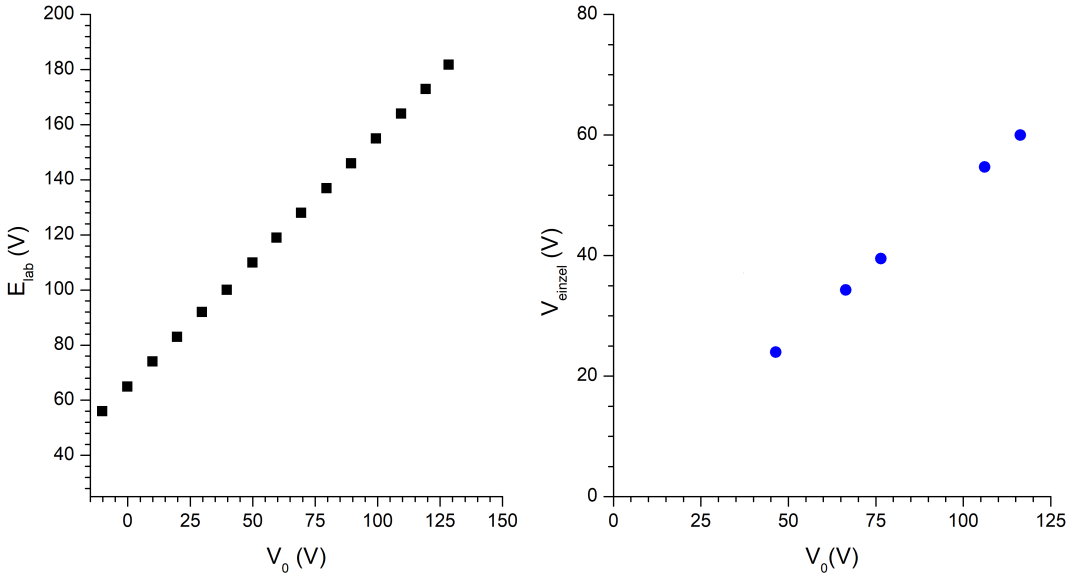

Figure 3.11: Calibration curves for lab frame kinetic energy, E_{lab}, and for the potential applied to the Einzel lens, V_{einzel} as a function of the mapping potential, V_0.

3.4.2 Software interface

For signal acquisition, friendly-user interfaces were developed using LabVIEW and Matlab 2017 (student's version). Both allow to control the number of scans and the energy loss range. A noise filter was implemented in Matlab's app using a Simple Moving Average (SMA, Finite Impulse Response - FIR) filter. The signal acquisition can work in two modes: energy loss and voltage measurement. The output will be presented as a function of the channels probed. Each channel will correspond to a specific pass energy, therefore a calibration curve is needed (see figure 3.12). Given that the energy loss scale is defined as the difference between the incident K° beam energy and the energy of the K^{+} beam after the collision, an energy profile of the primary beam is always needed before any energy loss measurement. Though it was made possible to edit the channels range for faster sweeping of the incident primary beam.

3.5 TOF mass spectrometer

Time-of-flight mass spectrometry is one of the many methods to identify ions formed from a molecular target and differentiate them, based on their m/z ratio. With this method, the ions formed in the collision region are accelerated towards a free-field region (FFR) and to a detector. Their m/z ratio is then determined considering their temporal dispersion, i.e. ions with different mass to charge ratio will have different transit times. The advantages of using such spectrometers are several but some of the most important features are the capability to obtain all ionic species simultaneously (unlike quadrupole

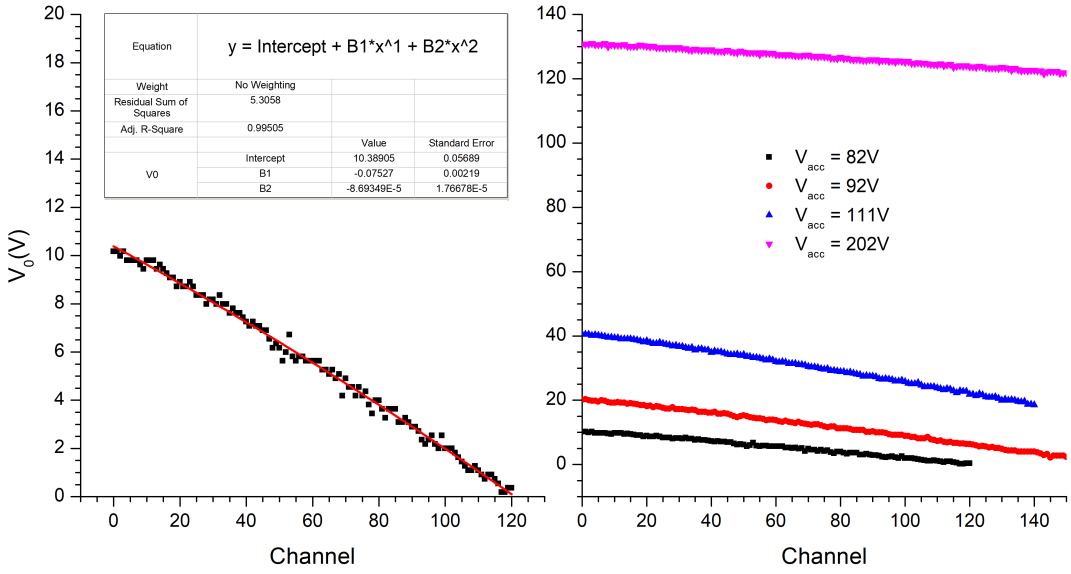

Figure 3.12: Calibration curves of V_0 as a function of the channel chosen.

mass spectrometers filter the ions according to a selected m/z), the transmission of a TOF analyser is usually higher and of course, the presence of no upper limit in mass detection. In general, it comprises an extraction region, an acceleration region, a FFR and a charged particle detector. Also, a start-stop arrangement for TOF measurements is needed. During the course of the research activities performed within the scope of this

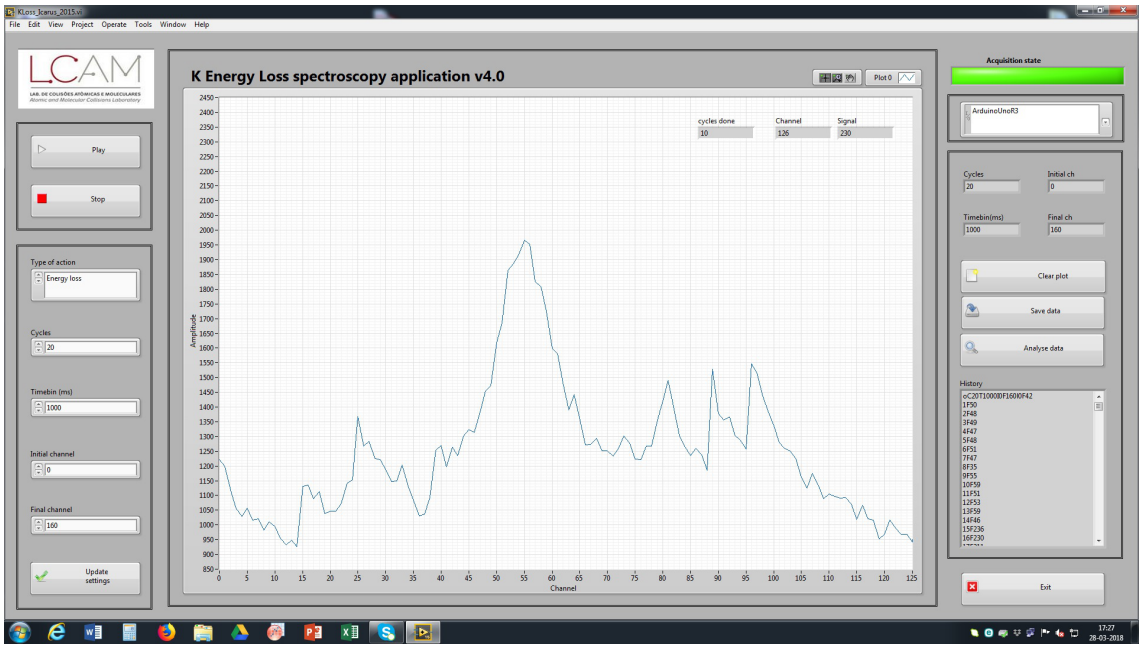

Figure 3.13: Picture taken from the LabVIEW interface during K^+ energy loss acquisition over a wide channel range.

thesis, two types of TOF mass spectrometers were used and will be briefly described.

3.5.1 TOF Working principles

The ions formed within the region of two mutual plates, are extracted by an electric field in that region. They may pass through a second stage where they are accelerated, by the voltage V, towards the entrance of a field-free region (FFR). During acceleration, the potential energy, $U = zV$, will be converted to kinetic energy of the ions, $K = \frac{1}{2}mv^2$.

$$zV = \frac{1}{2}mv^2 \tag{3.16}$$

where z is the charge, m is the mass and v is the velocity of the particle. The velocity of a ion will not change after the acceleration region since it moves in a FFR region. The TOF can then be determined by using simple kinematic equations. Let $v = L/t$, where L is the total flight length, the flight time, t, can be expressed by equation 3.17:

$$t^2 = \left(\frac{L^2}{2V}\right)\frac{m}{z} \tag{3.17}$$

The total TOF is given by

$$t = t_0 + t_e + t_a + t_L \tag{3.18}$$

where t_e represents the flight time in the extraction region, t_a the flight time in the acceleration zone and t_L the flight time in the field-free region. When an ion is formed after a certain time a trigger is set to start the TOF scale, here denoted t_0. The total energy as the ions travel through the FFR will be the sum of all contributions, i.e.

$$K_t = K_0 + K_e + K_a \tag{3.19}$$

where K_0 is the ion's initial kinetic energy, K_e is the kinetic energy after being extracted and K_a the kinetic energy passing the acceleration region.

3.5.2 Mass Resolution

The resolving power of a TOF spectrometer can written as:

$$Resolution = \frac{m}{\Delta m} = \frac{t}{2\Delta t} \tag{3.20}$$

Being Δm the difference in mass of adjacent peaks and Δt the corresponding difference in the time-of-flight. Hence,the resolution will be limited by the time sensitivity of the acquisition system. Such capability may be compromised by the response time of the detection system. From equation 3.17 the flight time is very sensitive to the length of the flight tube. Other main constraints for a high mass resolution are: the initial kinetic energy of the fragments (energy distribution); initial position of the ions (spatial distribution); and initial instant of ion formation (temporal) distribution). The influence of the initial kinetic energy and initial position can be suppressed by using an additional stage of acceleration [7].

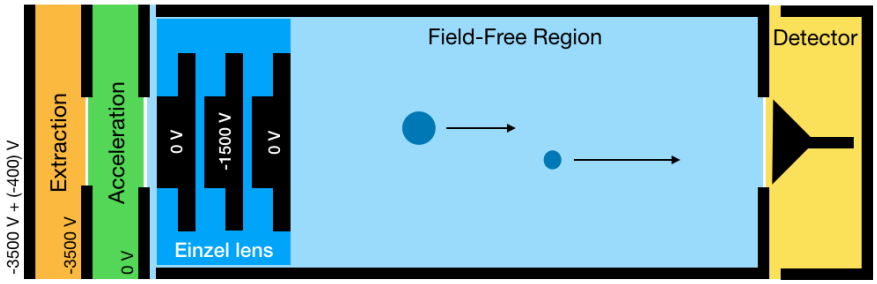

Figure 3.14: Schematic representation of the linear TOF mass spectrometer used in this thesis.

3.5.3 Wiley-McLaren TOF (with dual stage)

This configuration was introduced by Wiley and McLaren in 1950's [74] resulting in an enhancement in resolution with respect to the single-stage TOF spectrometer. The additional stage allows for m/z less energetic ions to reach together with the more energetic ions the focal plane where the detector is, increasing resolution by reducing the spatial distribution. A detailed description of the dual-stage TOF used in this work is not within the scope of this thesis and can be found elsewhere [7]. Briefly, the former TOF spectrometer, besides a stage for extraction, acceleration and drift, it also comprised an Einzel lens. The extraction region was defined by a repeller plate and an extraction grid 12 mm apart. It is in this region that both potassium and molecular target beams cross at right angles. A DC potential of -3500 V was constantly applied to both plates and a pulse up to -400 V was added (with 15 ns rise time) to the repeller plate through a Jordan D-1040 Pulser unit. The pulse duration was set according to the heavier mass being formed allowing time enough for its total extraction (typical values of 1-2μs were used). The acceleration region was defined by the extraction grid and acceleration grid that was grounded at a mutual separation of 12 mm. Ions were accelerated and left this region with high kinetic energy while the Einzel lens allowed focusing of the ions to a focal point without changing their kinetic energy. The voltage applied to the central electrode was -1500V and the outer electrodes were kept grounded. The FFR region consisted of a 1 m long stainless steel CF63 straight connector kept at ground potential with differential pumping provided by a turbomolecular pump connected to a backing pump. The detector used was a channeltron type detector, operating in pulse counting mode. For each ion impinging on the detector, a negative pulse of 20 mV (with 20 ns duration) was generated. This signal was preamplified through an ORTEC VT-120 C and entered the FastComtec P7888 multiscale board. By analysing the FWHM of the NO_2^- peak in nitromethane mass spectrum, Antunes [7] reported a mass resolution of ~125.

3.5.4 Reflectron TOF

Ion energy focusing in TOF spectrometers can be achieved using special focusing devices. The most common is the reflectron type and it was first suggested by Mamyrin [75, 76].

The main component is the ion mirror which comprises a series of annular electrostatic lenses placed at the opposite end of the drift tube, with respect to the optical bench. A repulsive voltage, V_r is applied to the lenses to deflect the ions into the detector, i.e. the ions are decelerated to zero velocity turn around and are accelerated backwards exiting the ion mirror with the same kinetic energy. The time spent inside the ion mirror will be

$$t_r = 2t_d \tag{3.21}$$

where $t_d = d/(v_i/2)$ and $v_i/2$ is the average velocity inside the ion mirror. Thus, equation 3.21 may be written as

$$t_r = \frac{4d}{v_i} \tag{3.22}$$

Assuming two charged particles with the same m/z ratio, it is possible to infer from equation 3.22, that charged particles with larger kinetic energy will spend more time inside the ion mirror, with larger trajectories, arriving at the detector about the same time as the less energetic particles. Our current set-up, assembled in the crossed molecular beam experiment is a dual-stage reflectron-TOF mass spectrometer with an additional stage that decelerates the ions by a high electric field losing part of their kinetic energy before entering the ion mirror (see figure 3.15). The detector in use is a Chevron micro channel plate with 25 mm diameter wide. Each micro channel is a continuous dynode electron multiplier. Currently, the maximum mass resolution achieved is around 1600.

3.6 Vacuum system

High-vacuum conditions in both chambers are guaranteed by two diffusion pumps with 1300 l/s and 1550 l/s pumping speed, respectively. A liquid nitrogen trap is coupled

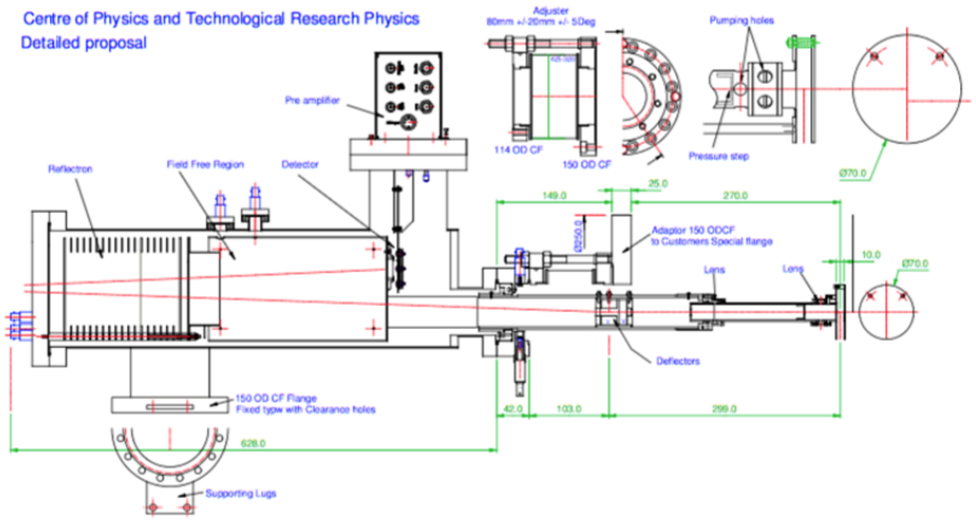

Figure 3.15: Technical drawing of the Re-TOF mass spectrometer recently installed from Kore Technology, UK.

to each pump to avoid oil migration into the chamber. During measurements, only a two-stage rotary pump with a pumping speed of 6 l/s was used as the backing pump and it ensured an ultimate pressure around $3 \times 10^{-2} hPa$ in both diffusion pumps. To avoid contamination of oil vapours from the rotary pump, a molecular sieve trap was installed. Another rotary pump provided primary vacuum onto the liquid and gas sample line. The TOF mass spectrometer is differentially pumped by a 600 l/s Turbo molecular pump from Pfeifer achieving an ultimate pressure of $1 \times 10^{-8} hPa$.

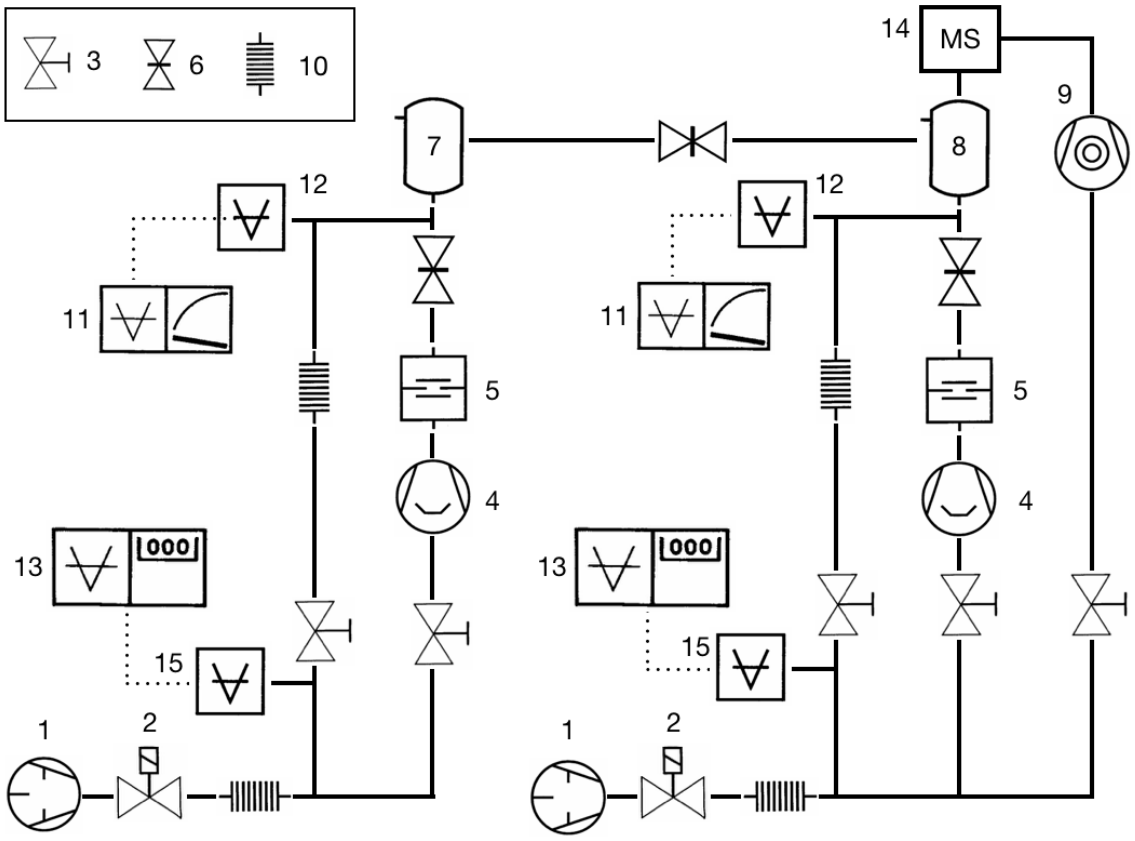

Figure 3.16: Vacuum system schematic. Symbols used according to norm DIN 28401 (2008-03): 1) Rotary pump; 2) Electro-magnetic valve ; 3) Membrane valve ; 4) Diffusion pump; 5) Baffle; 6) Gate valve; 7) Potassium chamber; 8) Collision chamber; 9) Turbo-molecular pump; 10) Flexible tube; 11) Vacuum gauge control unit with dial indicator; 12) Penning gauge; 13) Vacuum gauge control unit with digital indicator; 14) TOF mass spectrometer; 15) Pirani gauge.

Chapter 4

Site-selective bond excision in adenine upon electron transfer

"It's the man who does the science, an evident fact that is too often forgotten."

W. Heisenberg

This chapter is dedicated to novel results concerning bond- and site-selectivity in purine molecules that was observed for the first time in potassium collisions, as far as authors are aware. $(M\text{-}H)^-$ formation is selectively controlled, by tuning the collision energy between 4 and 68 eV. Such process proceeds not only through the breaking of the (C-H) against (N-H) bonds but also exclusively trough H abstraction from N9 position.

Communication: Site-selective excision of adenine upon electron transfer[1]

T. Cunha[a], M. Mendes[a], F. Ferreira da Silva[a], S. Eden[b], G. García[c] and P. Limão-Vieira[a 2]

[a] Laboratório de Colisões Atómicas e Moleculares (LCAM), CEFITEC, Physics Department, Universidade Nova de Lisboa, 2829-516 Caparica, Portugal

[b] School of Physical Sciences, The Open University, Walton Hall, MK7 6AA, Milton Keynes, UK

[c] Instituto de Física Fundamental, Consejo Superior de Investigaciones Científicas (CSIC), Serrano 113-bis, 28006, Madrid, Spain

Published: The Journal of Chemical Physics, 148, 021101 (2018)

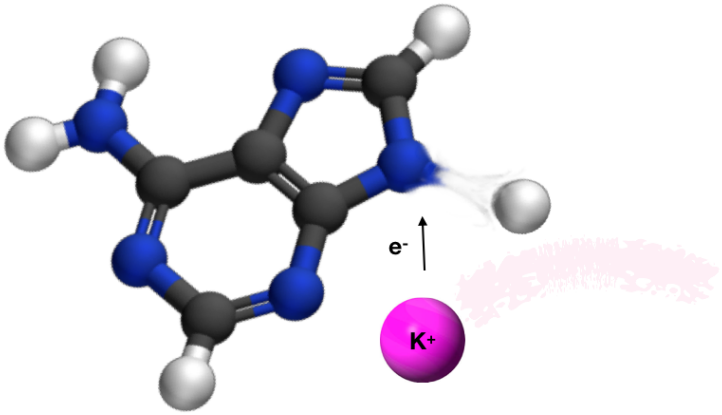

Abstract

This work demonstrates that selective excision of hydrogen atoms at a particular site of the DNA base adenine can be achieved in collisions with electronegative atoms by controlling the impact energy. The result is based on analysing the time-of-flight mass spectra yields of potassium collisions with a series of labelled adenine derivatives. Production of dehydrogenated parent anions is reminiscent of neutral H loss either from selective breaking of C-H or N-H bonds. These unprecedented results open up a new methodology in charge transfer collisions that can initiate selective reactivity as a key process in chemical reactions that are dominant in different areas of science and technology.

[1] Published by AIP Publishing. https://doi.org/10.1063/1.5018401

[2] Author to whom correspondence should be addressed: plimaovieira@ fct.unl.pt. Tel.: (+351) 21 294 78 59. Fax: (+351) 294 85 49.

4.1 Introduction

Radiation-driven control of reactivity is a major goal in chemical physics/physical chemistry. This has been reported previously using ultra-fast laser pulses [77], quantum molecular dynamics of photo-excited molecules [78] and coherent quantum manipulation [79]. However these methods are not readily scalable for many potential technological or medical applications. Therefore, the achievement of electron-induced site- and bond-specific dissociation (on surfaces using STM tips [80] and in the gas phase using low-energy electron beams [22, 23, 81, 82] in the mid-2000 was highly significant. The only previous control over dissociation pathways in atom-molecule collisions was demonstrated for potassium impact on gas-phase thymine and uracil [39]. By achieving controlled dissociation of purines, the present experiments show that selective reactivity in charge transfer collisions is not restricted to the particular case of pyrimidine nucleobases. Indeed, we anticipate that this new route for controlled chemistry can be adapted for numerous collision systems. As the most abundant secondary species produced by ionising radiation, low-energy electrons (defined here as <15 eV) are recognized as critically important reactive species in irradiated materials [83]. In particular, dissociative electron attachment (DEA) [4] and intermolecular charge transfer [84] play key roles in radiation damage to DNA. These results have stimulated extensive experimental and theoretical research into low-energy electron interactions with gas-phase DNA/RNA constituents, revealing detailed understanding of their transient negative ion states [85]. In aqueous conditions that evidently provide a closer approximation of biological environments [5], Wang et al. [9] have shown that deoxyribonucleotides comprising adenine and guanine are more efficient at capturing pre-hydrated electrons than those comprising thymine and cytosine. Therefore, we expect electron-capture induced reactive processes in the purine nucleobases to play a particularly important role in radiation-induced DNA damage. In these experiments an alkali atom, potassium, is used as an electron donor to the nucleobase molecules, adenine and its derivatives. The donor-acceptor interaction changes from covalent (neutral) to ionic at a particular distance, R_c, [64] i.e. the crossing of the covalent and ionic diabatic states. For large potassium-molecule distances the Van der Waals and induction forces can be neglected and consequently the covalent potential is zero and the ionic potential is purely coulombic ($\propto -1/R$). At infinite separation the energy difference ΔE between the ionic and covalent configurations (the endoergicity of the electron transfer process), is given by $IE(K^{\circ}) - EA(M)$, where IE(K) is the ionisation energy of the potassium atom and EA(M) is the electron affinity of the molecule. R_c is given by $14.41/\Delta E$ (Å), [43] where ΔE is expressed in eV. Taking the experimental vertical electron affinity of adenine as -0.54 eV [86] (adiabatic value of 11 meV [87]), the value found for R_c is $\sim$ 3.0 Å, meaning that the corresponding total cross sections for ion-pair formation (of the order of πR_c^2) is much larger (even one order of magnitude) than the corresponding gas kinetic cross sections. Another relevant aspect pertaining significant differences between electron transfer and DEA experiments needs to be properly accounted for within

the context of negative ion formation. Although the information gained in DEA experiments is relevant to assess which resonances may be involved in the attachment process, the role of a third body (K^+) in the vicinity of the temporary negative ion (TNI) is solely responsible to either shift or give access to other (diabatic) resonant states (i.e. in the K-M coordinate) probed in the collision dynamics. [43] Comparisons with electron scattering and DEA experiments are valuable when considering which temporary negative ion (TNI) states may be involved in collisional electron-transfer. However, the presence of the electron donor (pre- and post-transfer) can lead to major differences compared with DEA. These differences can be traced to shifting the energies of key orbitals in the neutral molecule and/or the TNI, as well as modifying TNI lifetimes with respect to electron auto-detachment. [88]

4.2 Experimental section

Negative ion mass spectra were obtained in a crossed beam set-up consisting of a potassium source, an oven and a time-of-flight (TOF) mass analyser. [13] The components were housed in two high-vacuum chambers at a base pressure of 10^{-5} Pa. A neutral potassium beam generated from a charge exchange chamber intersected at right angles an effusive molecular beam consisting of the target molecules. Atomic K^+ ions, obtained from a potassium ionic source, were accelerated through a chamber containing potassium vapour where they resonantly charge exchanged to form a beam of neutral K° fast atoms. The energy of the resultant K° neutral beam was established by the initial acceleration of the K^+ ions and the geometry of the collimating slits in the charge exchange source. The lab-frame collision energy ranged from 15 to 100 eV and the beam energy resolution at full width half maximum was 0.5 eV as measured with an energy loss analyser. The resulting neutral K° beam entered a high vacuum chamber where it was monitored by an iridium surface ionisation detector operating in a temperature regime that only allows detection of the fast beam. This sampled the beam intensity but did not interfere with the beam passing to the collision region. The biomolecular target beams were produced in a hot gas cell (oven) and admitted to vacuum by an effusive source through a 1 mm diameter orifice where they were crossed with the neutral hyperthermal potassium beam. The molecular oven was operated at a lower temperature (400 K measured by a platinum resistance probe, Pt_100) than previous experimental studies which reported no evidence for thermal decomposition of neutral adenine. [86, 89] The negative ions produced in the collision region were extracted by a 250 V/cm pulsed electrostatic field towards the entrance of the TOF where they were analysed and detected in single-pulse counting mode. In the present electron transfer experiments, the total energy available for anion excitation (the collision energy in the centre-of-mass frame minus the ionisation energy of potassium) varied from ~6 up to ~68 eV. Purine, adenine, 9-methyladenine and 6-dimethyladenine were supplied by Sigma Aldrich with stated purities of 98%, $\geqslant$ 99%, 97% and $\geqslant$ 98%, respectively and adenine-2-d (adenine deuterated at the C2 position)

was supplied by CDN Isotope Inc. with isotope enrichment of 97%. Experimental [90, 91] and theoretical [92–94] studies of adenine's tautomers have shown that the canonical form N(9)H dominates in the gas phase, while the N(7)H form is 33 kJ/mol (0.342 eV) higher in energy [91, 93, 94].

4.3 Results and discussion

Figure 4.1 shows the time-of-flight (TOF) mass spectra recorded at 100 eV lab frame collision energy of neutral potassium atoms with purine, adenine, 9-methyladenine, 6-dimethyladenine and adenine-2-d (63.6, 65.5, 67.0, 68.3 and 65.6 eV available energy in the centre-of-mass, respectively). The TOF mass spectra show no evidence of parent anion formation (M^-) and this communication focuses on the dehydrogenated parent anion yield $(M\text{-}H)^-$ only. $(M\text{-}H)^-$ is produced from all five molecules where in 6-dimethyladenine such yield is barely visible above background noise. Adenine branching

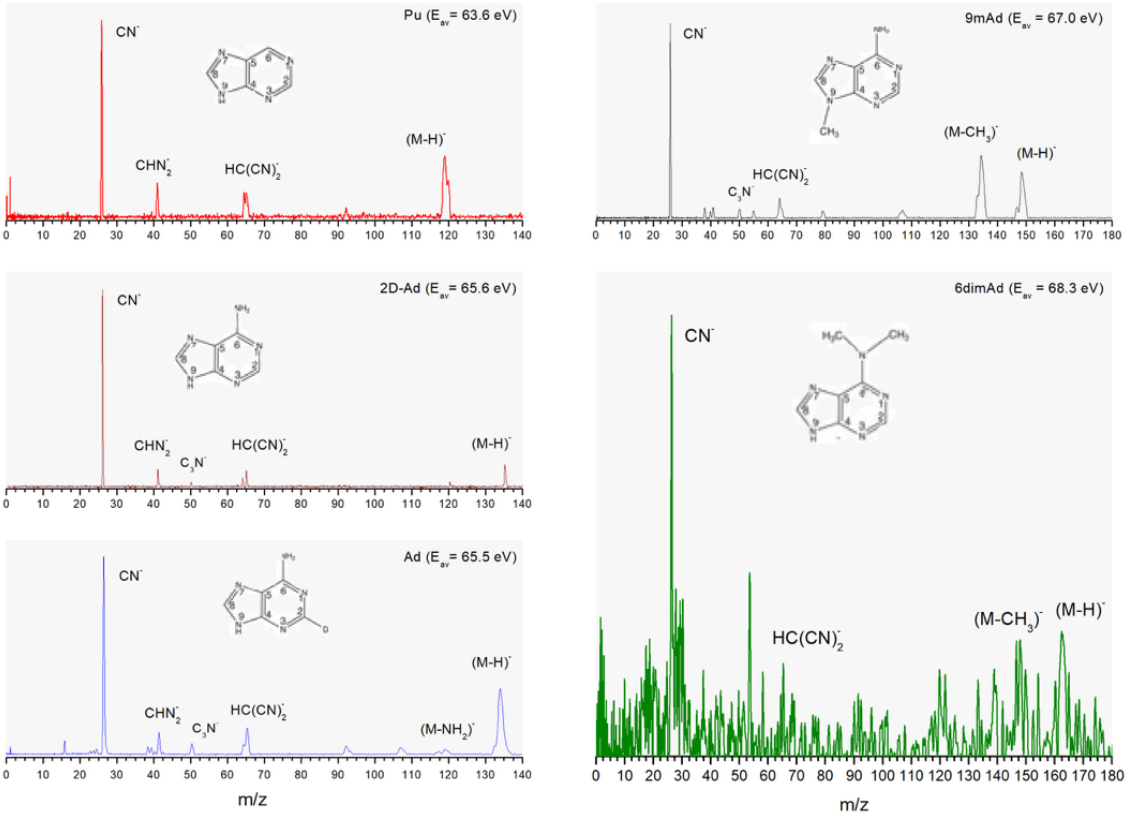

Figure 4.1: TOF mass spectra showing the anions produced following electron transfer from potassium to purine, adenine, methylated adenine at the N9 site (9-mAd), methylated at N-C6 site (6-dimAd) and deuterated adenine at C2 site (2-DAd) in collisions at 100 eV lab frame energy (63.6, 65.5, 67.0, 68.3 and 65.6 eV of available energy, E_{av}, respectively). $(M\text{-}H)^-$ represents the dehydrogenated parent anion.

ratios (see figure 5.7) reveal that loss of a neutral H atom is a precursor in the formation of other fragment anions. Such is discernible in figure 4.2 (15 eV lab frame collision

energy) where $(M\text{-}H)^-$ dominates for the case of adenine and 6-dimethyladenine. The threshold for electron transfer ($IE(K^\circ) - EA(M) \approx 4$ eV) is smaller than the collision energy, so the molecular anion can be formed with an excess of internal energy. For the molecular compounds investigated, 6-dimethyladenine exhibits the highest number of degrees of freedom (57 modes), from which the excess energy can be redistributed resulting in fragmentation (100 eV lab frame). However, if the lifetime of the metastable anion is long enough, intra-molecular energy redistribution may occur competing with direct dissociation. Such is the dominant case of longer collision times as revealed in the TOF mass spectra in figure 4.2. Clearly, all of the conceivable H loss reaction pathways (from the N9, C8, C6, and C2 sites of purine and from the N9, C8, (NH_2)C6, and C2 sites of adenine) are energetically accessible at the relatively high lab frame collision energy of 100 eV. However, the absence of an $(M\text{-}D)^-$ signal in the measurement on partially deuterated adenine indicates that hydrogen loss from the C2 position on adenine can be ruled out. This may be rationalised in terms of strong auto-detachment competing with dissociation for this specific channel. It is also interesting to consider the present results in the context of previously calculated electrostatic potential maps and isodensity maps of the lowest virtual σ^* molecular orbitals at the B3LYP/aug-cc-pVTZ level for purine, adenine and 6-dimethyladenine. [24] These show that for purine the regions accessible for H loss are around the N9-H and C8-H sites, whereas in adenine and 6-dimethyladenine an extra region around the NH_2 and $N(CH_3)_2$ groups is also available. Furthermore, these results show that there is no wave-function density in the C6-H region for purine. Figure 4.2 shows the negative ion yields of $(M\text{-}H)^-$ from purine, adenine, 9-methyladenine and 6-dimethyladenine with a lab frame collision energy of 15 eV (5.8, 6.1, 6.4 and 6.6 eV available energy in the centre-of-mass frame, respectively). Blocking the H positions at the amino group with CH_3, where NH_2 is replaced with a $N(CH_3)_2$ group in 6-dimethyladenine, it is obvious that H loss can also occur from the N9 or C8 positions. For a conclusive check of these two positions, we have performed an additional experiment on 9-methyladenine, thus blocking the N9 site. Significantly, the ion yield of $(M\text{-}H)^-$ is completely suppressed. This means that H loss proceeds from N9 site only. Denifl et al.[24] showed that selective H cleavage from the N9 site of adenine can be also be achieved in DEA, notably via resonances observed experimentally below around 1.07 eV. However, the present results cannot be understood purely on the basis of a direct analogy with DEA. In DEA to adenine, the calculated minimum electron energy required to cleave a hydrogen atom from N9-H, (NH_2)C6, C8-H and C2-H and hence produce a dehydrogenated parent anion varies between 0.94 to 3.63 eV, [24] respectively. This is distinctly lower than the available energies in the centre-of-mass frame in the collisions probed in figure 4.2. Therefore, the remarkable bond- and site-selectivity observed here for $(M\text{-}H)^-$ formation in potassium collisions with adenine does not result purely from energetic constraints. We expect that the electronic structures of the metastable anions accessed by electron transfer at different collision energies are most likely to be responsible for the present result. This seems reasonable since the presence of the electron donor may

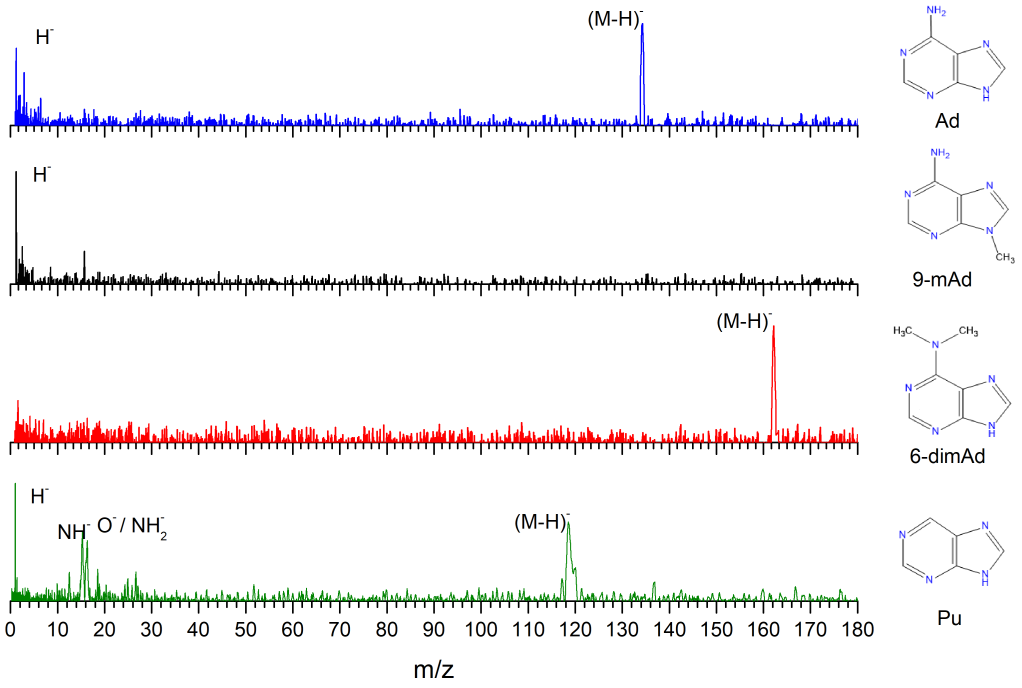

Figure 4.2: TOF negative ion mass spectra for Pu, Ad, 9-mAd and 6-dimAd in collisions with potassium atoms at 15 eV lab frame (5.8, 6.1, 6.4, and 6.6 eV available energy, E_{av}, respectively). The dehydrogenated parent anion $(M\text{-}H)^-$ is visible in all cases except for the 9-methyl adenine measurement. It is worth noting, for purine, NH^-, NH_2^- and CN^- are also formed.

affect the electronic structure of the target molecule (the lowest unoccupied molecular orbitals, LUMOs). Indeed, stabilization of specific orbitals of thymine and uracil due to presence of the potassium atom in the collision system have recently been reported in state-averaged CASSCF calculations. [95] Analogous theoretical studies of the effects of the incident potassium atom (pre- and post-electron transfer) on neutral and anionic adenine are required to better understand the mechanisms responsible for the presently observed selective H loss.

4.4 Final remarks

We show here that selective hydrogen removal from the adenine molecule can be achieved in collisional charge transfer experiments by tuning the collision energy. It is striking that such fine control over reactivity can be achieved in an energetic collision between an atom and a relatively complex molecule with numerous competing relaxation pathways. Indeed, the observed selectivity cannot be explained solely in terms of the threshold energies required to break specific bonds in the temporary negative ion. On the contrary, it reflects the specific dynamics of the three-body interaction involving the molecule,

the transferred electron, and the donor atom. Considerable progress has been made in recent years towards understanding these complex dynamics both experimentally and via *ab initio* calculations [90]. Therefore, there is great potential in the future to identify many more charge transfer collisions that can initiate selective reactivity of the kind demonstrated here, extending to tailored chemical control for industrial and even medical applications.

Acknowledgements

TC, MM and FFS acknowledge the Portuguese National Funding Agency FCT-MCTES through SFRH/BD/52538/2014, PD/BD/106038/2015 and researcher position IF-FCT IF/00380/2014, respectively, and together with PLV the research grant UID/FIS/00068/2013. This work was also supported by Radiation Biology and Biophysics Doctoral Training Programme (RaBBiT, PD/00193/2010); UID/Multi/ 04378/2013 (UCIBIO). GG acknowledges partial financial support from the Spanish Ministerio de Economia, Industria y Competitividad (Project No. FIS2016-80440). SE acknowledges the support the British EPSRC through a Career Acceleration Fellowship (EP/J002577/1).

Chapter 5

Electron transfer studies of purine derivatives in potassium collisions

"The ultimate goal of all science is to cover the greatest number of empirical facts by logical deduction from the smallest number of hypotheses or axioms."

Albert Einstein

This chapter is dedicated to a comprehensive analysis of the TOF mass spectra recorded in 13.5-90 eV collision energy range in the lab frame (5.8-68 eV available energy. The fragmentation patterns of adenine and other purine derivatives in dissociative electron transfer experiments is here further investigated as we try to understand the underlying dissociation mechanisms through the analysis of branching ratios obtained in this energy range, and with the help of *ab initio* theoretical calculations.

Electron transfer driven decomposition of adenine and selected analogues as probed by experimental and theoretical methods[1]

T. Cunha[a], M. Mendes[a], F. Ferreira da Silva[a], S. Eden[b], G. García[c], M.-C. Bacchus-Montabonel[d,#] and P. Limão-Vieira[a,#] [2]

[a] Laboratório de Colisões Atómicas e Moleculares (LCAM), CEFITEC, Physics Department, Universidade Nova de Lisboa, 2829-516 Caparica, Portugal
[b] School of Physical Sciences, The Open University, Walton Hall, MK7 6AA, Milton Keynes, UK
[c] Instituto de Física Fundamental, Consejo Superior de Investigaciones Científicas (CSIC), Serrano 113-bis, 28006, Madrid, Spain
[d] Univ. Lyon, Université claude Bernard Lyon 1, CNRS, Institut Lumière Matière, 69622 Villeurbanne, France

Published: The Journal of Chemical Physics, (2018)

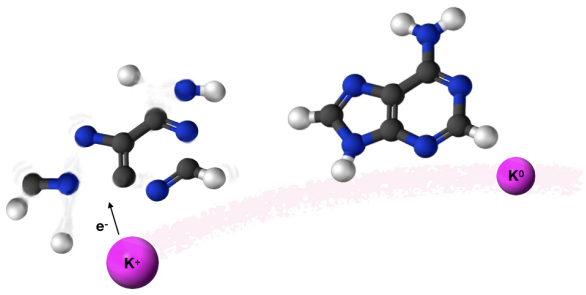

Abstract

We report on a combined experimental and theoretical study of electron-transfer-induced decomposition of adenine and a selection of analogue molecules in collisions with potassium (K°) atoms. Time-of-flight negative ion mass spectra have been obtained in a wide collision energy range (6-68 eV in the centre-of-mass frame), providing a comprehensive investigation of the fragmentation patterns of purine, adenine, 9-methyl adenine, 6-dimethyl adenine and 2-D adenine. Following our recent communication about selective hydrogen loss from the transient negative ions (TNIs) produced in these collisions [96], this work focuses on the production of smaller fragment anions. In the low-energy part of the present range, several dissociation channels that are accessible in free electron attachment experiments are absent from the present mass spectra, notably NH_2 loss from adenine and 9-methyl adenine. This can be understood in terms of a relatively long transit time of the K^+ cation in the vicinity of the temporary negative ion tending to enhance the likelihood of intramolecular electron transfer. In this case, the excess energy can redistributed through

[1] Published by AIP Publishing. https://doi.org/10.1063/1.5021888
[2] Authors to whom correspondence should be addressed: plimaovieira@ fct.unl.pt. Tel.: (+351) 212 947 859 and bacchus@univ-lyon1.fr, Tel.: (+33) 472 431 083.

the available degrees of freedom inhibiting fragmentation pathways. *Ab initio* theoretical calculations were performed for 9-methyl adenine (9-mAd) and adenine (Ad) in the presence of a potassium atom and provided a strong basis for the assignment of the lowest unoccupied molecular orbitals accessed in the collision process.

5.1 Introduction

It is now well-established within the international scientific community that low-energy electrons (e.g. <15 eV), as the most abundant secondary species produced by ionising radiation, play an important role in the modification of critical molecular structures in biological material. Such electron induced molecular decomposition processes have been demonstrated to yield substantial damage in plasmid DNA through single- and double-strand breaks. [4] Low-energy electrons can efficiently attach to DNA molecular constituents and derivatives to form transient negative ions (TNIs), which can subsequently dissociate and have been probed extensively in recent years using both experimental and theoretical methods. [85] Under aqueous conditions that approximate biological environments, TNI resonances can be shifted to lower energies [5]. Furthermore Wang and co-workers [9] found that significant quantities of single- and double-strand breaks of irradiated aqueous DNA are induced by pre-hydrated electrons. Wang et al.'s experiments on each deoxyribonucleotide (dXMP where X represents Thymine, Cytosine, Guanine or Adenine) have also shown that dGMP and dAMP are more efficient at capturing pre-hydrated electrons than dTMP and dCMP. Since most of the radiation damage in cellular DNA occurs through the generation of reactive species within the surrounding water, Wang et al.'s proposed mechanism of dissociative electron transfer may be responsible for a large portion of such damage. Given this rationale, electron transfer seems to be more prevalent under physiological conditions rather than simple electron attachment processes. Therefore, we argue that the present set of data on collisional electron-transfer induced dissociation of selected purine targets can advance our mechanistic understanding of radiation-induced in biological material on the molecular scale. By carrying out potassium-impact mass spectrometry experiments on partially labelled derivatives of adenine (Ad) and by means of quantum chemical calculations, we have explored the fragmentation patterns of negative ions formed in charge-transfer collisions.

Electron interactions with adenine ($C_5H_5N_5$) are well represented in the literature, including dissociative electron attachment (DEA) experiments, [97, 98] electron impact ionisation studies, [99] and charge-exchange collisions with laser-excited Rydberg atoms to probe dipole-bound anions. [100] Aflatooni et al.'s [86, 101] electron transmission data placed the three lowest electron affinities of π^* character at 0.54, 1.36 and 2.17 eV. More recently, site-selective bond excision of adenine yielding the dehydrogenated parent anion upon electron transfer in collision with neutral potassium atoms have been reported [96]. The influence of functional groups on site-specific dissociation of DNA bases by low-energy electron impact has been demonstrated via an effective loss of hydrogen located

at the specific nitrogen positions. [21, 22, 24] As far as theoretical investigations are concerned, we note elastic-scattering cross sections and resonance energies for low-energy electron impact on DNA/RNA bases [102], bound anionic states of adenine tautomers explored at the B3LYP/6-31+G** level of theory, [103] vertical and adiabatic ionisation energies of 12 adenine tautomers, [104] geometrical structures and energetic properties for different tautomers of adenine using multi-configurational wave functions, [105] and electronic spectra of purines [106] and purine tautomers. [92] Comprehensive studies on dissociative photo-ionisation of adenine following valence excitation [107] and reactivity in adenine–water clusters in multi-photon and electron impact ionisation studies, [108] have been also reported. Finally, hydrodynamic simulations have indicated that sequential HCN addition can be responsible for adenine formation during molecular cloud collapse. [109] Quantum chemical studies have recently shed light on the role of HCN and other prebiotic oligomers (e.g. HCCN, NH2CN and CN) to participate in gas-phase (and in the grain-phase) radical-radical and radical-molecule reactions on adenine formation within the interstellar medium. [110, 111]

5.2 Experimental method

The crossed molecular beam set-up used to study collisions of neutral potassium (K°) atoms with neutral purines, has been described in detail previously. [39, 112] Briefly, an effusive target molecular beam crosses a primary beam of fast neutral K° atoms and the product anions are analysed by time-of-flight (TOF) mass spectrometry. The K beam is produced in a resonant charge exchange chamber from the interaction of K^+ ions from a potassium ion source (12-100 eV in the lab frame) with gas-phase neutral potassium atoms from an oven source. Residual ions were removed from the primary beam by electrostatic deflecting plates outside the oven. The intensity of the neutral potassium beam was monitored using a Langmuir-Taylor ionisation detector before and after the collection of each TOF mass spectrum and the beam energy resolution in the collision energy range as measured as 0.5 eV (FWHM) using a hemispherical electrostatic energy loss analyser. Such energy resolution results from recording the K^+ ion beam signal at a fixed energy from collisions with nitromethane. The effusive beam of purines from an oven source was admitted into vacuum through a 1 mm diameter capillary where it was crossed with the neutral fast potassium beam. Negative ions formed in the collision region were extracted by a 250 V cm^{-1} pulsed electrostatic field. The typical base pressure in the collision chamber was 6×10^{-5} Pa and the working pressure was 4×10^{-4} Pa. Mass spectra (resolution $m/\Delta m \approx 125$) were obtained by subtracting background measurements (without the heated sample) from the sample measurements. Mass calibration was carried out on the basis of the well-known anionic species formed after potassium collisions with nitromethane. [13] Purine (Pu), adenine (Ad), 9-methyl adenine (9-mAd) and 6-dimethyl adenine (6-dimAd) were supplied by Sigma Aldrich with stated purities of 98%, ⩾ 99%, 97% and ⩾ 98%, respectively. Adenine-2-D (2-DAd) was supplied by CDN Isotope Inc.

with isotope enrichment of 97%. They were used as delivered. The samples were heated up to 400 K and the temperatures were controlled using a PID unit. In order to test for any thermal decomposition, the spectra were recorded at different temperatures. No differences were observed in relative peak intensities as a function of temperature. The extraction region and the TOF system were heated during the measurements in order to prevent any sample condensation and thus charge accumulation on the electrodes.

5.3 Theoretical method

The charge transfer in the collision of a neutral potassium atom K° and a nucleobase is described in the framework of the molecular representation looking at the evolution of the quasi-molecular system formed by the potassium projectile and the biomolecular target along the reaction coordinate. The one-dimension coordinate approximation is applied, as in previous ion/neutral-biomolecule collision systems. [95, 113, 114] The atom-nucleobase collision system is thus treated as a pseudo-diatomic molecule evolving along the coordinate associated with the distance between the impinging atom and the nucleobase. [115, 116] This approach does not consider the internal degrees of freedom of the biomolecule but may be used for very fast collision processes where nuclear vibration and rotation motions are much slower than the collision time and can be frozen during the collision. The geometry of adenine and 9-mAd has been optimized at the MP2 level of theory from the work of Fuentes-Cabrera et al. [117] A perpendicular approach of the potassium atom, pointing on the N9 atom (see figure 5.1) has been considered, as the charge transfer process has been clearly shown to be favoured in such orientation for the case of pyrimidine targets. [118, 119]

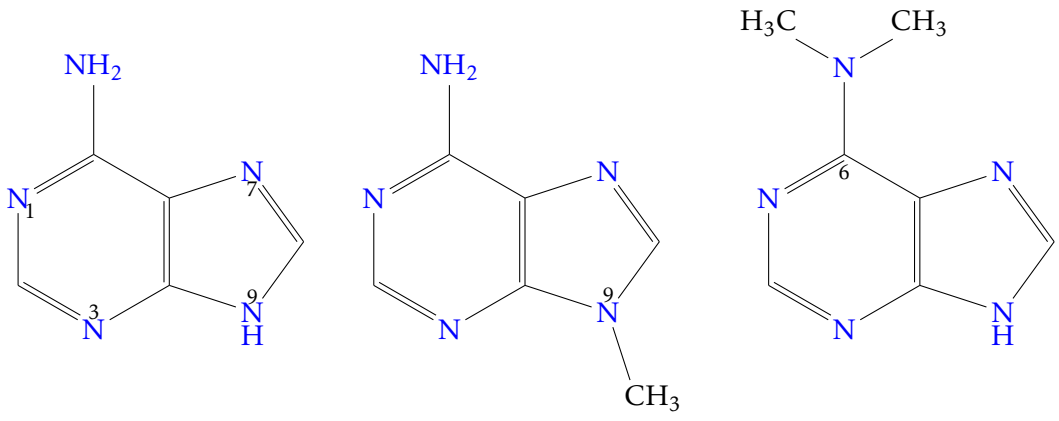

Figure 5.1: From left to right, molecular structure of adenine, 9-methyl adenine and 6-dimethyl adenine.

Ab-initio molecular calculations have been carried out with the MOLPRO code. [120] The nucleobase targets are kept frozen in their ground state geometry during the collision process. The calculation has been performed in Cartesian coordinates, with no symmetries. All electrons have been considered for C, N and H atoms with the 6-311G** basis

set, although the 18 core electrons of potassium have been treated through the ECP18sdf core-electron pseudopotential [121], with the corresponding basis set. The natural molecular orbitals for the K–Ad and K–9mAd have been determined by state-averaged CASSCF calculations for the reaction coordinate R = 10 Å corresponding to the asymptotic region. Similar active spaces have been considered for both targets in order to compare each system at the same level of accuracy. The 1s orbitals of carbon, nitrogen and oxygen are treated as frozen cores. The resultant highest occupied molecular orbitals (HOMOs) and lowest unoccupied molecular orbitals (LUMOs) for adenine and 9-methyl adenine are shown in figures 5.8 and 5.5, respectively, together with the corresponding orbitals without the presence of potassium. For adenine orbitals, the present results are in good agreement with a recent study using the CAP/SAC-CI method. [**ref39**] The polarization by the potassium atom induces a global shift in energy of about 2 eV for the π orbitals but the effect remains weak on the σ orbitals.

5.4 Results and discussion

Our recent short communication on electron transfer from neutral potassium atoms to Pu, Ad, 9-mAd, 6-dimAd, and 2-Dad showed that dehydrogenated parent anion formation can be achieved by selective breaking of C-H or C-N bonds, depending on the collision energy. [96] Based on the same experiments, the present work extends the analysis to the full fragmentation pattern of the TNIs. The two papers are complementary and the reader is recommended to read both for a full investigation of the collision dynamics. Dissociative electron transfer TOF mass spectra were recorded at lab-frame collision energies of 12-100 eV (3.8-68.3 eV in the centre-of-mass frame and from now on referred as available energy). Table 5.1 is a compilation of all fragment anions detected at 12, 15, 30, 50, 70, 100 eV lab frame collision energies. Figure 5.2 shows the negative ion TOF mass spectra recorded at 30 eV for Pu, Ad and 6-dimAd, figure 5.3 for Ad and Pu at 70 eV, and figure 5.6 for Pu, Ad, 2-DAd and 9-mAd at 100 eV lab frame collision energies with neutral potassium atoms. Branching ratios (BRs) for the major fragments of Ad and Pu as a function of the collision energy are presented in figure 5.7. The TOF mass spectra show no evidence of parent anion formation (M^-) and are, generally speaking dominated by the cyanide anion (CN^-). Absence of M^- formation seems plausible since in the case of adenine the vertical electron affinity is -0.54 eV. [86] The loss of different HCN units from the dehydrogenated parent anion of Pu and Ad, $(M\text{-}H)^-$, is schematically presented in Table 5.1. Another interesting aspect to discuss is the role of the potassium cation in the vicinity of the temporary negative ion (TNI) formed upon electron transfer, i.e. $K^\circ + M \longrightarrow (K^+ + M^-)$ and how the strong Coulomb interaction may affect the decomposition of the TNI. This is comprehensively investigated here and a mechanism is proposed with the help of quantum chemical calculations below. From the calculations, we also note that the lowest-lying π^* states are considerably shifted to higher energies (~2 eV) in the presence of a potassium cation (some of the calculated MOs without the presence of K^+ appear in

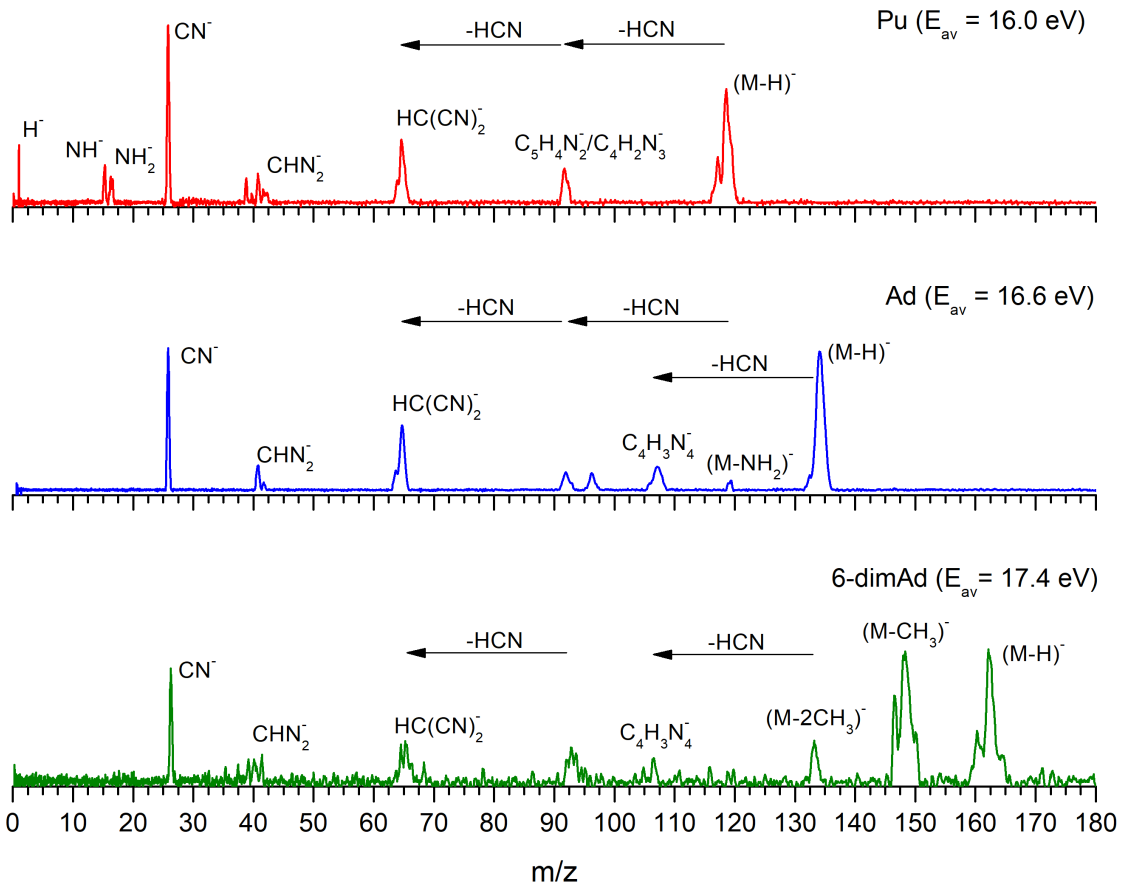

Figure 5.2: TOF negative ion mass spectra in potassium-purine (Pu), -adenine (Ad) and -6-dimethyl adenine (6-dimAd) collisions at 30 eV lab frame energy (16.0, 16.6 and 17.4 eV available energy in the centre-of-mass, respectively). See text for details.

the parentheses in figures 5.8 and 5.5.

Finally, accessing a π^* state does not lead to direct bond breaking unless a repulsive σ^* state does not lead to direct bond breaking unless a repulsive σ^* state is crossed diabatically. However, the available energy is enough to give access to intra-molecular electron transfer ($\pi \rightarrow \sigma$), which is possible if the nuclear wavepacket survives long enough along the reaction coordinate to allow diabatic coupling between the two states. This is discussed below within the scope of the different π^* and σ^* MOs involved in the formation of particular fragment anions.

5.4.1 $(M\text{-}H)^-$, $(M\text{-}2H)^-$, and $(M\text{-}3H)^-$ formation

The dehydrogenated closed shell anion $(M\text{-}H)^-$ is observed for all the molecular targets studied here and is formed via the ion-pair reaction:

$$K^\circ + M \longrightarrow K^+ + (M)^{\#-} \longrightarrow K^+ + (M-H)^- + H \quad (1)$$

Reaction (1) represents a direct cleavage of the (C-H) and/or (N-H) bonds (the specific H removal can be selected using the collision energy as reported in Ref. [96] and $(M)^{\#-}$ means a TNI formed with an excess of internal energy. Formation of the parent ion with H abstraction has been reported in DEA experiments of adenine through vibrational Feshbach resonances [24] and a weak "0 eV" contribution, the latter attributed to vibrationally excited molecules. [99] Adenine BRs as a function of the available energy (figure 5.7), show that $(Ad\text{-}H)^-$ is the most abundant fragment anion in the low energy collision region and its threshold of formation is below 4.0 eV (12 eV in the lab frame). This is in agreement with DEA resonances at 1.07 and 1.4 eV (1.36 eV [86]) attributed to N9-H excision and 2.2 eV (2.17 eV [86]) to C6N-H bond breaking. [24] Another interesting aspect of adenine BRs is that $(Ad\text{-}H)^-$ yield is generally speaking greater than 50% below 16 eV and strongly dominates at 6.1 eV. Above this energy, $(Ad\text{-}H)^-$ BR decreases while $(CN)^-$ BR increases, becoming dominant above 30 eV. This indicates that the dehydrogenated

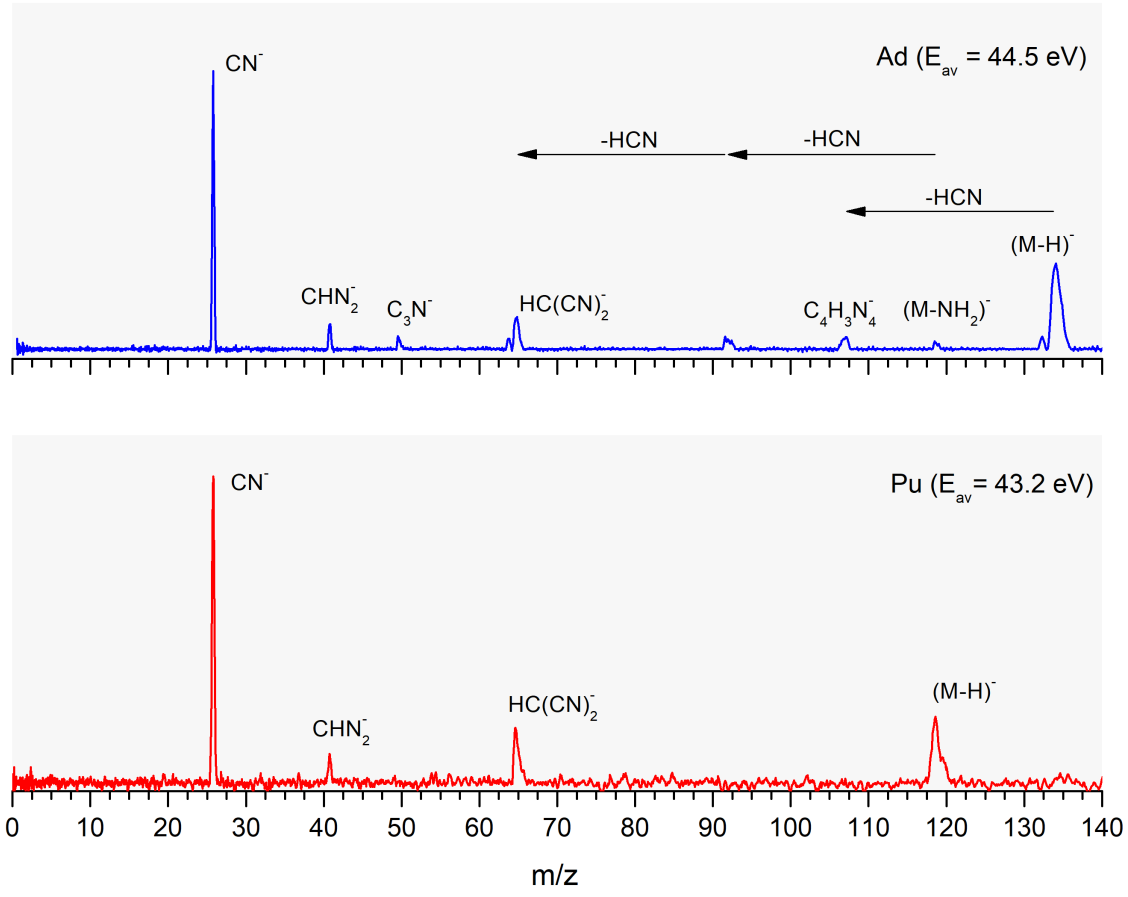

Figure 5.3: TOF negative ion mass spectra in potassium-adenine (Ad) and -purine (Pu) collisions at 70 eV lab frame energy (44.5 and 43.2 eV available energy in the centre-of-mass, respectively).

parent anion is a precursor in the formation of other fragment anions (except NH_2^- formation, see discussion below). Although $(Pu\text{-}H)^-$ (figure 5.7) is the dominant fragment

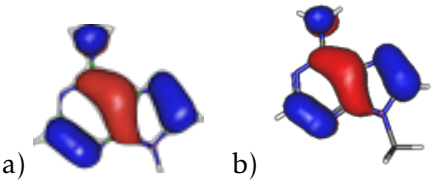

Figure 5.4: Calculated highest occupied molecular orbitals for: a) adenine and b) 9-methyl adenine.

anion from purine at K collision energies below 16 eV, it only accounts for (70 ± 7)% of the total anion yields at 5.8 eV and falls to just (35 ± 7)% at 3.8 eV available energy. At this low collision energy (12 eV in the lab frame), $(Pu\text{-}H)^-$ and NH^- are the prevalent yields, with the latter contributing to 20 % of the fragmentation pattern. By analogy with adenine where the threshold for H abstraction from N9 in DEA experiments is 0.94 eV, [24] we expect that any fragment anion has to be formed after H abstraction from purine TNI. We also observe strong competition with CN^- formation which is visible a lab frame collision energies above 30 eV for both adenine and purine.

From Table 5.1 we observe loss of more than one hydrogen atom for Pu, Ad, 9-mAd and 6-dimAd. In the case of 2-DAd we have detected only $(2\text{-}DAd\text{-}H)^-$ at 100 eV lab frame collision energy. Huber et al.'s [98] DEA experiments on adenine have reported the loss of two H atoms through reactions yielding $(M\text{-}2H)^-$ + H_2 and/or $(M\text{-}2H)^-$ + 2H formation. Loss of H_2 was attributed to the 0.7 eV resonance whereas H + H formation was accessible from the two high energy resonances at 7 and 10.6 eV, and loss of an H_2 + H (or three H atoms) was reported at 6.5 and 10.9 eV resonances. [98] As these fragment anions are discernible in the present mass spectra since above a lab frame collision energy of 30 eV (16.6 eV available energy), we conclude that these reactions are also accessible in potassium-adenine collisions. The lack of $(M\text{-}D)^-$ signal from 2-DAd was proposed in terms of strong auto-detachment competing with dissociation as well as to the lack of electron spin density in the C2 position. For more details see Ref. [96] Finally, the underlying molecular mechanisms yielding $(M\text{-}2H)^-$ and $(M\text{-}3H)^-$ formation are still not yet clear altought we suggest H_2 or 2H formation (depending on the specific states involved) and the loss of H_2 plus an H radical or H + H + H, respectively, as proposed by Huber and co-workers. [98] In the case of 2-DAd, however, $(M\text{-}HD)^-$ formation is absent which can be related to the lack of electrostatic potentials around C2 as well as to enhanced auto-detachment due to isotopic labelling. Further investigations are needed to clarify these processes, notably with isotopic labelling in other positions.

5.4.2 $(M\text{-}CH_3)^-$ and $(M\text{-}NH_2)^-$ formation

Formation of $(M\text{-}CH_3)^-$ and $(M\text{-}NH_2)^-$ from potassium collisions with 9-methyl adenine occurs at 67 eV in the centre-of-mass frame (see figure 5.6). The electron spin densities in figure 5.5 for 9-mAd suggest that the electron may be initially transferred to the π_2^*

and π_3^* states and subsequently to the σ_1^* state, resulting in dissociation. Alternatively, a direct initial transfer to the σ_1^* state and subsequent dissociation may occur. The present work does not provide evidence to assess the relative contributions of these two plausible pathways. It is interesting to note that similar dynamics have been discussed by Almeida and co-workers [122] in pyrimidine bases. In the case of 3-methyl uracil, the closeness of the vertical transition energies of π^* and σ^* states did not allow us to specify the dominant pathway to dissociation.

The loss of a CH_3 group is only visible from 9-mAd and 6-dimAd (respectively, yielding ions with m/z 134 and 148 – see figures 5.2 and 5.6), but there is no evidence for these channels at 15 eV lab frame. [96] This suppresion can be rationalised in terms of a slow collision process (~68 fs) enhancing Coulomb stabilization of the TNI by the proximate K^+ ion, increasing the probability of intra-molecular electron transfer that may favour dissociation (as is the case of NH_2^- formation, see section 5.4.6) or may favour auto-detachment (suppresing dissociation). As far as authors are aware, no DEA experiments have been produced these fragment anions.

Now we turn to the loss of an NH_2 group from adenine (Table 5.1) producing a negative ion with m/z 119 (see also figure 5.2). The DEA data of Huber et al. [98] reveals a dissociation channel at low electron energies, with a notably strong resonance feature at 0 eV indicating an exothermal character to the decomposition reaction. The TOF mass spectrum at 12 eV (not shown here) and 15 eV lab frame collision energy [96] show no traces of $(Ad\text{-}NH_2)^-$ formation. This can be explained under the same rationale of longer transit time of K^+ near the TNI promoting either auto-detachment or an alternative dissociation, which are reasonable arguments given the prominent decrease of $(Ad\text{-}H)^-$ BR at these energies as well as other fragment anions formation (see figure 5.7)).

5.4.3 Loss of HCN

Hydrogen cyanide abstraction is more evident in the TOF mass spectra of Pu, Ad and 9-mAd (figure 5.6) leading to ring opening, with assignment of the fragment anions indicated in Table 5.1, where arrows indicate the sequential HCN abstractions. The HOMOs of Ad and 9-mAd in figure 5.4 are localized on the rings showing relevant π character while the LUMOs appear with strong π^* anti-bonding with nodes along the C-N bonds (see figure 5.8 and 5.5). Such electron spin densities are indicative of favourable bond breaking in particular where curve crossing in the diabatically frame description may be relevant (i.e. $\pi_4{}^*/\sigma_2{}^*$). Though such cleavage, e.g. C2-N1, C4-N3 and C5-N7, C8-N9, may leave the remaining neutral HCN intact. Within the collision energy range studied for adenine and its derivatives, i.e. for the available energy (3.8-68.3 eV), such loss of HCN units is operative since the estimated threshold of the decomposition reaction requires 3.89 eV given that $\Delta_f H_g^\circ$ ($C_5H_5N_5$) = 225.7 kJ/mol (2.34 eV), [123] $\Delta_f H_g^\circ$ $(C_4H_3N_4)^-$ = 248 kJ/mol (2.57 eV), [124] $\Delta_f H_g^\circ$ (HCN) = 135.14 kJ/mol (1.4 eV) [124] and $\Delta_f H_g^\circ$ (H) = 218 kJ/mol (2.26 eV). [124] It is interesting that the loss of HCN from 9-mAd follows

methyl abstraction from the TNI, whereas in Pu and Ad it takes place after dehydrogenation of the parent anion. In the case of adenine, Huber et al. [98] reported that fragment anion 107 u, $(C_4H_3N_4)^-$, is formed through loss of HCN from the dehydrogenated parent anion since this reaction is energetically more favourable that CN radical and H_2 formation.

5.4.4 C_3N^- formation

The formation of fragment anion with m/z 50 from Ad, 9-mAd and 2-DAd (figure 5.6) is just visible at 100 eV lab frame collision energy and totally suppressed at 15 eV. [96] Harrison and Tennyson [125] have recently reported that C_3N^- supports a number of very weakly bound excited sates responsible to allow accommodation of the extra electron (resonances), with nuclear excited states lying in the continuum. The BR of C_3N^- in figure 5.7 shows the threshold of formation at $\sim$ 31 eV available energy and increases as a function of the collision energy. We also observe that above this energy the cyanide anion is relevant within the BRs. Although C_3N has higher electron affinity (4.54 eV [126]) than CN (3.862 eV [127]), the former anion results from combined fragmentation of both of rings with a considerable energy requirement. Owing to the molecular structure of Ad, C_3N^- can only result from the pyrimidine-like structure decomposition whereas CN^- formation may proceed from the breaking of the five member ring in particular in the lower energy regime (see discussion below). Interesting to note that we have observed previously in electron transfer experiments of potassium collisions with thymine formation of C_3N^-. [128] We suggest that in the case of adenine, this fragment anion may be

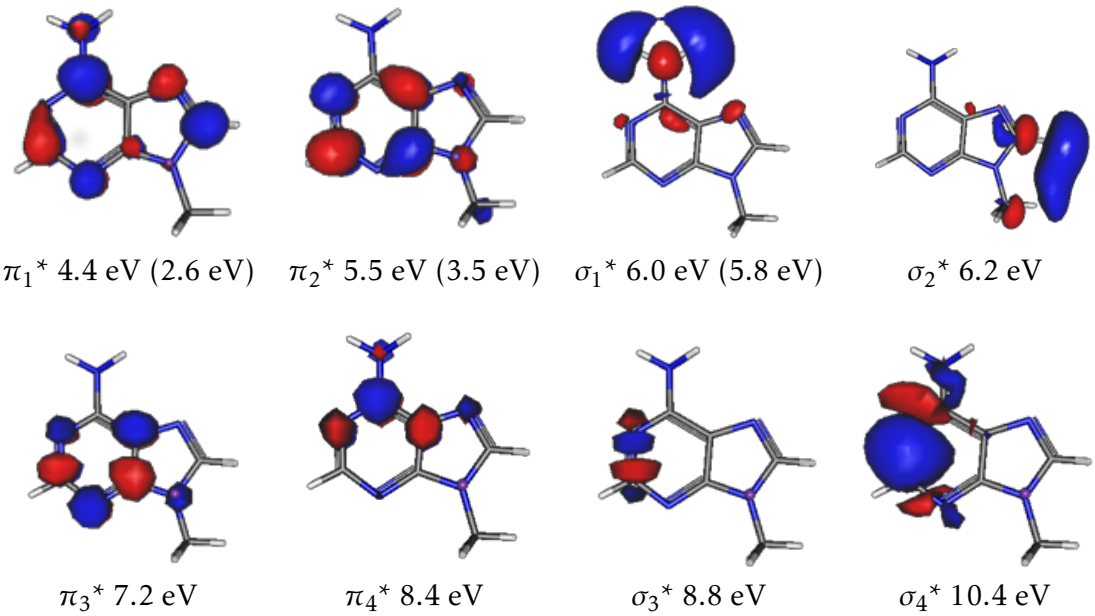

Figure 5.5: Calculated lowest unoccupied molecular orbitals (LUMOs) for 9mAd in the presence of a potassium cation in the perpendicular geometry poiting on the N9 atom. In parenthesis values calculates without the presence of potassium. Energies in eV.

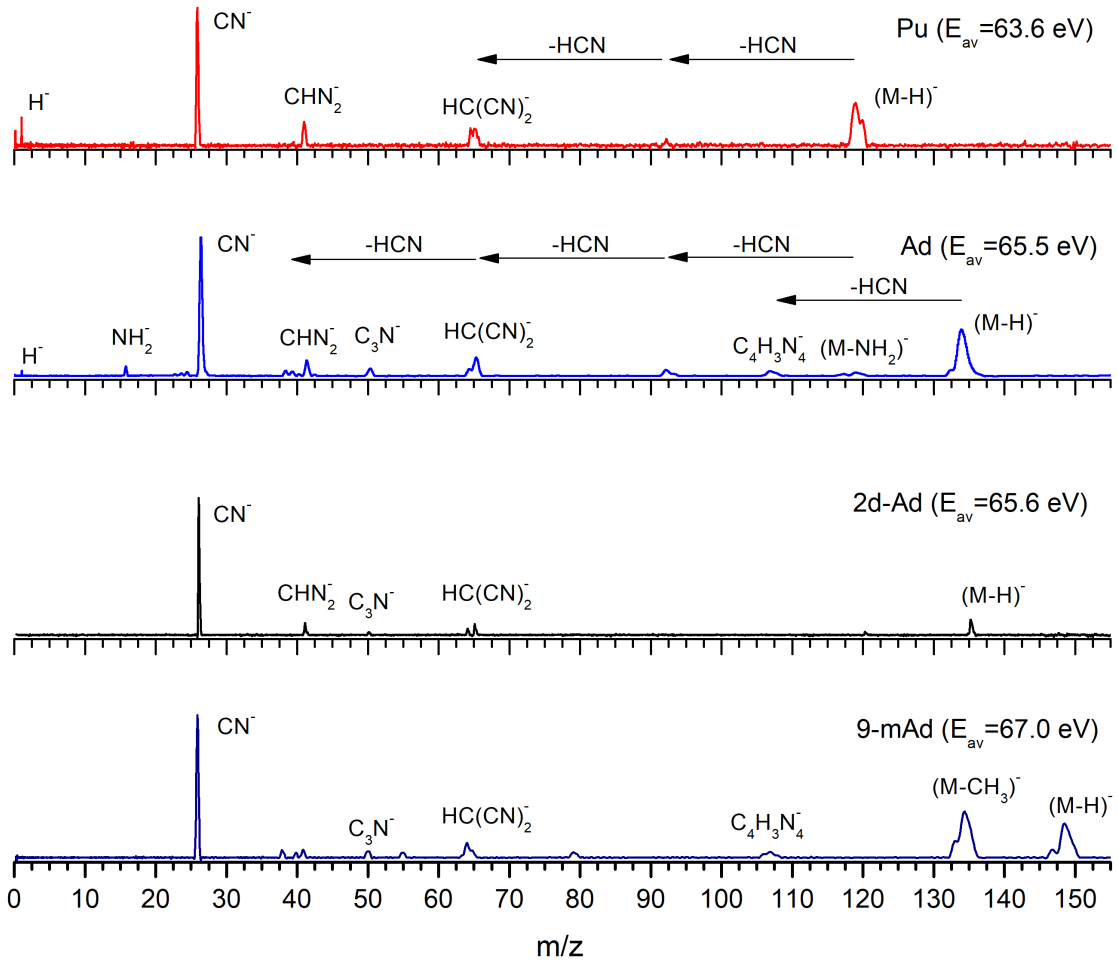

Figure 5.6: TOF negative ion mass spectra in potassium-purine (Pu), -adenine (Ad), -adenine-2-d (2-DAd), and -9-methyl adenine (9-mAd) collisions at 100 eV lab frame collision energy (63.6, 65.5, 65.6, and 67.0 eV available energy respectively).

formed via concerted mechanisms involving the six-member ring.

5.4.5 CN^- formation

The TOF mass spectra in figure 5.6 at 100 eV lab frame collision energy are dominated by the cyanide anion whereas at low collision energies, only $(M\text{-}H)^-$, H^-, NH^-, and NH_2^- are discernible. [96] Hence we can conclude that in the unimolecular decomposition process, the dehydrogenated parent anion is a precursor in the formation of fragments that require bond cleavages in the rings, namely CN^-. Such a decomposition process was previously observed for the pyrimidines investigated in collisional electron transfer experiments. [129] DEA experiments on adenine show that CN^- is the most intense anion at electron energies above 5 eV, with resonances at 5.8, 6.7 and 11.5 eV. [98] In order to aid our understanding of the underlying molecular mechanisms and the accessed states that are responsible for CN^- formation in adenine-potassium collisions, figure 5.8 shows three

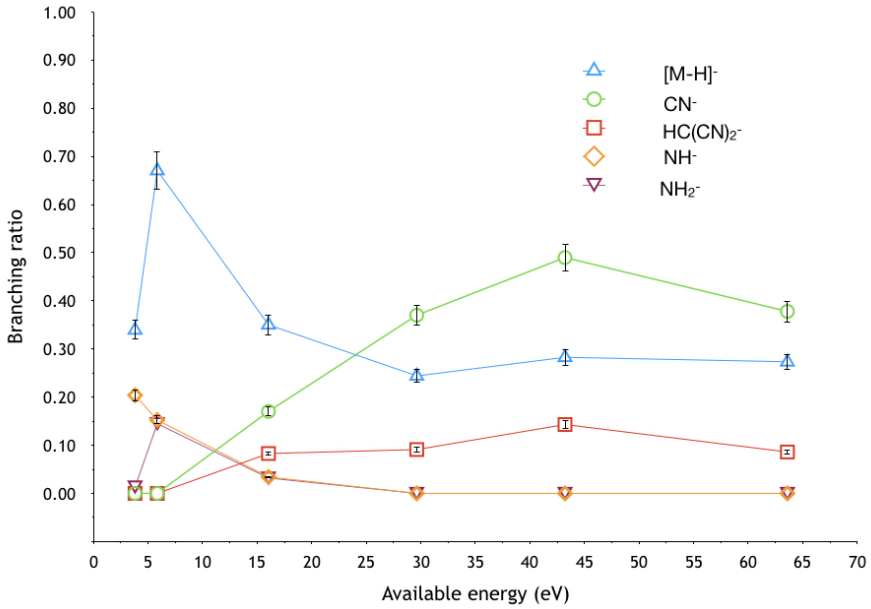

(a) Purine

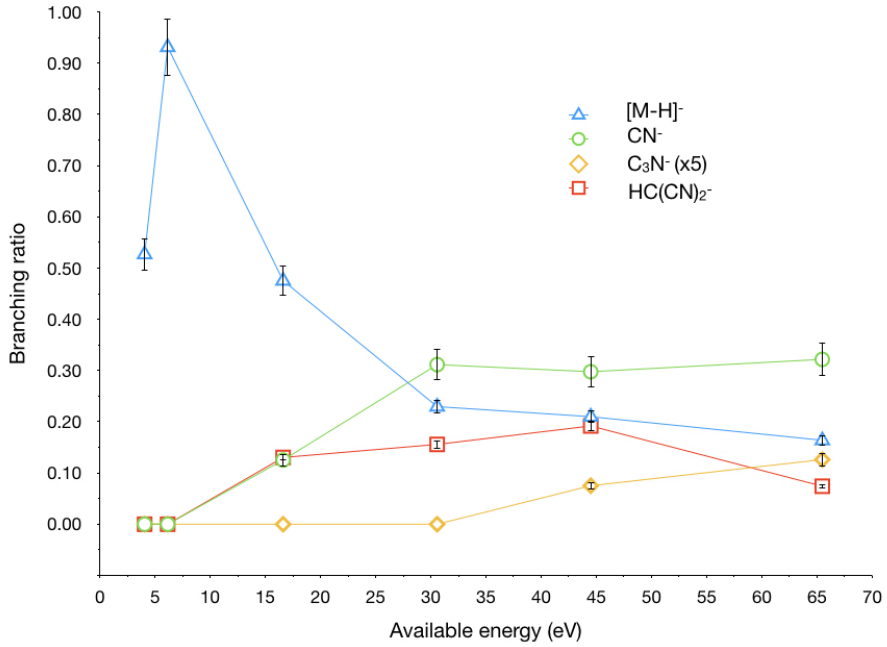

(b) Adenine

Figure 5.7: Branching ratios (fragment anion yield/total anion yield) as a function of the collision energy in the centre-of-mass frame for adenine and purine..

calculated π^* orbitals at 4.3 eV ($\pi_1{}^*$), 5.5 eV ($\pi_2{}^*$) and 7.0 eV ($\pi_3{}^*$). At higher energies two σ^* resonances at 8.8 ($\sigma_2{}^*$) and 10.3 eV ($\sigma_3{}^*$) are present, with $\sigma_3{}^*$ along the C2–N1 bond. Note that there is no appreciable difference as to the energy of 9-mAd LUMOs (figure figure 5.5). Accordingly, the adenine BRs in figure 5.7 show that CN^- cannot be produced $\leqslant$ 6.1 eV ($\leqslant$ 15 collision energy) which can be related to an electron promotion

to the π_2^*/π_3^* orbital. Accessing π_3* is achiedved by increasing the collision energy, and so CN^- yield, with bond-breaking certainly occuring through access of the σ* states. Now, a question that stands to be answered is where does CN^- formation proceed from? At threshold, it is initially formed from the fragmentation of the five-membered ring or is it the result of a combined contribution of breaking both rings? A careful inspection of figure 5.6 (100 eV lab frame collision energy) for Ad and 9-mAd shows a weak fragment anion at 107 u that has been assigned in table 5.1 to $(C_4H_3N_4)^-$ but is totally suppressed at 15 eV lab frame collision energy. [96] The BRs in figure 5.7 indicate that fragment anions (with the exception of NH_2^-) result from decomposition of the dehydrogenated parent anion, and this rationale also holds for 9-mAd. By analogy with Denifl et al.'s [24] DEA experiments, this signifies that H abstraction is already operative at ~1 eV. In the case of potassium-adenine collisions, the dehydrogenated parent anion may be formed with an excess of internal energy resulting in fragmentation yielding two complementary channels

$$(M-H)^{\#-} \longrightarrow CN^- + C_4H_3N_4 + H \ (2a)$$

$$(M-H)^{\#-} \longrightarrow CN + C_4H_3N_4^- + H \ (2b)$$

Such fragmentation pathways may proceed through two routes which involve breaking of N1-C6 and C6-C5 bonds (six member ring), and N7-C8 and N9-C4 bonds (five member ring). $(C_4H_3N_4)^-$ formation may procceed from both routes at high collision energies, typically 100 eV in the lab frame. Breaking N7-C8 and N9-C4 bonds is the most probable route at low collision energies, in agreement with the calculated π_2* and π_3* molecular

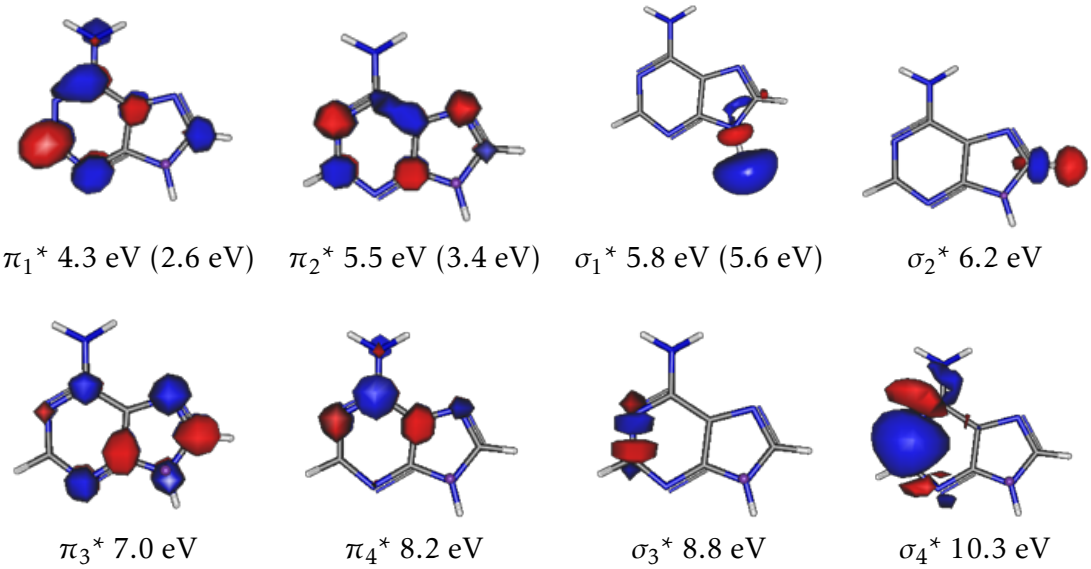

Figure 5.8: Calculated lowest unoccupied molecular orbitals (LUMOs) for Ad in the presence of a potassium cation in the perpendicular geometry poiting on the N9 atom. In parenthesis values calculates without the presence of potassium. Energies in eV.

Table 5.1: Negative ion formed in potassium collisions with purine (Pu), adenine (Ad), 9-methyl adenine (9-mAd), 6-dimethyl adenine (6-dimAd) and adenine-2-d (2-DAd).

m/z	Pu	Ad	2-DAd	9-mAd	6-dimAd
1	H^-	H^-	H^-		
15	NH^-				
16	NH^{-2}	NH^{-2}		NH^{-2}	
26	CN^-	CN^-	CN^-	CN^-	CN^-
38		C_2N^-		C_2N^-	
40				$CN_2^-/C_2H_2N^-$	
41	$CHN_2^-/C_2H_3N^-$	$CHN_2^-/C_2H_3N^-$	$CHN_2^-/C_2H_3N^-$	$CHN_2^-/C_2H_3N^-$	$CHN_2^-/C_2H_3N^-$
42	$CH_2N_2^-/C_2H_4N^-$	$CH_2N_2^-/C_2H_4N^-$			
50		C_3N^-	C_3N^-	C_3N^-	
55				$C_3H_5N^-$	
64	$C_3N_2^-$	$C_3N_2^-$	$C_3N_2^-$	$C_3N_2^-$	
65	$((CN)_2HC)^-$	$((CN)_2HC)^-$	$((CN)_2HC)^-$		$((CN)_2HC)^-$
79				$C_4H_3N_2^-$	
80				$C_4H_3N_2^-$	
92	$(Pu\text{-}H\text{-}HCN)^-$	$C_5H_4N_2^-$			$C_5H_4N_2^-$
96		$C_3H_4N_4^-$			
107		$C_4H_3N_4^-$		$C_4H_3N_4^-$	
108		$C_4H_4N_4^-$			
117		$(Ad\text{-}H(NH_3))^-$			
118	$(Pu\text{-}2H)^-$				
119	$(Pu\text{-}H)^-$	$(Ad\text{-}NH_2)^-$			
120			$(2\text{-}DAd\text{ -}NH_2)^-$		
132		$(Ad\text{-}3H)^-$			
133		$(Ad\text{-}2H)^-$		$(9\text{-}mAd\text{ -}HCH_3)^-$	$(6\text{-}dimAd\text{ -}(CH_3)_2)^-$
134		$(Ad\text{-}H)^-$		$(9\text{-}mAd\text{ - }CH_3)^-$	
135			$(2\text{-}DAd\text{-}H)^-$		
146					$(6\text{-}dimAd\text{ -}NH_3)^-$
147				$(9\text{-}mAd\text{-}2H)^-$	
148				$(9\text{-}mAd\text{-}H)^-$	$(6\text{-}dimAd\text{ -}CH_3)^-$
160					$(6\text{-}dimAd\text{ -}3H)^-$
162					$(6\text{-}dimAd\text{ -}H)^-$

orbitals, and most likely leading to the formation of CN^- in view of its high electron affinity (3.8620 ± 0.0050 eV). [124]

5.4.6 NH_2^- and NH^- formation

The TOF mass spectrum of Pu at 15 eV lab frame collision energy [96] shows a significant contribution of NH^- and NH_2^- relative to the $(Pu\text{-}H)^-$ yield. In the case of Ad at 12 eV (see its BR in figure 5.7) we observe that $NH_2^-/(Ad\text{-}H)^-$ appears at a ratio of 1:2. The NH_2^- threshold of formation from adenine in DEA was estimated at 3.1 eV given that $D(C\text{–}NH_2) = 3.9$ eV [130] and $EA(NH_2) = (0.771 \pm 0.005)$ eV. [131] The BRs in figure 5.7, show that NH_2^- is not formed by dissociation of the dehydrogenated parent anion. At 12 eV lab frame collision energy, the available energy amounts to 4.0 eV which is enough to yield the NH_2 anion. At 6.1 eV available energy (15 eV in the lab frame), the TNI is formed with an excess of internal energy which can be statistically distributed over the internal degrees of freedom, resulting in NH_2^- formation even with a modest electron affinity. Such assumption seems reasonable since the electrostatic potential maps of Ad

show a region of positive electron spin density around the $–NH_2$ group. [24] However, the high relative intensity of the NH_2^- signal in the present data at low collision energies can only be attributed to the presence of K^+ in the vicinity of the TNI allowing intramolecular electron transfer from the ring to $–NH_2$. In the case of Pu, NH^- and NH_2^- formation mechanism may substantially differ from Ad. The isodensity map of purine in Ref. [24], shows that the region strongly favourable for electron capture is around the N9–H and the neighbouring C8–H sites. As such, NH^- formation upon electron transfer to purine may proceed through the breaking of C4–N9 and C8–N9 bonds and electron capture at NH. Taking D(C–N) = 3.1 eV and EA(NH) = (0.370 ± 0.004) eV, [124] the estimated threshold is 5.83 eV. The available energy at a lab frame collision energy of 15 eV is slightly higher than this value and hence this formation mechanism is plausible in the present experiments. Finally, regarding NH_2^- formation from purine, we note from figure 5.7) that its yield is slightly lower than NH^- formation. The NH_2^- / NH^- ratio remains approximately constant when the collision energy is increased to 30 eV lab frame (16 eV available energy, figure 5.7)) indicating that the two fragments derive from a common excited precursor. The mechanism for amino radical anion formation must involve NH combining with a proton transferred from the C8 position. Identifying the specific mechanism is beyond the scope of this contribution and quantum chemical calculations would be very helpful clarifying the routes of NH_2^- formation.

5.4.7 H^- formation

The formation of H^- can be schematically represented by the reaction:

$$K^\circ + M \longrightarrow K^+ + (M)^{\#-} \longrightarrow K^+ + (M-H) + H^-(3)$$

The H^- yield is clearly visible in 30 eV lab frame collisions (figure 5.2) from Pu only. We do not have a strong basis to explain the absence (with the present signal/noise ratios) of this anion in the equivalent mass spectra of Ad and 6-dimAd. Huber et al [98] have reported H^- formation via two resonances at 6 and 11 eV, the former almost three times more intense than the latter. The resonance at 6 eV may be accessed in potassium collision at 15 eV lab frame (~6 eV available energy). We observe H^- formation from adenine in 100 eV lab frame collisions (figure 5.6), albeit with a very low yield. This may suggest that its absence in the present measurements at low collision energies is linked to strong competition with other fragment anion channels with energetically similar resonances.

5.5 Final remarks

The present work provides a comprehensive investigation of the decomposition mechanisms of purine, adenine, 9-methyl adenine, 6-dimethyl adenine and 2-D adenine in collisions with potassium atoms. The major fragment anion formation has been investigated as a function of the available energy in the centre-of-mass frame. In the case

of adenine, the dehydrogenated parent anion is shown to be a precursor in the formation of the smaller fragment anions, with the exception of NH_2^-. We report for the first time formation of $(M\text{-}CH_3)^-$ from 9-mAd and 6-dimAd. Additionally, C_3N^- formation is proposed to proceed through the six-membered ring structure decomposition, while the cyanide anion may proceed from the breaking of the five-membered ring particularly in low energy collisions. The theoretical calculations reveal how the electronic structures of Ad and 9-mAd are modified by the presence of the electron donor and hence provide insights into the electronic states that are most likely to participate in the major fragment anion channels. The clear differences in fragment anion production from adenine in the present electron transfer collisions compared with DEA provide further evidence that the specifics of the electron delivery mechanisms need to be properly taken into account in nanoscale models of radiation damage to DNA.

Acknowledgements

T.C., M.M. and F.F.d.S. acknowledge the Portuguese National Funding Agency FCT-MCTES through SFRH/BD/52538/2014, PD/BD/106038/2015 and researcher position IF-FCT IF/00380/2014, respectively, and together with P.L.V. the research grant UID/FIS/00068/ 2013. This work was also supported by Radiation Biology and Biophysics Doctoral Training Programme (RaBBiT, PD/00193/2010); UID/Multi/04378/2013 (UCIBIO). G.G. acknowledges partial financial support from the Spanish Ministerio de Economia, Industria y Competitividad (Project No. FIS2016-80440). S.E. acknowledges the support of the British EPSRC through a Career Acceleration Fellowship (EP/J002577/1) and a Research Grant (EP/L002191/1) Career Acceleration Fellowship (EP/J002577/1). M.-C.B.-M. acknowledges support from the computational resources from the CCIN2P3 in Villeurbanne and CCRT/CINES/IDRIS by GENCI (Grand Equipement National de Calcul Intensif) under the Allocation No. x2017087662.

Chapter 6

Alkali energy loss spectroscopy

"The opposite of a correct statement is incorrect assertion. However, the opposite of a profound truth may also be another profound truth."

N. Bohr

In order to further our knowledge of the underlying molecular mechanisms of biological relevant molecules, namely purines, an alkali energy loss set-up was implemented. The knowledge obtained from these measurements may allow to identify the prevalent electronic transitions in the transient negative ion formation. To validate the set-up we focused on the study of two molecules which have been thoroughly studied in both DEA and alkali collisions, namely, nitromethane and tetrachloromethane.

6.1 Overview

Energy loss spectroscopy (ELS) is commonly related with electron scattering experiments. Such technique consists in the study of the energy distribution of electrons which have interacted with atomic or molecular targets, hence providing key structural [132] and chemical information [133]. As so, such energy loss technique can be used in atom-molecule collision experiments. The energy loss from scattered ions can also be measured by using an energy analyser in which the transmitted signal is presented as a function of the energy loss, ΔE, for all scattered K^+ ions, within the solid angle accepted by the analyser. Briefly, in the set-up used in this thesis a hyperthermal K° atom is forced to collide with a molecular target M, and during the collision an ion-pair is formed (K^+ + M^-). The resultant K^+ ions are then focused into the analyser entrance slit through an Einzel lens arrangement. This type of lens has the particular ability to focus a charge particle beam without changing its energy. Only the K^+ ions matching the pass energy of the analyser will be transmitted within the analyser and reaching the detector. The pass energy will vary according to the contact potentials applied to the electrodes. By sweeping the pass energy we can then obtain energy loss spectra having as a reference the incident K° beam kinetic energy – this energy is experimentally determined *a priori*. Hence, the energy loss ΔE is defined as the difference between the incident K° atoms and the scattered K^+ ions, and relates with the transition energy, E, to an anionic state of the molecular target:

$$\Delta E = IE(K^\circ) + E \tag{6.1}$$

As already mentioned in previous chapters, the anionic states that can be accessed during collision, are dependent of the system's available energy E_{av}.

6.1.1 Energy loss scale calibration

During energy loss experiments we have observed shifts in the energy scale of ~1eV throughout the measurements. Thus, we opted to normalize the energy loss scale using the TNI formation threshold energy, i.e. the minimum energy, that is experimentally determined by TOF mass spectrometry, and is require to form a stable anion.

6.1.2 FWHM analysis

The FWHM profiles observed in an energy loss spectrum are of high interest, first because they are not dependent – or in other words, not influenced – by the energy scale calibration, and second they can show evidences of where bond pre-stretching is more prominent or barely visible.

6.2 Tetrachloromethane (CCl_4)

Tetrachloromethane, also known as carbon tetrachloride, CCl_4, is widely used as a cleaning agent, in polymerization chemical processes, as well as a feed gas in plasma processing. CCl_4 has been widely used in research investigations due to its high cross section for electron attachment at approximately 0 eV [134, 135] making it suitable for setting the electron energy scale in these experiments. Molecules with such an interesting property as high cross section values (~40 Å [136]) at 0 eV electron attachment can be used in devices in which it is necessary to quickly extinguish flames, plasmas or arcs. Therefore, this has motivated many studies on electron attachment to CCl_4. [56, 137–139] Experiments measuring rate constants at near thermal energies using flow afterglow Langmuir-Taylor probe technique were reported [140, 141]. Su et al. [142] used Photoemission Electron Attachment Ion Mobility Spectroscopy to measure the rate of electron attachment to CCl_4 in the energy range 0.29-0.96 eV. In dissociative electron attachment studies, Sheunemann and Matejcik observed the formation of Cl^-, Cl_2^-, CCl_2^-, CCl_3^- fragment ions [134, 143]. In Rydberg electron transfer experiments, the CCl_4^- anion has also been detected with a lifetime of 7.5-30 ps [56, 144, 145]. Dispert and Lacmann [146] reported CCl_4^- formation, in potassium collisions (as 0.1 % of the total anion yield), at an appearance potential of 2.3 eV. Several temperature dependence studies of dissociative electron attachment (DEA) to CCl_4 in the gas phase have been performed in crossed beam experiments [56, 137, 147] and they all demonstrated that DEA to CCl_4 is not enhanced by increasing temperature, indicating no activation energy for this process. Thermal decomposition was detected only above 470 K for this molecule [138]. Other electron attachment studies using Laser Photoelectron Attachment method [139] were performed with very high resolution (down to 1 meV), and cross-sections for Cl^- and Cl_2^- formation have been reported in the electron energy range from 0.1 meV to 1.85 eV. The vertical attachment energy (VAE), associated with occupation of the LUMO of CCl_4, is reported by Burrow et al. [148] to be slightly negative, i.e. the anion state lies below the neutral potential energy surface in the equilibrium geometry by 0.08-0.32 eV [149] and thus was not reported by ETS (electron transmission spectroscopy) experiments [101]. This anion state with σ^* character must cross through the lowest vibrational levels of the neutral state being largely repulsive along the C-Cl bond efficiently yielding Cl^- [148]. DEA studies performed by Oster et al. [135] revealed that below 0.6 eV electron energy only Cl^- ions are produced. Ion yields for Cl_2^- and CCl_3^- showed resonances at 1.7 eV (small intensity) and at 6.0 eV. This is in fair agreement with Hotop et al. [139] DEA results. Attachment into the next higher lying empty orbital, the triply degenerate $^2T_2$ orbital occurs at 0.94 eV [148] and gives rise to a peak in the DEA cross section at 0.80 eV [137]. Hence, Cl^- formation shows two features: the first, most intense at around 0 eV due to capture of s-wave electrons through a $^2A_1$ resonance and the second at 0.8 eV with leading p-wave component due to electron capture to a triply degenerate $^2T_2$ excited state of the negative

ion. In alkali collisions, Lacmann and Maneira [150] performed K^+ energy loss measurements in the forward direction and interestingly, observed a maximum at (5.25 ± 0.20) eV which gives an anionic state at 0.9 eV (taking into account the ionisation energy of potassium $5.25 - 4.34 \approx 0.9$ eV) which they assigned to a transition to a purely repulsive $^2A_1$ state. Furthermore, they determined the adiabatic electron affinity to be (2.0 ± 0.2) eV [124]. More recently, Li et al. [151] reported the direct observation of CCl_3 radical by DEA to CCl_4 and measured the appearance of all the other neutral species through Stepwise Electron Spectroscopy (SES) in the gas phase.

6.2.1 Results

From TOF mass spectra of anions formed in collisions of fast potassium atoms with CCl_4, five fragments have been assigned: Cl^-, Cl_2^-, CCl_2^- and CCl_3^- along with their expected isotopic ratios – Cl (35/37) being 100:32.4, Cl_2 (70/72/74) being 100:64.8:10.5,CCl_2 (82/84/86) being 100:64.8:10.5, and CCl_3 (117/119/121/123) being 100:97.2:31.5:3.4, as depicted in figure 6.1. The dominant fragment anion is Cl^- while the other fragments are considerably less intense as appeared also in DEA experiments [134, 152] and electron transfer experiments (see figure 6.1). From figure 6.1 we determine that Cl^- formation corresponds to more than 90 % of the total yield over a wide collision energy range (not shown here). Such behaviour dictates the fragmentation pattern, hence CCl_4 can be described as a quasi-diatomic molecule as far as fragmentation is concerned. No parent anion was observed for all collision energies probed, i.e. from 8 up to 900 eV.

Figure 6.2 shows the total relative cross section of CCl_4 in potassium collisions with two visible maxima. Tipically, the first maximum, at low collision energies is characterised by a sharp rise, achieving a maximum cross section followed by a sudden drop. Such behaviour is attributed to bond stretching and/or pre-stretching effects of a C-Cl bond resulting in dissociation enhancement. The second maximum, observed at ~ 300 eV ($t_{col} << t_{vib}$), is considered to be a Landau-Zener maximum. [153] In the latter region we can treat the molecular target as effectively "frozen" during the collision, i.e. non-rotating and non-vibrating, and the movement of the atom approaching the molecular target can be described classicaly. We can conlude that < 100 eV collision energy in the lab frame, bond stretching effects are influencing the negative ion yield resulting in a maximum around 30 eV lab frame (~21 eV c.m.). Indeed, similar behaviour observed in alkali collisions with Cl_2, Br_2, F_2, etc. [153] Pre-stretching and bond stretching, are explained in terms of the time spent by the electron donor (K^+) in the vicinity of the molecular target during the collision, which appears to be the major influence in this type of collisions. Furthermore, if we assume an effective impact parameter, $b_{eff} = 2R_c/\sqrt{2}$, and assuming R_{c2} does not change during collision ($R_{c1} = R_{c2} = R_c$), the collision time at maximum cross section for CCl_4 is approximately given by:

$$t_{col} = \frac{2R_c}{v\sqrt{2}} \tag{6.2}$$

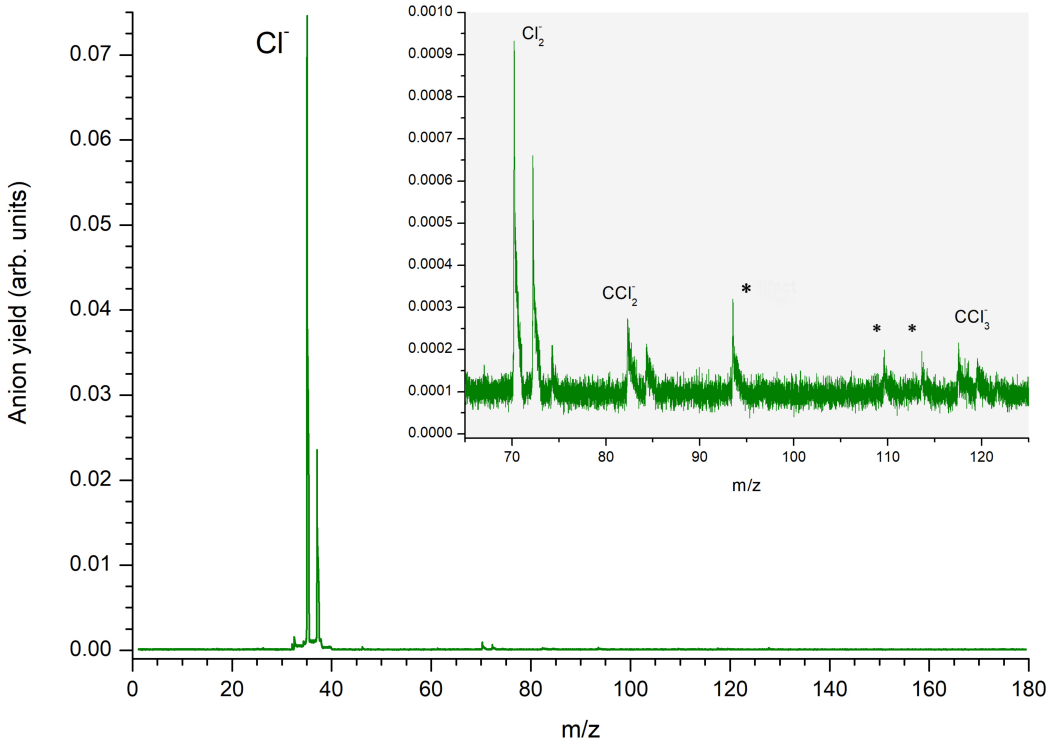

Figure 6.1: Typical TOF negative ion mass spectra of CCl_4 at 100 eV collision energy in the lab frame. *Artifact.

resulting in ~ 31.9 fs (at 30 eV lab frame). This collision time appears to be comparable to ~ 74 % of C-Cl bond vibration – stretching mode, 776 cm^{-1} (43 fs). Bond stretching effects are no longer relevant above 200 eV lab frame collision energy where a second maximum is observed, described by the Landau-Zener model. At high energy collisions the molecule can then be described as a single particle, and a maximum cross section is achieved when covalent scattering probability is equal to the ionic scattering (p_1=p_2=p=0.5). Above this energy, covalent scattering is expected to prevail. From the landau-Zener maximum cross section v_{max} can be determined and the coupling factor between both covalent and ionic state ($K^\circ + M \longleftrightarrow K^+ + M^-$)obtained. Such allows to determine the non-adiabatic transition probability between those states. The velocity v_{max} relates with H_{12} by the following semi-empirical expression [153]:

$$H_{12} = 0.58\left(\frac{v_{max}}{R_c^2}\right)^{1/2} \quad (eV) \tag{6.3}$$

with H_{12} equals to 0.28 eV. Being the non-adiabatic transition probability proportional to the product $H_{12}R_c$ (P $\propto$ $-H_{12}R_c$), it may be indicative of a small non-adiabatic transition probability, hence the crossing is adiabatic at low (and may be even at intermediate) velocities . R_c was calculated using equation 2.16, where the vertical electron affinity used was determined by energy loss spectroscopy (EA_v ~0.8 eV).

In the differential cross section experiments, the energy loss of the K^+ ions formed

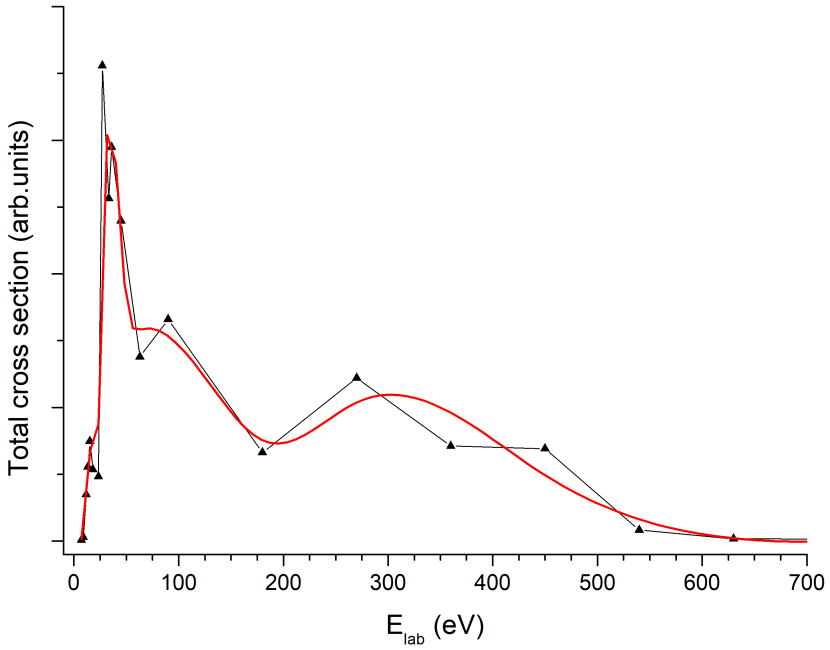

Figure 6.2: Total anion yield for CCl_4 from potassium collisions over a wide energy range (7-700 eV lab frame). Red curve is a moving average interpolation.

after electron transfer in the forward direction ($\theta \approx 0$) was measured at ~79 eV c.m. collision energy (100 eV in the lab frame). It is worth mentioning that these measurements were not performed in coincidence with TOF mass spectrometry. The energy loss scale was calibrated in *situ* from the the minimum energy required to form a TNI [150]. Typical K^+ energy loss spectrum obtained at 79 eV c.m. collision energy is presented in figure 6.3 and we immediately observed an intense peak lying around $\Delta E \approx (5.1 \pm 0.2)$ eV which is in fair agreement with the results reported by Lacmann and Maneira [150] (5.25 ± 0.20) eV. A careful inspection of the energy loss peak shows an asymmetric shape which may indicate the presence of an adjacent contribution that can be decomposed by Gaussian fitting. In potassium-molecule collisions yielding ion-pair formation, the energy loss required to access a particular electronic state, ΔE is given by the difference between the ionisation energy of K° and the vertical electron affinity of the molecular target for the corresponding state [43]:

$$\Delta E = IE(K) - EA_{Imax} \tag{6.4}$$

Hence, from the energy loss spectrum a vertical electron affinity of (-0.8± 0.2) eV is obtained. The crossing distance R_c can then be calculated using equation 2.16 and, which for the purposes of our discussion we shall assume in a first approach, to be constant, since Lacmann and Maneira did not observe any shift of the energy loss peak above 30 eV c.m. collision energy. [150] The calculation indicates a crossing radius $R_c \approx 2.8$Å$(\sim 5a_0)$ meaning that electron transfer occurs at very large distances with an estimation of the cross section given by $\pi R_c^2 \approx 25$Å^2. Using the multi peak fit approach, three new peaks

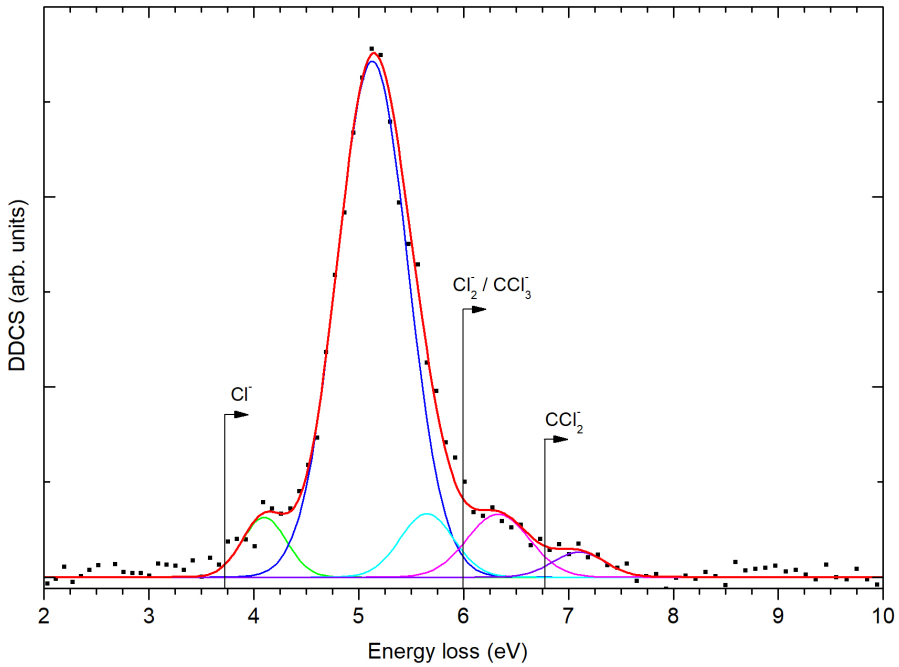

Figure 6.3: Energy loss spectrum of K^+ ions formed in the forward direction of K atoms in collisions with CCl_4 at 79 eV in the centre-of-mass frame. Arrows indicate the threshold of formation of the different anionic species.

are unveiled. We clearly notice features at 4.1, 6.2 and 7.0 eV not reported before, which are now discernible due to a higher and (most of all) constant resolution of the present set-up. By comparing with DEA results and appearance potentials obtained by Lacmann et al. [146] in alkali collisions, peaks at 4.1, 6.2 and 7.0 eV can be assigned to anionic states leading to Cl^-, Cl_2^-/CCl_3^- and CCl_2^- formation, respectively (see table 6.1).

6.2.1.1 Cl^- and CCl_3^- formation

In collision of neutral potassium atoms with neutral CCl_4 molecules, an electron is transferred from the alkali to the target yielding ion-pair formation. Moreover, if the temporary negative ion is formed with an excess of internal energy and competes with auto-detachment, it may decompose resulting in a neutral radical and a negative ion:

$$K^\circ + CCl_4 \rightarrow K^+ + CCl_4^{\#-} \rightarrow K^+ + CCl_3 + Cl^-$$

In the present potassium collisions experiments, Cl^- is observed as the most intense anion, hence it is reasonable to assume that the most intense peak in the energy loss measurements corresponds to a transition that mainly yields this fragment. From the spectrum analysis, we extract an energy value of (5.1 ± 0.2) eV. Taking out the energy required for potassium ionisation we obtain a negative electron affinity ~(-0.8 ± 0.2) eV. Previously, Lacmann et al [150] assigned this transition to a purely repulsive $^2A_1$ state. However, it should be noted the presence of a triply degenerate $^2T_2$ state characterised

Table 6.1: Peaks observed in K^+ energy loss spectroscopy and in DEA experiments. *

ΔE	Electronic state energies	DEA resonances [152]	Observed fragments in DEA [152]
4.10	~0	0.0±0.05	Cl^-
5.13	0.8±0.2	0.75±0.05	Cl^-
5.65	1.3±0.2	1.1/1.3±0.1	Cl_2^-, CCl_3^-
6.33	2.0±0.2	1.7±0.1	CCl_2^-
7.10	2.8±0.2	-	-
-	-	6.00	CCl_2^-

*All energies in electron-volt units.

by leading p-wave components, at this energy. [137] Such electron affinity EA_v correlates also with the resonance observed by Scheunemann et al [143] at an electron energy of (0.75 ± 0.05) eV. Furthermore, we observe a peak at a lower energy, ~4.1 eV (4.1 – 4.34 = −0.24 ± 0.2 ≈ 0 eV). Since CCl_4^- was not detected in the present measurements, such feature at ~ 0 eV must be attributed, as in DEA, to Cl^- formation through direct transition to a highly repulsive $^2A_1$ state (i.e. this σ^* state crosses the ground state of the neutral molecule). However, as depicted in figure 6.4, for that to be possible, pre-stretch of the bond C-Cl must occur. It is also worth noting the relative intensities of both resonant features yielding Cl^-. In contrast to the present energy loss spectrum, DEA shows a resonance at (0.75 ± 0.05) eV with much lesser intensity than that at ~ 0 eV. This may be explained in terms of bond stretching that enhances the transition to this anionic state yielding CCl_3^- while strongly competing with auto-detachment. Since Lacmann et al. [146] determined the threshold for CCl_3^- at ~ 6 eV, auto-detachment will be the main contribution to the observed K^+ ion yield. CCl_3^- is formed through the dissociation channel expressed below competing with Cl^- formation.

$$K^+ + CCl_4^{\#-} \rightarrow K^+ + Cl + CCl_3^-$$

CCl_3^- yield may then contribute to the appearence of a tail in the right side of the main energy loss feature reported by Lacmann and Maneira [150]. These authors assigned only up to 9 % of this fragmentation pathway to result in CCl_3^- formation. However, our present mass spectra presents a much lower yield. In fact, Cl_2^- is the second most intense fragment anion. This supports the discussion of strong competition with auto-detachment for the dissociation channel yielding CCl_3^-. From this fitting method, our threshold value is estimated to be at ~(5.0 ± 0.2) eV (4.34 + 0.6 = 4.94 eV), which seems consistent with the energy thresholds observed by Scheunemann et al, ~0.6 eV [143]. Now we can estimate the CCl_3-Cl bond dissociation energy:

$$\begin{aligned} D(CCl_3 - Cl) &= AE(CCl_3^-) + IE(K^\circ) - EA(CCl_3) \\ &= 5.0 - 4.34 + 2.16 \\ &= (2.8 \pm 0.2) \end{aligned} \tag{6.5}$$

This value agrees well with Hotop and co-workers dissociation energy D(CCl_3-Cl) of 3.07 eV [154].

From the collisional data, the potential energy curves can be estimated taking the assymetric stretch vibration to be the most important mode [150], with the dissociation

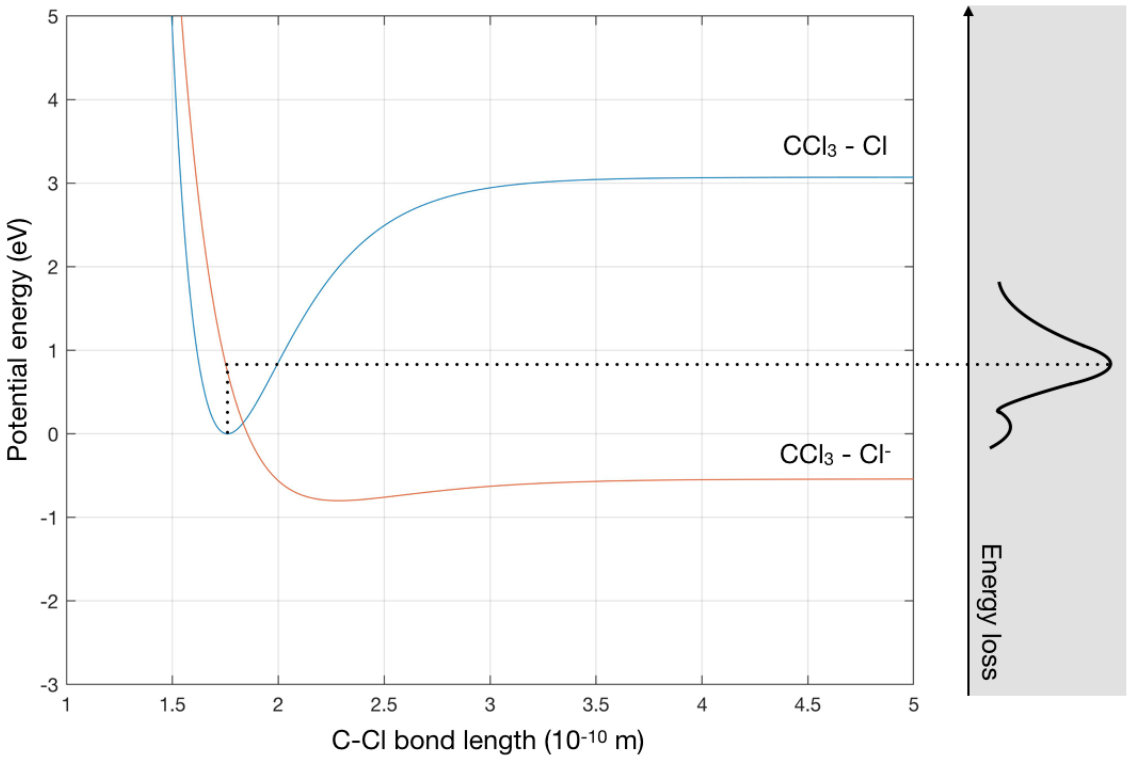

Figure 6.4: Potential energy curves obtained along CCl_3-Cl bond with neutral sate $^1A_1$ (in blue) and $^2A_1$ state (in red) that leads into dissociation yielding Cl^-.

Table 6.2: Parameters used in drawing the potential curves for CCl_4.

State	ν_e(cm^{-1}	R_e(Å)	D_e(eV)
$^1A_1$	778 [150]	1.76 [156]	3.07 [154]
$^2A_1$	170*	2.3*	0.26**

*Fitted parameters. ** Calculated dissociation energy from EA(CCl_4) [157] and EA(Cl) [124].

yield mainly due to the anionic fragments Cl^- and CCl_3^-. The parameters used to compute these potential energy curves, are listed in table 6.2. Using a Morse function [155]:

$$V(R) = D_e\left[1 - e^{-\beta(R-R_{eq})}\right]^2 \tag{6.6}$$

where,

$$\beta = 2\pi\nu_e\sqrt{\frac{\mu}{2D_e}} \tag{6.7}$$

with ν_e the frequency of classical small vibrations, R_{eq} the inter-atomic equilibrium distance, D_e the dissociation energy and μ the reduced mass. Equation 6.8 can now be written as:

$$V(R) = 1.356\times10^{-3}\nu_e\sqrt{\frac{\mu}{D_e}} \tag{6.8}$$

where ν_e is in cm^{-1}, D_e is in eV and μ is in u units.

6.2.1.2 Cl_2^- formation

Formation of Cl_2^- most probably proceeds through the following reaction:

$$K^\circ + CCl_4 \rightarrow K^+ + CCl_4^{\#-} \rightarrow K^+ + CCl_2 + Cl_2^-$$

This anion is the second most intense fragment in the TOF mass spectra contributing to 3-4 % of the total anion yield. Lacmann et al. [146] obtained the energy threshold around 6 eV while Scheunmann [143] reported Cl_2^- formation even at 0.6 eV in DEA reactions (thus in potassium collisions we estimate a threshold around $0.60 + 4.34 \approx 5$ eV). Taking $EA(Cl_2) = 2.9 \pm 0.3$ eV [152], $D(CCl_3 - Cl) = 3.07$ eV and a typical bond dissociation energy $D(C - Cl) = (3.3 \pm 0.3)$ eV [152] for the second C-Cl bond break, the enthalpy formation is given as:

$$\begin{aligned} \Delta_f H_g^\circ(Cl_2^-) &= D(CCl_3 - Cl) + D(C - Cl) - D(Cl - Cl) - EA(Cl_2) \\ &= 3.07 + 3.3 - 2.48 - 2.9 \\ &\approx 1 \end{aligned} \tag{6.9}$$

assuming the fragmentation mechanism below:

$$CCl_4^{\#-} \rightarrow Cl_2^- + CCl_2$$

Thus, it yields a minimum energy of ~ 1 eV [143] (which corresponds roughly to 5.3 eV from the alkali collisions) to form Cl_2^-. From the energy loss data analysis, a threshold of (5.5 ± 0.2) eV is obtained.

6.2.1.3 CCl_2^- formation

For the formation of CCl_2^-, two mechanisms can be proposed:

$$K^\circ + CCl_4 \rightarrow K^+ + CCl_4^{\#-} \rightarrow K^+ + Cl_2 + CCl_2^- \ (pathway 1)$$

$$K^\circ + CCl_4 \rightarrow K^+ + CCl_4^{\#-} \rightarrow K^+ + 2Cl + CCl_2^- \ (pathway 2)$$

This fragment anion is only responsible for 1-2 % of the total anion yield. It has the lowest electron affinity (1.590 ± 0.006) eV [124] In our present measurements, the appearance energy was estimated to be $\sim(6.5 \pm 0.2)$ eV, peaking at 7.1 eV. In alkali collisions performed by Lacmann et al. [150], the threshold was reported at 6.8 eV. The minimum energy required to form such fragment is calculated below considering two distinct dissociation pathways 1 and 2:

$$\begin{aligned} &\textit{Pathway 1} \\ \Delta_f H_g^\circ(CCl_2^-) &= D(CCl_3 - Cl) + D(C - Cl) - D(Cl - Cl) - EA(CCl_2) + IE(K) \\ &= 3.07 + 3.3 - 2.48 - 1.59 + 4.34 \approx (6.6 \pm 0.3)\ eV\ (2.3eV) \\ &\textit{Pathway 2} \\ \Delta_f H_g^\circ(CCl_2^-) &= D(CCl_3 - Cl) + D(C - Cl) - EA(CCl_2) + IE(K) \\ &\approx (9.0 \pm 0.3)\ eV\ (4.8eV) \end{aligned} \tag{6.10}$$

In the present measurements, no evidence of CCl_2^- formation is observed at ∼9 eV (from the energy loss spectra no K^+ ion yield is observed in that energy region), which indicates that in alkali collisions, CCl_2^- formation most likely follows through dissociation pathway 1. Pathway 1 is more favourable than pathway 2 from an energetic point-of-view. The present energy loss data suggests that the peak at ∼7 eV yields CCl_2^- along with Cl_2 molecules. Pathway 2 seems rather unlikely to occur since no discernible energy loss feature is observed at ∼9-10 eV. It is interesting to note that the available energy in the centre-of-mass frame is much greater than the required for that process to occur (E_{av} = 75 eV), meaning the electronic structure may play a role in such pathway.

6.3 Nitromethane (CH_3NO_2)

Nitromethane has been thoroughly studied in the gas-phase by free electron attachment [158, 159], alkali atom collisions [13, 51, 54], and Rydberg electron transfer experiments [55, 160, 161]. It is considered as a relevant atmospheric compound, is a popular solvent in organic and electro-analytical chemistry and is also widely used for explosives and as a propellent. The high dipole moment, 3.46D [55], makes it possible to accommodate dipole bound anion states (DBS) which have been shown to be a doorway into valence states that lead to molecular dissociation [27, 55]. Electron transmission spectroscopy results [162] and electron attachment experiments [158, 159] both report a negative vertical Franck-Condon transition from the neutral ground $^1A_1$ to a $^2B_1(\pi^*)$ state at low energy, which then decays mostly into dissociation due to an avoided crossing with a dissociative $^2A_1(\sigma^*)$ state yielding NO_2^- [163]. In free electron experiments, the major product of dissociation is by far NO_2^- although O^-, OH^-, CN^-, CNO^- and CH^- are also observed. [13, 158, 159] In DEA reactions, the resonance assigned to NO_2^- formation was reported at 0.6 eV by Sailer et al. [158] using a high energy resolution (140 meV) electron beam from 0-10eV impact energy. Alizadeh et al. [159] reported the same feature at ∼0.5 eV. In this experiment however, a high mass-resolution sector field instrument with an energy resolution ∼1 eV was used,for electron impact energies from 0 up to 16 eV. These experimental results are in agreement with theoretical calculations that determined a negative electron affinty of ∼ 0.7 eV. [51, 164] It is worth noting that in dissociative electron attachment studies, no parent anion was observed which is in sharp contrast with alkali collisions and Rydberg electron transfer studies where it appears as one of the most dominant fragments. [52, 54] Dispert et al. [52] determined by potassium collisions with nitromethane, an adiabatic electron affinity of (0.35 ± 0.20) eV. In K^+ energy loss measurements [165], from 20 to 300 eV collision energy, these authors showed evidence of a dominantly dissociative $^2A_1(\sigma^*)$ state, and two π^* states with $^2B_1$ character. Concerning the energy loss spectrum, only two peaks were observed in the forward direction, at 6.5 eV which is the most intense, and the other at 8.5 eV [165]. The lowest energy loss feature is related to a negative vertical electron affinity of (−2.16±0.20 eV) [165] that was assigned to the $^2A_1$ state that can decay through auto-detachment as well as dissociation yielding

NO_2^- contributing to 65-80 % of the total anion formation [13]. Indeed, Walker et al. [51] have observed in DEA experiments, that direct transition from the neutral state to this anionic state decays solely through auto-detachment to the vibrationally excited ground state of the neutral molecule. These authors also reported five other anionic states at 0.7, 4.0, 5.6, 6.1, and ~8 eV. They all lead to dissociation in contrast to the $^2A_1$ state at 2.4 eV reported by Walker et al. [51] . Such formation mechanisms shall now be discussed on the light of novel spectroscopic results obtained using a high resolution hemispherical analyser in energy loss experiments.

6.3.1 Results

Figure 6.5 shows a typical energy loss spectrum of K^+ ions from collisions of potassium atoms with nitromethane with our recently implemented hemispherical analyser. The

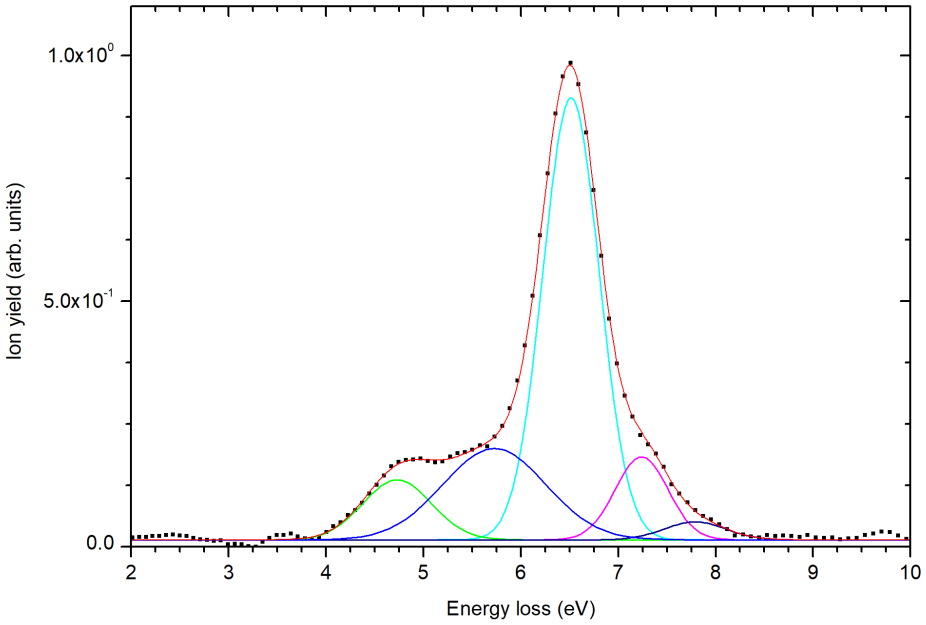

Figure 6.5: Energy loss spectrum of K^+ ions formed in the forward direction of K atoms in collisions with nitromethane at 84 eV collision energy in the centre-of-mass frame. Arrows indicate the threshold of formation of the different anionic species.

energy loss scale is expressed in terms of the centre-of-mass frame where the intensities correspond to a relative double differential cross section. A value of 3.99 eV obtained by Compton et al. [52] in threshold measurements was used to set the minimum energy to form the parent anion, $CH_3NO_2^-$. From the different energy loss spectra (see figure 6.6), we observe that the most intense peak shifts to higher energy losses as the collision energy increases. A tail extending up to 9 eV, is also observed, at higher collision energies. The shift to higher energies can be explained either in terms of higher momentum transfer favouring dissociative ionisation against non-dissociative ionisation (i.e. above 100 eV

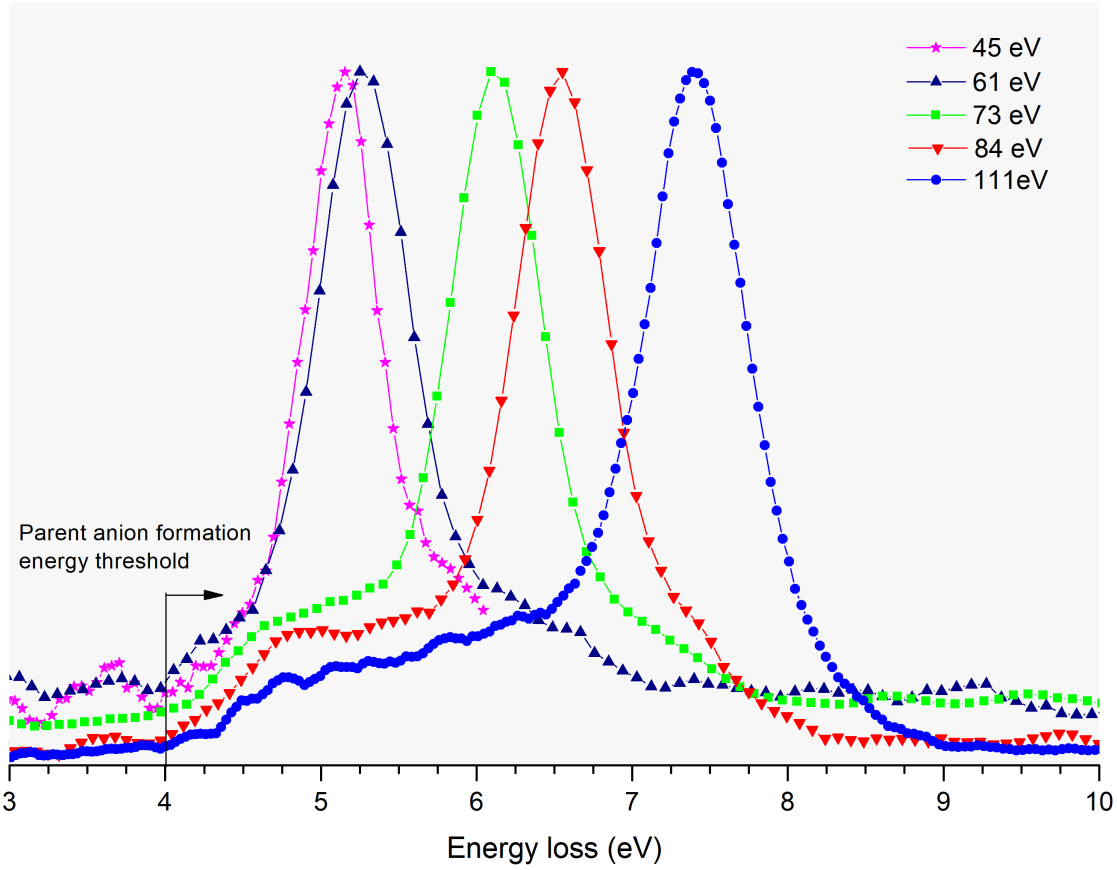

Figure 6.6: Energy loss spectra obtained at different collision energies in potassium-nitromethane collisions.

collision energy, positive ion formation is more likely to occur while below 100 eV, ion-pair formation is the dominant mechanism [166]), or in terms of the anionic states that are predominantly being accessed for each collision energy. In the energy range below 61 eV collision energy in the centre-of-mass frame, a single intense peak at 5.1 eV is observed. Such peak is related to a crossing radius, $R_c = 14.4/\Delta E = 2.8$Å ($5a_0$, with $a_0 = 0.529$Å). At low energies ionic scattering is dominant, i.e. due to strong dependence of the coupling factor H_{12} with R_c, the system follows adiabatically at the first crossing and maintains ionised at the second crossing, thus proceeding along the ionic path. [64]. We can also conclude from the high R_c value, that the crossing point occurs at large internuclear distances. Therefore, the interaction potential between the TNI and hyperthermal K^+ ion can be considered as entirely Coulombic. The peaks at maximum intensity, observed in Figure 6.6, are due to energy losses of 5.1, 6.1, 6.5 and 7.4 eV. After taking the ionisation energy of the potassium atom, the energy required to accommodate the electron in one of the free virtual orbitals is shown in (Table 6.3). The expected anionic states, from ETS measurements [162] are at 0.75, 2.4, 4.0, 5.6, 6.1, and 8.6 eV, where at 2.4 eV , as far as electron attachment is concerned, this anionic state is known to strongly compete with auto-detachment [163]. Therefore the present results suggest that a transition from the

ground state to a $^2B_1(\pi^*)$ state at (0.8 ± 0.2) eV, is the dominant mechanism at energies below 61 eV in the centre-of-mass frame which due to an avoided crossing with a dissociative $^2A_1(\sigma^*)$ leads to NO_2^- formation. [163]. Furthermore, the branching ratios [13] for 30 eV (17eV c.m.), 70 eV (39 eV c.m.), and 100 eV (55 eV c.m.) show that NO_2^- and the parent anion yields have similar behaviour between 70 eV and 100 eV lab frame collision energy (from 39 to 55 eV c.m., respectively). This strongly indicates that these fragmentation channels originate from the same anionic state [13] which may be assigned to a π^* state with $^2B_1$ character. Above 60 eV centre-of-mass frame collision energy, however, the states attainable are different. A intense peak located at (2.1 ± 0.2) eV is observed for a collision energy of 84 eV c.m.. At a collision energy of 73 eV c.m., a energy loss peak is observed at 1.7 eV. The former was assigned to the $^2A_1(\sigma^*)$ state while the latter was only reported by Sailer et al. [158] yielding CN^- and CNO^-. From Figure 6.7 in the 73-111 eV c.m. collision energy range, the electron is directly promoted mainly to the $^2A_1$ (σ^*) state. Such state leads to no negative ion formation as far as electron attachment is concerned. This is a clear evidence of the role of K^+ cation in the vicinity of the molecular target by stabilising the complex $[K^+ + M^-]$, where M^- represents the parent anion. Indeed, if bond stretching is allowed in the target molecule during electron transfer, strong vibronic coupling may occur [13], suppressing auto-detachment and yielding NO_2^-. To support this rationale, it is interesting to note that C-N stretch mode has an energy of 1080-1360 cm^{-1} [167] which corresponds to a time period between 24.5 and 30.9 fs. We observe an enhancement in the K^+ ion yield in a collision energy range corresponding to a collision time roughly half stretch of the C-N bond, which corresponds to electron capture into a $^2A_1$ state (see Figure 6.7) with an energy loss of 2.1-2.4 eV (see Table 6.4). However, we

Table 6.3: Peaks observed in K^+ energy loss measurements *.

Anionic states			**Present work**					**Assignment** [51]
Sailer [158]	Alizadeh [159]	Fluendy [51]	45eV	61eV	73eV	84eV	111eV	
0.6	0.5/1	0.72	0.8	0.9	0.8	0.4	0.8	$^2B_1$
1.7	1.5/2	-	-	1.7	1.6	1.3	1.7	
-	-	2.4		-	2.4	2.2	2.4	$^2A_1$
-	-	-	-	-	-	3.0	3.1	$^3B_2$
-	-	-	-	-	-	3.7	3.7	$^3B_1$
4.0	4/4.5	4.0	-	-	-	-	4.0	$^1A_2$
5.6	5/5.5	5.6						
6	6	6.1						
8.6	7/8.5	8.6						

*All values in electron-volt.

Table 6.4: Collision time for the present energy loss measurements *.

E_{cm} (eV)	v (m/s)	$t_{col}(fs)$
45	2.0×10^4	20.5
61	2.3×10^4	17.6
73	2.5×10^4	16.1
84	2.7×10^4	15.0
111	3.1×10^4	13.1

*Collision time was calculated using R_c = 2.8Å.

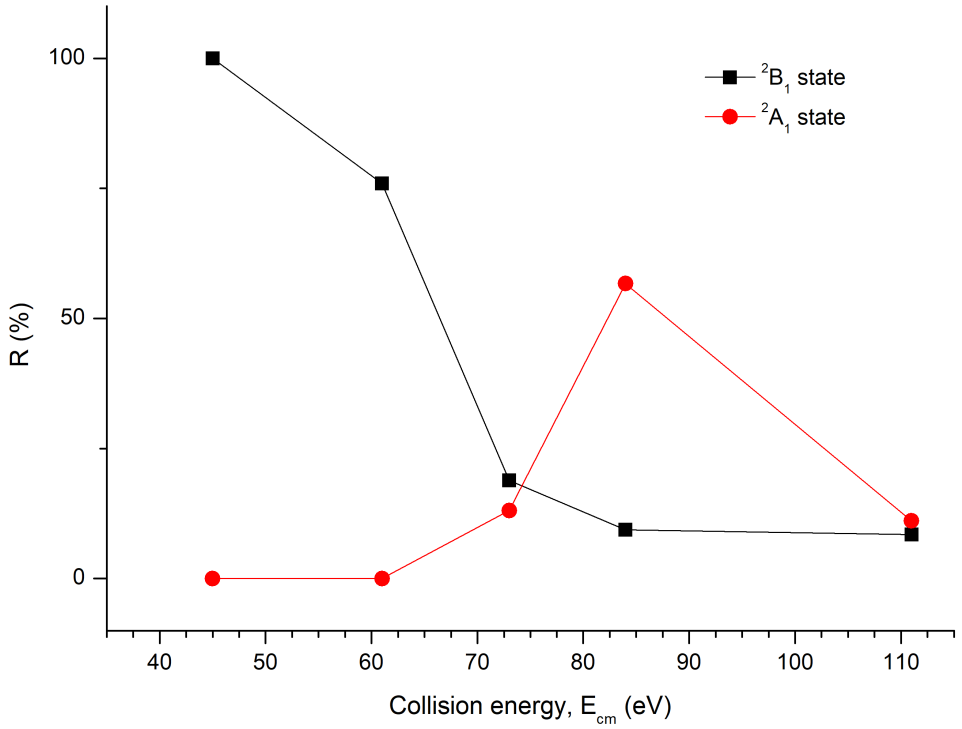

Figure 6.7: Ratio of the main anionic states $^2B_1$ and $^2A_1$ involved in electron transfer studies of potassium atoms with nitromethane molecules.

notice from the branching ratios reported by Antunes et al. [13] that there is a sudden decrease in this anion yield above 70 eV lab frame (39 eV c.m.). Since in this energy range NO_2^- seems to be formed mainly through a transition to a $^2A_1$ (σ^*) state, this is indicative that auto-detachment strongly competes with dissociation. Indeed, Lobo et al [165] reported electrons from auto-detachment and noted that NO_2^- was only detected from the covalent scattering, i.e. electron transfer at the second crossing. By spending less time in the $^2A_1$ state it is possible to compete successfully with auto-detachment [165] [51]. This is in agreement with our experimental results since we expect that at higher collision energies, the probability of ionic scattering decreases and electron transfer occurs predominantly by covalent scattering (see Chapter 2). Concerning the energy loss peak observed at 1.7 eV, Sailer et al. [158] reported a resonance at this energy concerning OH^- formation. For DEA reactions, to form OH^- there are three possible dissociation mechanisms:

$$e^- + CH_3NO_2 \longrightarrow (CH_3NO_2)^{\#-} \longrightarrow CH_2 + NO + OH^- \quad (a)$$

$$(CH_3NO_2)^{\#-} \longrightarrow HCN + OH + OH^- \quad (b)$$

$$(CH_3NO_2)^{\#-} \longrightarrow H_2O + CN + OH^- \quad (c)$$

A threshold formation of ~4 eV for reaction (a) to occur was reported by Gutsev et al. [168]. For reactions (b) and (c) internal rearrangement of the bonds is required, with thermochemical thresholds at 1.22 and 1.42 eV, respectively. Since only at 111 eV c.m. collision

energy a contribution at 4 eV is discernible, it seems that OH^- most likely is formed through internal rearrangement of the bonds for low collision energies. Such process is probably facilitated due to the presence of the alkali in vicinity of the molecule and its ability to stabilize the ion-pair complex through Coulomb interaction. Another energy loss peak is observed at 3.1 eV. From angular distribution measurements of inelastically scattered electrons, Flicker and co-workers [169] located a triplet excited state, $^3B_2$, in this energy range (~3.8 eV) with the onset at 3.1 eV. Flicker [169] attributed this feature to at least one singlet-triplet transition that may play a central role in the photolysis of nitromethane. The triplet states $^3B_1$ and $^3A_2$ are expected to be close in energy. Other minor features are observed as we increase the collision energy that can be analysed by multipeak fitting method (See Appendix A). It is also worth noting that, all the discussed transitions are always observed as long the available energy of the system is greater than the energy required to access these states. As we increase the collision energy, only the intensity of these transitions is affected due to the collision dynamics. Another important aspect of the energy loss measurements, is the width of the peaks, which is independent of the energy scale calibration, hence not influenced by energy scale shifts. The change of the peaks width can then be studied and used to assess the behaviour of the electron affinity as a function of the collision energy. This is shown in Figure 6.8 where the FWHM of the peaks with maximum intensity increases from low to high collision energies tending to an asymptotic value that corresponds to the vertical electron affinity [43]. This can be interpreted in terms of stretching the C-N bond that occurs during electron capture due to the presence of the K^+ ion in the vicinity of the temporary negative ion formed in the electron transfer process. Moreover, this effect will be more prominent for low collision velocities and it seems to gradually disappear with increasing velocity. Such is

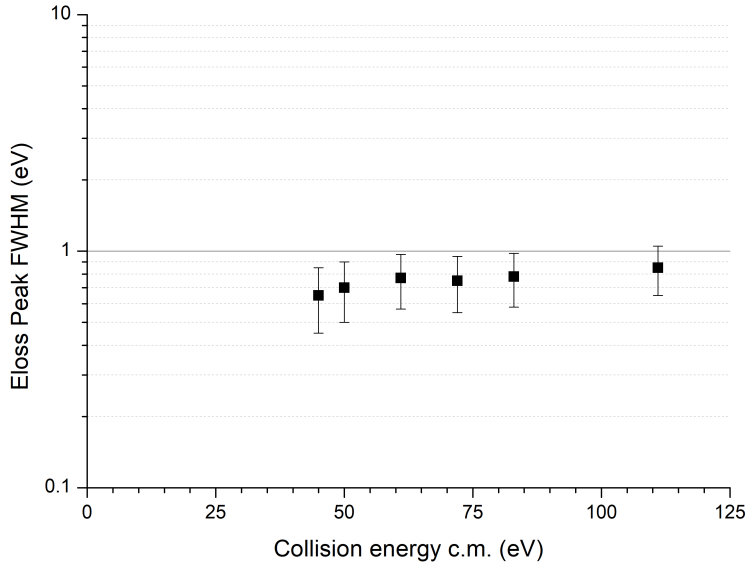

Figure 6.8: Energy loss FWHM behaviour as a function of the collision energy in the centre-of-mass frame.

in agreement with the assumption that at low collision velocities, the potassium cation spends more time in the molecule's vicinity.

6.4 Final Remarks

From the recently implemented hemisperical analyser, the potassium beam energy distribution shows a Gaussian shape with FWHM $\approx$ 0.6 eV in the lab frame. The present energy loss spectra of nitromethane constitute a follow up of earlier studies which unveiled new features, and as far as authors are aware not observed before in neutral alkali collisional studies mostly due to energy resolution limitations. The anionic state associated with the formation of $CH_3NO_2^-$ has been referred to be a vibrationally excited $^2B_1(\pi^*$ NO) state, which is subsequently stabilised by the potassium positive core into a long lived anion [51]. The NO_2^- formation was associated with a repulsive $^2A_1(\sigma^*$ CN) , that competes with auto-detachment. At low and even intermediate collision velocities, bond stretching along the C-N bond can efficiently suppress auto-detachment favouring a direct transition from the ground state to a highly dissociative $^2A_1$ state that results in dissociation yielding NO_2^-. Such state was reported from free electron experiments to decay only by auto-detachment. For the present range of collision energies, the available energy for electron transfer to occur is well above the energy formation thresholds and the resonances measured in DEA. This means that all anionic states are accessible from an energetic point-of-view. Thus, the present results suggest that the collision dynamics is mainly influenced by the collision time. Particularly, when ($t_{col} \approx t_{vib}$), it enhances bond-stretching effects having a strong influence in the collision dynamics.

Concerning CCl_4, a vertical electron affinity is reported at (-0.8 ± 0.2) eV, which is consistent with previous measurements in the literature. Due to a better energy resolution other (new) features were also observed.

Chapter 7

Conclusions

7.1 Concluding remarks

The main objective was to study negative ion formation in purine molecules - potassium collisions through TOF mass spectrometry. However, in order to achieve a better understanding of the fragmentation mechanisms involved in electron transfer processes of this kind, we have implemented a K^+ energy loss set-up in the forward direction. Thus, we can separate the work presented in this thesis in two parts: Experimental results of purine derivatives obtained in potassium collisions through TOF mass spectrometry analysis; and the development of an energy loss set-up capable of performing energy loss measurements in the forward direction to obtain key information regarding the mechanisms involved in ion-pair formation. Thus, they will be addressed separately. To conclude, we will discuss some future work as a follow-up of the work presented here.

7.1.1 Negative ion formation in purines-potassium collisions

A significant amount of attention was given in understanding the basic fundamental mechanisms that govern electron transfer with purines and some of its derivatives (in particular adenine) in potassium collisions. Site and bond selectivity in hydrogen excision was shown in adenine for collision energies < 15 eV lab frame, and the role of the potassium cation in the collision complex was further explored, both through studying chemical derivatives, such as 9-mAd and 6-dimAd as a function of the available energy in the centre-of-mass frame. The results suggest that these electrons, rather than yielding the dehydrogenated parent anion, will mostly lead to extensive damage to purines aromatic rings – that is required to form CN^- or a stable neutral HCN molecule. Such damage that results from ring breaking may be more complex to repair than the damage that results

from hydrogen abstraction, which was shown to be site selective. Intra-molecular electron transfer has also been proposed in the low-energy collision region, where prevalent Coulomb interaction of the transient K^+ cation with the TNI allows time enough for such internal charge redistribution yielding NH_2^- and NH^- fragments. Furthermore, sequential HCN loss was observed as a very relevant fragmentation pathway, and may have implications in gas-phase (and in the grain-phase) radical-radical and radical-molecule reactions on adenine formation and other purine analogues, within the interstellar medium.

7.1.2 Alkali energy loss spectroscopy

In order to investigate the anionic states accessed in electron transfer processes, as a result of collisions involving fast potassium atoms and a molecular target, an alkali energy loss set-up was implemented. The development of such set-up started with the implementation of an electrostatic energy retarder that was later replaced by a high resolution hemispherical energy analyser, followed by optimisation of the latter along with the rest of the set-up components. Furthermore, the development of a user-friendly software interface was required, suitable to our needs. For that purpose, two interfaces (in LabVIEW and Matlab2017 student version) to manage the acquisition and control system in the 0-15 eV energy range were developed. The system was tested by first performing energy loss experiments with nitromethane and tetrachloromethane, whose results revealed new information regarding the transitions that result in the formation of the most intense fragments (NO_2^- and Cl^-, respectively). With this information it was possible to draw the potential curves.

Due to an improved and constant energy resolution during measurements relative to prior results obtained by other research groups, it was possible to unveil new features, not reported before. The experimental results also showed evidences of bond stretching effects, pre- and/or post- electron transfer, that have an influence on dissociation channels that are being accessed. Adding the stabilising effect of the Coulomb complex $K^+ + M^-$, altogether may result in enhanced or even new fragmentation pathways. The latter effect varies with the projectile velocity that can be fine tuned, and it appears to have a major influence on the fragment yield when the collision time correlates with the molecular target vibrational modes, $t_{col} \approx t_{vib}$.

7.2 Future work

As far as the collision energy is concerned, it would be important to optimize the beam intensity in the low-energy collision region, either by: implementing a set of focusing lenses increasing beam transmission coefficient, and consequently the signal rate; or by shortening the potassium's optical path, i.e. placing the ion source closer to the collision region.

As far as ion-pair formation is concerned, with the currently implemented Re-TOF mass spectrometer, it will now be possible to measure more complex molecules, such as nuleosides (like adenosine), with improved mass resolution. However, and according to the literature, these molecular systems are easily decomposed when heated (our atom-molecule collision experiment is limited to gas-phase). Instead, other biologically relevant molecules can be studied. For instance, 4-aminopyrimidine, imidazole, or pyrimidine are excellent study cases and they will, for sure, contribute to a better understanding of the process of adenine fragmentation. TOF mass spectra of guanine and other xanthine class molecules would also be very interesting to compare with adenine's in order to understand the effects of the amide (-CONH-) functional group, in the collision dynamics. Furthermore, the study of halogenated purines would be highly relevant. Halogen nucleotide bases have already been suggested and used as radiosensitisers applied in concomitant chemotherapy treatments. In this way, the detailed study of the mechanisms of fragmentation at the molecular level is of high interest. Furthermore, with our recently acquired Re-TOF mass spectrometer it is now possible to study metastable decay, which seems to play an important role in the fragmentation patterns of purine molecules.

Finally, concerning the energy loss set-up, it is relevant to make it possible to accurately measure differential cross sections at different angles to probe both covalent and ionic scattering with collision energy. This will, for sure, increase the scientific contribution that this technique can provide not only to the field of radiation-induced DNA damage, but also to other areas such as astrochemistry [14]. From a technical point-of-view, there is some improvements that should be performed, such as: increase energy loss range; assemble a differential vacuum system; and improve the heating system of either the analyser and the molecular target oven.

References

[1] H. Varmus. "The new era in cancer research." In: *Science* 312 (2006), pp. 1162–1165.

[2] M. A. Śmiałek. "Early models of DNA damage formation." In: *Journal of Physics: Conference Series* 373 (2012), p. 012013.

[3] M. Folkard and K. Prise. "Investigating Mechanisms of Radiation-Induced DNA Damage Using Low-Emergy Photons." In: *Acta Physica Polonia Series A* 109 (2006), p. 265.

[4] B. Boudaïffa, P. Cloutier, D. Hunting, M. A. Huels, and L. Sanche. "Resonant formation of DNA strand breaks by low-energy (3 to 20 eV) electrons." In: *Science* 287 (2000), pp. 1658–1660.

[5] L. Sanche. "Biological chemistry: beyond radical thinking." In: *Nature* 461 (2009), p. 358.

[6] E. Alizadeh and L. Sanche. "Precursors of solvated electrons in radiobiological physics and chemistry." In: *Chemical Reviews* 112 (2012), pp. 5578–5602.

[7] R. Antunes. "The role of halouracils in radiotherapy studied by electron transfer in atom-molecule collisions experiments." In: PhD thesis, Universidade NOVA de Lisboa, Portugal (2011).

[8] J. Raviraj, V. K. Bokkasam, V. S. Kumar, U. S. Reddy, and V. Suman. "Radiosensitizers, radioprotectors, and radiation mitigators." In: *Indian Journal of Dental Research* 25 (2014), p. 83.

[9] C.-R. Wang, J. Nguyen, and Q.-B. Lu. "Bond breaks of nucleotides by dissociative electron transfer of nonequilibrium prehydrated electrons: a new molecular mechanism for reductive DNA damage." In: *Journal of the American Chemical Society* 131 (2009), pp. 11320–11322.

[10] V. Cobut, Y. Frongillo, J. Patau, T. Goulet, M. Fraser, and J. Jay-Gerin. "Monte Carlo simulation of fast electron and proton tracks in liquid water-I. Physical and physicochemical aspects." In: *Radiation Physics and Chemistry* 51 (1998), pp. 229–244.

[11] M. A. Huels, B. Boudaïffa, P. Cloutier, D. Hunting, and L. Sanche. "Single, double, and multiple double strand breaks induced in DNA by 3- 100 eV electrons." In: *Journal of the American Chemical Society* 125 (2003), pp. 4467–4477.

[12] S. Denifl, T. M ark, and P. Scheier. In: *Radiation Damage in Biomolecular Systems*. Ed. by G. G. Gómez-Tejedor and M. C. Fuss. Springer Science & Business Media, 2012. Chap. The Role of Secondary electrons in Radiation Damage.

[13] R. Antunes, D. Almeida, G. Martins, N. Mason, G. Garcia, M. Maneira, Y. Nunes, and P. Limão-Vieira. "Negative ion formation in potassium–nitromethane collisions." In: *Physical Chemistry Chemical Physics* 12 (2010), pp. 12513–12519.

[14] D. Almeida. "The role of electron transfer in DNA building blocks: evaluation of strand breaks and their implications." In: PhD thesis, Universidade NOVA de Lisboa, Portugal (2013).

[15] A. S. Burton, J. C. Stern, J. E. Elsila, D. P. Glavin, and J. P. Dworkin. "Understanding prebiotic chemistry through the analysis of extraterrestrial amino acids and nucleobases in meteorites." In: *Chemical Society Reviews* 41 (2012), pp. 5459–5472.

[16] P. Ehrenfreund, M. Spaans, and N. G. Holm. "The evolution of organic matter in space." In: *Philosophical Transactions of the Royal Society of London A: Mathematical, Physical and Engineering Sciences* 369 (2011), pp. 538–554.

[17] K. M. Menten and F. Wyrowski. "Molecules Detected in Interstellar Space." In: *Interstellar Molecules* (2011), pp. 27–42.

[18] J. Moffat and K. Tang. "A theoretical study of the reactive dimerization of HCN." In: *Journal of theoretical biology* 58 (1976), pp. 83–95.

[19] J. F. Henderson and A. R. P. Paterson. *Nucleotide metabolism: an introduction*. Academic Press, 2014.

[20] L. Sanche. "Low energy electron-driven damage in biomolecules." In: *The European Physical Journal D-Atomic, Molecular, Optical and Plasma Physics* 35 (2005), pp. 367–390.

[21] S. Gohlke, H. Abdoul-Carime, and E. Illenberger. "Dehydrogenation of adenine induced by slow (< 3 eV) electrons." In: *Chemical Physics Letters* 380 (2003), pp. 595–599.

[22] H. Abdoul-Carime, S. Gohlke, and E. Illenberger. "Site-specific dissociation of DNA bases by slow electrons at early stages of irradiation." In: *Physical Review Letters* 92 (2004), p. 168103.

[23] S. Ptasinska, S. Denifl, P. Scheier, E. Illenberger, and T. D. Märk. "Bond-and Site-Selective Loss of H Atoms from Nucleobases by Very-Low-Energy Electrons (< 3 eV)." In: *Angewandte Chemie International Edition* 44 (2005), pp. 6941–6943.

[24] S. Denifl, P. Sulzer, D. Huber, F. Zappa, M. Probst, T. D. Märk, P. Scheier, N. Injan, J. Limtrakul, R. Abouaf, et al. "Influence of functional groups on the site-selective dissociation of adenine upon low-energy electron attachment." In: *Angewandte Chemie International Edition* 46 (2007), pp. 5238–5241.

[25] I. Bald, J. Kopyra, and E. Illenberger. "Selective Excision of C5 from D-Ribose in the Gas Phase by Low-Energy Electrons (0–1 eV): Implications for the Mechanism of DNA Damage." In: *Angewandte Chemie International Edition* 45 (2006), pp. 4851–4855.

[26] P. Burrow, G. A. Gallup, A. M. Scheer, S Denifl, S Ptasinska, T Märk, and P Scheier. "Vibrational Feshbach resonances in uracil and thymine." In: *The Journal of chemical physics* 124 (2006), p. 124310.

[27] T. Sommerfeld. "Dipole-bound states as doorways in (dissociative) electron attachment." In: *Journal of Physics: Conference Series*. Vol. 4. 2005, p. 245.

[28] L. Pray. "Discovery of DNA structure and function: Watson and Crick." In: *Nature Education* 1 (2008), p. 100.

[29] S. Ptasińska, S. Denifl, S. Gohlke, P. Scheier, E. Illenberger, and T. D. Märk. "Decomposition of Thymidine by Low-Energy Electrons: Implications for the Molecular Mechanisms of Single-Strand Breaks in DNA." In: *Angewandte Chemie International Edition* 45 (2006), pp. 1893–1896.

[30] B. Barc, M. Ryszka, Spurrell, M. Dampc, P. Limao-Vieira, R. Parajuli, N. Mason, and S. Eden. "Multi-photon ionization and fragmentation of uracil: Neutral excited-state ring opening and hydration effects." In: *The Journal of Chemical Physics* 139 (2013), p. 244311.

[31] H. Abdoul-Carime, M. Huels, F. Brüning, E. Illenberger, and L. Sanche. "Dissociative electron attachment to gas-phase 5-bromouracil." In: *The Journal of Chemical Physics* 113 (2000), pp. 2517–2521.

[32] K. Tanzer, L. Feketeová, B. Puschnigg, P. Scheier, E. Illenberger, and S. Denifl. "Reactions in Nitroimidazole Triggered by Low-Energy (0–2 eV) Electrons: Methylation at N1-H Completely Blocks Reactivity." In: *Angewandte Chemie International Edition* 53 (2014), pp. 12240–12243.

[33] H. Abdoul-Carime, P. Limão-Vieira, S. Gohlke, I. Petrushko, N. J. Mason, and E. Illenberger. "Sensitization of 5-bromouridine by slow electrons." In: *Chemical Physics Letters* 393 (2004), pp. 442–447.

[34] J Kopyra, A. Keller, and I. Bald. "On the role of fluoro-substituted nucleosides in DNA radiosensitization for tumor radiation therapy." In: *Rsc Advances* 4 (2014), pp. 6825–6829.

[35] C. Moertel, S. Frytak, R. Hahn, M. O'Connell, R. Reitemeier, J. Rubin, A. Schutt, L. Weiland, D. Childs, M. Holbrook, et al. "Therapy of locally unresectable pancreatic carcinoma: A randomized comparison of high dose (6000 rads) radiation alone, moderate dose radiation (4000 rads+ 5-fluorouracil), and high dose radiation+ 5-fluorouracil. The gastrointestinal tumor study group." In: *Cancer* 48 (1981), pp. 1705–1710.

[36] H. Abdoul-Carime, M. Huels, E. Illenberger, and L. Sanche. "Sensitizing DNA to secondary electron damage: Resonant formation of oxidative radicals from 5-halouracils." In: *Journal of the American Chemical Society* 123 (2001), pp. 5354–5355.

[37] J. J. Lokich. "Improved cancer chemotherapy: Benefits of delivery by infusion." In: *Postgraduate medicine* 87 (1990), pp. 239–246.

[38] S. Denifl, S. Ptasińska, G. Hanel, B. Gstir, M. Probst, P. Scheier, and T. Märk. "Electron attachment to gas-phase uracil." In: *The Journal of Chemical Physics* 120 (2004), pp. 6557–6565.

[39] D. Almeida, F. Ferreira da Silva, G. García, and P. Limao-Vieira. "Selective bond cleavage in potassium collisions with pyrimidine bases of DNA." In: *Physical Review Letters* 110 (2013), p. 023201.

[40] D. Almeida, F. Ferreira da Silva, G. García, and P. Limão-Vieira. "Dynamic of negative ions in potassium-D-ribose collisions." In: *The Journal of Chemical Physics* 139 (2013), p. 114304.

[41] D. Almeida, F. Ferreira da Silva, S. Eden, G. García, and P. Limão-Vieira. "New Fragmentation Pathways in K–THF Collisions As Studied by Electron-Transfer Experiments: Negative Ion Formation." In: *The Journal of Physical Chemistry A* 118 (2014), pp. 690–696.

[42] D. Almeida, F. Ferreira da Silva, J. Kopyra, G. García, and P. Limão-Vieira. "Anion formation in gas-phase potassium–uridine collisions." In: *International Journal of Mass Spectrometry* 365 (2014), pp. 243–247.

[43] A. Kleyn and A. Moutinho. "Negative ion formation in alkali-atom-molecule collisions." In: *Journal of Physics B: Atomic, Molecular and Optical Physics* 34 (2001), R1.

[44] M. Polanyi. *Atomic reactions*. Williams & Norgate, 1932.

[45] K. Wilson and D. Herschbach. "Correlation of Sodium Atom Reaction Rates with Electron Capture Cross-sections." In: *Nature* 208 (1965), p. 182.

[46] J. L. Magee. "The mechanism of reactions involving excited electronic states the gaseous reactions of the alkali metals and halogens." In: *The Journal of Chemical Physics* 8 (1940), pp. 687–698.

[47] J. Birely and D. Herschbach. "Reactive Scattering in Molecular Beams: Velocity Analysis of KBr Formed in the K+ Br_2 Reaction." In: *The Journal of Chemical Physics* 44 (1966), pp. 1690–1701.

[48] R. Cross Jr, E. Gislason, and D. Herschbach. "Dipole—Dipole Scattering in Molecular Beams. Variation of Total Cross Section with Velocity and Rotational Overlap." In: *The Journal of Chemical Physics* 45 (1966), pp. 3582–3593.

[49] D. Herschbach. "Molecular beams." In: *Advances in Chemical Physics* 10 (2009), pp. 319–393.

[50] S. J. Riley, P. E. Siska, and D. R. Herschbach. "Reactions of alkali metal atoms with carbon tetrachloride. Rainbow-like coupling of product angle and energy distributions." In: *Faraday Discussions of the Chemical Society* 67 (1979), pp. 27–40.

[51] M. Fluendy and S. Lunt. "Electron transfer in alkali atom CH_3NO_2 collisions." In: *Molecular Physics* 49 (1983), pp. 1007–1016.

[52] R. Compton, P. Reinhardt, and C. Cooper. "Collisional ionization between alkali atoms and some methane derivatives: Electron affinities for CH_3NO_2, CF_3I, and CF_3Br." In: *The Journal of Chemical Physics* 68 (1978), pp. 4360–4367.

[53] W. Vassen, C. Cohen-Tannoudji, M. Leduc, D. Boiron, C. I. Westbrook, A. Truscott, K. Baldwin, G. Birkl, P. Cancio, and M. Trippenbach. "Cold and trapped metastable noble gases." In: *Reviews of Modern Physics* 84 (2012), p. 175.

[54] J. Stockdale, F. Davis, R. Compton, and C. Klots. "Production of negative ions from CH_3X molecules (CH_3NO_2, CH_3CN, CH_3I, CH_3Br) by electron impact and by collisions with atoms in excited Rydberg states." In: *The Journal of Chemical Physics* 60 (1974), pp. 4279–4285.

[55] R. Compton, H. Carman Jr, C. Desfrancois, H. Abdoul-Carime, J. Schermann, J. Hendricks, S. Lyapustina, and K. Bowen. "On the binding of electrons to nitromethane: Dipole and valence bound anions." In: *The Journal of Chemical Physics* 105 (1996), pp. 3472–3478.

[56] R. Popple, C. Finch, K. Smith, and F. Dunning. "Dissociative electron attachment to CCl_4: Lifetime of the $CCl_4{}^{*-}$ intermediate." In: *The Journal of Chemical Physics* 104 (1996), pp. 8485–8489.

[57] A Amaya-Tapia, R Hernández-Lamoneda, and H Martínez. "Single-electron capture cross section in 1-500 keV H^+ - Mg collisions." In: *Journal of Physics B: Atomic, Molecular and Optical Physics* 34 (2001), p. 769.

[58] T. Morgan and F. Eriksen. "Formation of metastable hydrogen atoms by charge exchange of fast protons in magnesium and barium vapors." In: *Physical Review A* 19 (1979), p. 2185.

[59] A. Baede, A. Moutinho, A. De Vries, and J. Los. "Total cross sections for charge transfer between Alkali Atoms and Halogen Molecules." In: *Chemical Physics Letters* 3 (1969), pp. 530–531.

[60] S. Edelstein and P. Davidovits. "Cross Sections for the Alkali-Metal-Halogen Molecule Reactions: Na, K, Rb, and Cs with I_2." In: *The Journal of Chemical Physics* 55 (1971), pp. 5164–5170.

[61] A. Moutinho, J. Aten, and J. Los. "Chemi-ionization in alkali-methylhalogen collisions." In: *Chemical Physics* 5 (1974), pp. 84–94.

[62] J. Aten, M. Hubers, A. Kleyn, and J. Los. "Simple trajectory calculations on ion pair formation in alkali atom—halogen molecule collisions." In: *Chemical Physics* 18 (1976), pp. 311–319.

[63] I. Bald, J. Langer, P. Tegeder, and O. Ingólfsson. "From isolated molecules through clusters and condensates to the building blocks of life." In: *International Journal of Mass Spectrometry* 277 (2008), pp. 4–25.

[64] A. W. Kleyn, J. Los, and E. A. Gislason. "Vibronic coupling at intersections of covalent and ionic states." In: *Physics Reports* 90 (1982), pp. 1–71.

[65] C. Lin and F. Martín. "Fast and slow collisions of ions, atoms and molecules." In: *Scattering*. Elsevier, 2002, pp. 1025–1042.

[66] C. Zhu, Y. Teranishi, and H. Nakamura. "Nonadiabatic transitions due to curve crossings: complete solutions of the landau-zener-stueckelberg problems and their applications." In: *Advances in Chemical Physics, Volume 117* (2001), pp. 127–233.

[67] URL: www.simion.com.

[68] F. Stienkemeier, M. Wewer, F. Meier, and H. Lutz. "Langmuir–Taylor surface ionization of alkali (Li, Na, K) and alkaline earth (Ca, Sr, Ba) atoms attached to helium droplets." In: *Review of Scientific Instruments* 71 (2000), p. 3480.

[69] R. Wilson. "Surface ionization ion sources." In: *IEEE transactions on nuclear science* 14 (1967), pp. 72–74.

[70] J. Aten and J. Los. "Space charge related energy deficit in beams from charge exchange sources." In: *Journal of Physics E: Scientific Instruments* 8.5 (1975), p. 408.

[71] J. H. Moore, C. C. Davis, M. A. Coplan, and S. C. Greer. *Building Scientific Apparatus*. Cambridge University Press, 2009.

[72] T. Cunha. "Analisador de dispersão de energia." In: MSc Thesis, Universidade NOVA de Lisboa, Portugal (2013).

[73] O. Sise, T. Zouros, M. Ulu, and M. Dogan. "Novel and traditional fringing field correction schemes for the hemispherical analyser: comparison of first-order focusing and energy resolution." In: *Measurement Science and Technology* 18 (2007), p. 1853.

[74] W. Wiley and I. H. McLaren. "Time-of-flight mass spectrometer with improved resolution." In: *Review of Scientific Instruments* 26 (1955), pp. 1150–1157.

[75] B. Mamyrin, V. Karataev, D. Shmikk, and V. Zagulin. "The mass-reflectron. A new nonmagnetic time-of-flight high resolution mass-spectrometer." In: *Zhurnal Ehksperimental'noj i Teoreticheskoj Fiziki* 64 (1973), pp. 82–89.

[76] B. Mamyrin and D. Shmikk. "Linear mass reflectron." In: *Zh. Eksp. Teor. Fiz* 76 (1979), pp. 1500–1505.

[77] E. Potter, J. Herek, S. Pedersen, Q. Liu, and A. Zewail. "Femtosecond laser control of a chemical reaction." In: *Nature* 355 (1992), p. 66.

[78] H. Rabitz, R. de Vivie-Riedle, M. Motzkus, and K. Kompa. "Whither the future of controlling quantum phenomena?" In: *Science* 288 (2000), pp. 824–828.

[79] L. Ratschbacher, C. Zipkes, C. Sias, and M. Köhl. "Controlling chemical reactions of a single particle." In: *Nature Physics* 8 (2012), p. 649.

[80] P. A. Sloan and R. Palmer. "Two-electron dissociation of single molecules by atomic manipulation at room temperature." In: *Nature* 434 (2005), p. 367.

[81] S. Ptasińska, S. Denifl, V. Grill, T. D. Märk, E. Illenberger, and P. Scheier. "Bond- and site-selective loss of H^- from pyrimidine bases." In: *Physical Review Letters* 95 (2005), p. 093201.

[82] V. S. Prabhudesai, A. H. Kelkar, D. Nandi, and E. Krishnakumar. "Functional group dependent site specific fragmentation of molecules by low energy electrons." In: *Physical Review Letters* 95 (2005), p. 143202.

[83] L. Sanche. "Radiation induced molecular phenomena in nucleic acids: low energy electrons damage to DNA." In: ed. by M Shukla and J Leszczynski. Springer Netherlands, Dordrecht, 2008. Chap. 19.

[84] A. Kumar and M. D. Sevilla. "Proton-coupled electron transfer in DNA on formation of radiation-produced ion radicals." In: *Chemical Reviews* 110 (2010), pp. 7002–7023.

[85] I. Baccarelli, I. Bald, F. A. Gianturco, E. Illenberger, and J. Kopyra. "Electron-induced damage of DNA and its components: Experiments and theoretical models." In: *Physics Reports* 508 (2011), pp. 1–44.

[86] K. Aflatooni, G. Gallup, and P. Burrow. "Electron attachment energies of the DNA bases." In: *The Journal of Physical Chemistry A* 102 (1998), pp. 6205–6207.

[87] S. Carles, F. Lecomte, J. Schermann, and C. Desfrancois. "Gas-phase experimental and theoretical studies of adenine, imidazole, pyrrole, and water non-covalent complexes." In: *The Journal of Physical Chemistry A* 104 (2000), pp. 10662–10668.

[88] F. Ferreira da Silva, G. Meneses, O. Ingólfsson, and P. Limão-Vieira. "Side chain effects in reactions of the potassium-tyrosine charge transfer complex." In: *Chemical Physics Letters* 662 (2016), pp. 19–24.

[89] J. Tabet, S. Eden, S. Feil, H. Abdoul-Carime, B. Farizon, M. Farizon, S. Ouaskit, and T. Märk. "Mass spectrometry (fragmentation ratios) of DNA base molecules following 80 keV proton impact with separation of direct ionization and electron capture processes." In: *International Journal of Mass Spectrometry* 292 (2010), pp. 53–63.

[90] C. Plützer, E. Nir, M. De Vries, and K. Kleinermanns. "IR–UV double-resonance spectroscopy of the nucleobase adenine." In: *Physical Chemistry Chemical Physics* 3 (2001), pp. 5466–5469.

[91] C. Plützer and K. Kleinermanns. "Tautomers and electronic states of jet-cooled adenine investigated by double resonance spectroscopy." In: *Physical Chemistry Chemical Physics* 4 (2002), pp. 4877–4882.

[92] A. C. Borin, L. Serrano-Andrés, M. P. Fülscher, and B. O. Roos. "A theoretical study of the electronic spectra of N9 and N7 purine tautomers." In: *The Journal of Physical Chemistry A* 103 (1999), pp. 1838–1845.

[93] M. Hanus, M. Kabelac ˇ , J. Rejnek, F. Ryjac ˇ ek, and P. Hobza. "Correlated ab initio study of nucleic acid bases and their tautomers in the gas phase, in a microhydrated environment, and in aqueous solution. Part 3. Adenine." In: *The Journal of Physical Chemistry B* 108 (2004), pp. 2087–2097.

[94] Y.-F. Wang and S. X. Tian. "Shape resonance states of the low-energy electron attachments to DNA base tautomers." In: *Physical Chemistry Chemical Physics* 13 (2011), pp. 6169–6175.

[95] D. Almeida, M.-C. Bacchus-Montabonel, F. Ferreira Da Silva, G. García, and P. Limão-Vieira. "Potassium-Uracil/Thymine ring cleavage enhancement as studied in electron transfer experiments and theoretical calculations." In: *The Journal of Physical Chemistry A* 118 (2014), pp. 6547–6552.

[96] T. Cunha, M. Mendes, F. Ferreira da Silva, S. Eden, G. García, and P. Limão-Vieira. "Communication: Site-selective bond excision of adenine upon electron transfer." In: *The Journal of Chemical Physics* 148 (2018), p. 021101.

[97] H. Abdoul-Carime, J. Langer, M. Huels, and E. Illenberger. "Decomposition of purine nucleobases by very low energy electrons." In: *The European Physical Journal D-Atomic, Molecular, Optical and Plasma Physics* 35 (2005), pp. 399–404.

[98] D. Huber, M. Beikircher, S. Denifl, F. Zappa, S. Matejcik, A. Bacher, V. Grill, T. Märk, and P. Scheier. "High resolution dissociative electron attachment to gas phase adenine." In: *The Journal of Chemical Physics* 125 (2006), p. 084304.

[99] B. Minaev, M. Shafranyosh, Y. Y. Svida, M. Sukhoviya, I. Shafranyosh, G. Baryshnikov, and V. Minaeva. "Fragmentation of the adenine and guanine molecules induced by electron collisions." In: *The Journal of Chemical Physics* 140 (2014), p. 05601.

[100] C. Desfrançois, H Abdoul-Carime, and J. Schermann. "Electron attachment to isolated nucleic acid bases." In: *The Journal of Chemical Physics* 104 (1996), pp. 7792–7794.

[101] K. Aflatooni, A. Scheer, and P. Burrow. "Total dissociative electron attachment cross sections for molecular constituents of DNA." In: *The Journal of Chemical Physics* 125 (2006), p. 054301.

[102] S. Tonzani and C. H. Greene. "Low-energy electron scattering from DNA and RNA bases: Shape resonances and radiation damage." In: *The Journal of Chemical Physics* 124 (2006), p. 054312.

[103] M. Harańczyk, M. Gutowski, X. Li, and K. H. Bowen. "Bound anionic states of adenine." In: *Proceedings of the National Academy of Sciences* 104 (2007), pp. 4804–4807.

[104] C. Fonseca Guerra, F. Bickelhaupt, S. Saha, and F. Wang. "Adenine tautomers: relative stabilities, ionization energies, and mismatch with cytosine." In: *The Journal of Physical Chemistry A* 110 (2006), pp. 4012–4020.

[105] L. M. Salter and G. M. Chaban. "Theoretical study of gas phase tautomerization reactions for the ground and first excited electronic states of adenine." In: *The Journal of Physical Chemistry A* 106 (2002), pp. 4251–4256.

[106] M. P. Fülscher, L. Serrano-Andrés, and B. O. Roos. "A theoretical study of the electronic spectra of adenine and guanine." In: *Journal of the American Chemical Society* 119 (1997), pp. 6168–6176.

[107] S. Pilling, A. Lago, L. Coutinho, R. De Castilho, G. De Souza, and A. N. De Brito. "Dissociative photoionization of adenine following valence excitation." In: *Rapid Communications in Mass Spectrometry* 21 (2007), pp. 3646–3652.

[108] B. Barc, M. Ryszka, J.-C. Poully, E. J. Al Maalouf, Z. El Otell, J. Tabet, R. Parajuli, P. Van Der Burgt, P. Limão-Vieira, and P. Cahillane. "Multi-photon and electron impact ionisation studies of reactivity in adenine–water clusters." In: *International Journal of Mass Spectrometry* 365 (2014), pp. 194–199.

[109] S. Chakrabarti and S. K. Chakrabarti. "Can DNA bases be produced during molecular cloud collapse?" In: *arXiv preprint astro-ph/0001079* (2000).

[110] R. Glaser, B. Hodgen, D. Farrelly, and E. McKee. "Adenine synthesis in interstellar space: mechanisms of prebiotic pyrimidine-ring formation of monocyclic HCN-pentamers." In: *Astrobiology* 7 (2007), pp. 455–470.

[111] V. Gupta, P. Tandon, P. Rawat, R. Singh, and A. Singh. "Quantum chemical study of a new reaction pathway for the adenine formation in the interstellar space." In: *Astronomy & Astrophysics* 528 (2011), A129.

[112] F. Ferreira da Silva, D. Almeida, R. Antunes, G. Martins, Y. Nunes, S. Eden, G. García, and P. Limão-Vieira. "Electron transfer processes in potassium collisions with 5-fluorouracil and 5-chlorouracil." In: *Physical Chemistry Chemical Physics* 13 (2011), p. 21621.

[113] M.-C. Bacchus-Montabonel and Y. S. Tergiman. "Radiation damage on biomolecular systems: dynamics of ion induced collision processes." In: *Computational and Theoretical Chemistry* 990 (2012), pp. 177–184.

[114] M.-C. Bacchus-Montabonel and F. Calvo. "Nanohydration of uracil: emergence of three-dimensional structures and proton-induced charge transfer." In: *Physical Chemistry Chemical Physics* 17 (2015), pp. 9629–9633.

[115] L. Salem. *Electrons in chemical reactions: first principles*. John Wiley & Sons, 1982.

[116] M.-C. Bacchus-Montabonel, D. Talbi, and M. Persico. "Quantum chemical determination of the rate coefficients for radiative association of CH_3^+ and H_2." In: *Journal of Physics B: Atomic, Molecular and Optical Physics* 33 (2000), p. 955.

[117] M. Fuentes-Cabrera, B. G. Sumpter, and J. C. Wells. "Size-expanded DNA bases: An ab initio study of their structural and electronic properties." In: *The Journal of Physical Chemistry B* 109 (2005), pp. 21135–21139.

[118] M. Bacchus-Montabonel and Y. Tergiman. "Anisotropic effect in the charge transfer of C q+ ions with uracil." In: *Physical Review A* 74 (2006), p. 054702.

[119] M.-C. Bacchus-Montabonel and Y. S. Tergiman. "An ab initio study of ion induced charge transfer dynamics in collision of carbon ions with thymine." In: *Physical Chemistry Chemical Physics* 13 (2011), pp. 9761–9767.

[120] H. Werner, P. Knowles, G Knizia, F. Manby, M Schütz, P Celani, T Korona, R Lindh, A Mitrushenkov, G Rauhut, et al. *MOLPRO, version 2012.1, a Package of ab initio Programs, Cardiff, UK*. 2012.

[121] A. Nicklass, M. Dolg, H. Stoll, and H. Preuss. "Ab initio energy-adjusted pseudopotentials for the noble gases Ne through Xe: Calculation of atomic dipole and quadrupole polarizabilities." In: *The Journal of Chemical Physics* 102 (1995), pp. 8942–8952.

[122] D. Almeida, D. Kinzel, F. Ferreira da Silva, B. Puschnigg, D. Gschliesser, P. Scheier, S. Denifl, G. García, L González, and P. Limão-Vieira. "N-site de-methylation in pyrimidine bases as studied by low energy electrons and ab initio calculations." In: *Physical Chemistry Chemical Physics* 15 (2013), pp. 11431–11440.

[123] O. V. Dorofeeva and N. Vogt. "Enthalpies of Formation of DNA and RNA Nucleobases from G3X Theory." In: *Journal of Chemical & Engineering Data* 54 (2009), pp. 1348–1352.

[124] URL: http://webbook.nist.gov/chemistry(2018).

[125] S. Harrison and J. Tennyson. "Bound and continuum states of molecular anions C_2H^- and C_3N^-." In: *Journal of Physics B: Atomic, Molecular and Optical Physics* 44 (2011), p. 045206.

[126] K. Graupner, T. Field, and L. Feketeova. "Dissociative electron attachment to the unstable carbon monosulfide molecule CS." In: *New Journal of Physics* 8 (2006), p. 314.

[127] S. E. Bradforth, E. H. Kim, D. W. Arnold, and D. M. Neumark. "Photoelectron spectroscopy of CN^-, NCO^-, and NCS^-." In: *The Journal of Chemical Physics* 98 (1993), pp. 800–810.

[128] D. Almeida, R. Antunes, G. Martins, S. Eden, F. Ferreira da Silva, Y. Nunes, G. Garcia, and P. Limão-Vieira. "Electron transfer-induced fragmentation of thymine and uracil in atom–molecule collisions." In: *Physical Chemistry Chemical Physics* 13 (2011), pp. 15657–15665.

[129] F. Ferreira Da Silva, C. Matias, D. Almeida, G. García, O. Ingólfsson, H. D. Flosadóttir, B. Ómarsson, S. Ptasinska, B. Puschnigg, and P. Scheier. "NCO–, a Key Fragment Upon Dissociative Electron Attachment and Electron Transfer to Pyrimidine Bases: Site Selectivity for a Slow Decay Process." In: *Journal of the American Society for Mass Spectrometry* 24 (2013), pp. 1787–1797.

[130] H. Abdoul-Carime, J. Langer, M. Huels, and E. Illenberger. "Decomposition of purine nucleobases by very low energy electrons." In: *The European Physical Journal D-Atomic, Molecular, Optical and Plasma Physics* 35 (2005), pp. 399–404.

[131] C. T. Wickham-Jones, K. M. Ervin, G. B. Ellison, and W. C. Lineberger. "NH_2 electron affinity." In: *The Journal of Chemical Physics* 91 (1989), pp. 2762–2763.

[132] F. Hofer, F.-P. Schmidt, W. Grogger, and G. Kothleitner. "Fundamentals of electron energy-loss spectroscopy." In: *IOP Conference Series: Materials Science and Engineering* 109 (2016), p. 012007.

[133] D. Spence, R. Huebner, H. Tanaka, M. Dillon, and R.-G. Wang. "Electronic structure of Cl2 from 5 to 15 eV by electron energy loss spectroscopy." In: *The Journal of Chemical Physics* 80 (1984), pp. 2989–2996.

[134] S. Matejcik, A. Kiendler, A. Stamatovic, and T. Märk. "A crossed beam high resolution study of dissociative electron attachment to CCl_4." In: *International Journal of Mass Spectrometry and Ion Processes* 149 (1995), pp. 311–319.

[135] T. Oster, A. Kühn, and E. Illenberger. "Gas phase negative ion chemistry." In: *International Journal of Mass Spectrometry and Ion Processes* 89 (1989), pp. 1–72.

[136] R. K. Jones. "Absolute total cross sections for the scattering of low energy electrons by CCl_4, CCl_3F, CCl_2F_2, $CClF_3$, and CF_4." In: *The Journal of Chemical Physics* 84 (1986), pp. 813–819.

[137] S. Chu and P. Burrow. "Dissociative attachment of electrons in the chloromethanes." In: *Chemical Physics Letters* 172 (1990), pp. 17–22.

[138] Š Matejčík, V. Foltin, M Stano, and J. Skalnỳ. "Temperature dependencies in dissociative electron attachment to CCl_4, CCl_2F_2, $CHCl_3$ and $CHBr_3$." In: *International Journal of Mass Spectrometry* 223 (2003), pp. 9–19.

[139] M. Braun, S. Marienfeld, M. Ruf, and H. Hotop. "High-resolution electron attachment to the molecules CCl_4 and SF_6 over extended energy ranges with the (EX) LPA method." In: *Journal of Physics B: Atomic, Molecular and Optical Physics* 42 (2009), p. 125202.

[140] H. Shimamori, Y. Tatsumi, Y. Ogawa, and T. Sunagawa. "Low-energy electron attachment to molecules studied by pulse-radiolysis microwave-cavity technique combined with microwave heating." In: *The Journal of chemical physics* 97 (1992), pp. 6335–6347.

[141] P. Spanel, S. Matejcik, and D. Smith. "The varying influences of gas and electron temperatures on the rates of electron attachment to some selected molecules." In: *Journal of Physics B: Atomic, Molecular and Optical Physics* 28 (1995), p. 2941.

[142] D. Su, W. Niu, S. Liu, C. Shen, C. Huang, H. Wang, H. Jiang, and Y. Chu. "Electron attachment rate constant measurement by photoemission electron attachment ion mobility spectrometry (PE-EA-IMS)." In: *Radiation Physics and Chemistry* 81 (2012), pp. 1869–1873.

[143] H.-U. Scheunemann, E Illenberger, and H Baumgärtel. "Dissociative Electron Attachment to CCl_4, $CHCl_3$, CH_2Cl_2 and CH_3Cl." In: *Berichte der Bunsengesellschaft für physikalische Chemie* 84 (1980), pp. 580–585.

[144] A Kalamarides, R. Marawar, M. Durham, B. Lindsay, K. Smith, and F. Dunning. "Use of Rydberg atoms to probe negative ion lifetimes." In: *The Journal of Chemical Physics* 93 (1990), pp. 4043–4046.

[145] X Ling, B. Lindsay, K. Smith, and F. Dunning. "Rydberg-atom collisions with SF_6 and CCl_4 at very high n." In: *Physical Review A* 45 (1992), p. 242.

[146] H. Dispert and K. Lacmann. "Negative ion formation in collisions between potassium and fluoro-and chloromethanes: Electron affinities and bond dissociation energies." In: *International Journal of Mass Spectrometry and Ion Physics* 28 (1978), pp. 49–67.

[147] J. Ayala, W. Wentworth, and E. Chen. "Thermal electron attachment rate to carbon tetrachloride, chloroform, dichloromethane, and sulfur hexafluoride." In: *The Journal of Physical Chemistry* 85 (1981), pp. 3989–3994.

[148] P. Burrow, A. Modelli, N. Chiu, and K. Jordan. "Temporary negative ions in the chloromethanes $CHCl_2F$ and CCl_2F_2: Characterization of the σ^* orbitals." In: *The Journal of Chemical Physics* 77 (1982), pp. 2699–2701.

[149] P. Burrow and A. Modelli. "On the treatment of LUMO energies for their use as descriptors." In: *SAR and QSAR in Environmental Research* 24 (2013), pp. 647–659.

[150] K. Lacmann, M. Maneira, A. Moutinho, and U. Weigmann. "Total and double differential cross sections of ion-pair formation in collisions of K atoms with SnCl4 and CCl4." In: *The Journal of Chemical Physics* 78 (1983), pp. 1767–1776.

[151] Z. Li, A. R. Milosavljević, I. Carmichael, and S. Ptasinska. "Characterization of neutral radicals from a dissociative electron attachment process." In: *Physical Review Letters* 119 (2017), p. 053402.

[152] E. Illenberger. "Energetics of Negative Ion Formation in Dissociative Electron Attachment to CCl_4, $CFCl_3$, CF_2Cl_2, and CF_3Cl." In: *Berichte der Bunsengesellschaft für physikalische Chemie* 86 (1982), pp. 252–261.

[153] M. Hubers, A. Kleyn, and J. Los. "Ion pair formation in alkali-halogen collisions at high velocities." In: *Chemical Physics* 17 (1976), pp. 303–325.

[154] T. Andersen, H. Haugen, and H. Hotop. "Binding energies in atomic negative ions: III." In: *Journal of Physical and Chemical Reference Data* 28 (1999), pp. 1511–1533.

[155] N. Slater. "Classical motion under a Morse potential." In: *Nature* 180 (1957), p. 1352.

[156] N. Zhang, P. Blowers, and J. Farrell. "Ab initio study of carbon- chlorine bond cleavage in carbon tetrachloride." In: *Environmental Science & Technology* 39 (2005), pp. 612–617.

[157] P. Staneke, G. Groothuis, S. Ingemann, and N. Nibbering. "Formation, stability and structure of radical anions of chloroform, tetrachloromethane and fluorotrichloromethane in the gas phase." In: *International Journal of Mass Spectrometry and Ion Processes* 142 (1995), pp. 83–93.

[158] W. Sailer, A. Pelc, S. Matejcik, E. Illenberger, P. Scheier, and T. Märk. "Dissociative electron attachment study to nitromethane." In: *The Journal of Chemical Physics* 117 (2002), p. 7989.

[159] E. Alizadeh, F. Ferreira Da Silva, F. Zappa, A. Mauracher, M. Probst, S. Denifl, A. Bacher, T. Märk, P. Limão-Vieira, and P. Scheier. "Dissociative electron attachment to nitromethane." In: *International Journal of Mass Spectrometry* 271 (2008), pp. 15–21.

[160] F. Lecomte, S. Carles, C. Desfrancois, and M. Johnson. "Dipole bound and valence state coupling in argon-solvated nitromethane anions." In: *The Journal of Chemical Physics* 113 (2000), p. 10973.

[161] L. Suess, R. Parthasarathy, and F. Dunning. "Rydberg electron transfer to CH_3NO_2: Lifetimes and characteristics of the product $CH_3NO_2^-$ ions." In: *The Journal of Chemical Physics* 119 (2003), p. 9532.

[162] A. Di Domenico and J. Franklin. "Negative ions in the mass spectrum of nitromethane." In: *International Journal of Mass Spectrometry and Ion Physics* 9 (1972), pp. 171–184.

[163] I. C. Walker and M. A. Fluendy. "Spectroscopy and dynamics of nitromethane (CH_3NO_2) and its anionic states." In: *International Journal of Mass Spectrometry* 205 (2001), pp. 171–182.

[164] A. Lopes, S. d. Sanchez, and M. Bettega. "Elastic scattering of low-energy electrons by nitromethane." In: *Physical Review A* 83 (2011), p. 062713.

[165] R. Lobo, A. Moutinho, K. Lacmann, and J. Los. "Excitation of the nitro group in nitromethane by electron transfer." In: *The Journal of Chemical Physics* 95 (1991), pp. 166–175.

[166] D. Almeida, R. Antunes, G. Martins, G Garcia, R. McCullough, S. Eden, and P. Limão-Vieira. "Mass spectrometry of anions and cations produced in 1–4 keV H^-, O^-, and OH^- collisions with nitromethane, water, ethanol, and methanol." In: *International Journal of Mass Spectrometry* 311 (2012), pp. 7–16.

[167] *http://www2.ups.edu/faculty/hanson/Spectroscopy/IR/IRfrequencies.html*. accessed in February 14^{th} 2018.

[168] G. L. Gutsev, P. Jena, and R. J. Bartlett. "Thermodynamical stability of CH_3ONO and CH_3ONO-: A coupled-cluster and Hartree–Fock-density-functional-theory study." In: *The Journal of Chemical Physics* 110 (1999), pp. 403–411.

[169] W. M. Flicker, O. A. Mosher, and A. Kuppermann. "Variable angle electron-impact excitation of nitromethane." In: *The Journal of Chemical Physics* 72 (1980), pp. 2788–2794.

[170] F. Ferreira da Silva, J. Rafael, T. Cunha, D. Almeida, and P. Limão-Vieira. "Electron transfer to aliphatic amino acids in neutral potassium collisions." In: *International Journal of Mass Spectrometry* 365 (2014), pp. 238–242.

[171] E. Lange, G. Meneses, T. Cunha, J. Krasuska, J. Kopyra, G. García, F. Ferreira da Silva, and P. Limão-Vieira. "Electron induced fragmentation of sulphur containing biological prototypes: thiaproline and taurine." In: *Journal of Physics: Conference Series* 635 (2015), p. 072069.

[172] P. Limão-Vieira, G. Meneses, T. Cunha, A. Gil, M. Calhorda, G. Garcia, and F. Ferreira Da Silva. "Complex internal rearrangement processes triggered by electron transfer to acetic acid." In: *Journal of Physics: Conference Series* 635 (2015), p. 012002.

[173] G. Meneses, C. Widmann, T. Cunha, A. Gil, F. Ferreira da Silva, M. Calhorda, and P. Limão-Vieira. "Unravelling the dissociation pathways of acetic acid upon electron transfer in potassium collisions: experimental and theoretical studies." In: *Physical Chemistry Chemical Physics* 19 (2017), pp. 1083–1088.

[174] K. Regeta, T. Cunha, F. Ferreira da Silva, G. García, and P. Limão-Vieira. "Electron-transfer studies in potassium collisions with tetrachloromethane." In: *Journal of Physics: Conference Series* 875 (2017), p. 102015.

[175] A. Rebelo, T. Cunha, M. Mendes, F. Ferreira da Silva, G. García, and P. Limão-Vieira. "Kinetic-energy release distributions of fragment anions from collisions of potassium atoms with D-Ribose and tetrahydrofuran." In: *The European Physical Journal D* 70 (2016), p. 130.

APPENDIX A

FITTING RESULTS: ENERGY LOSS

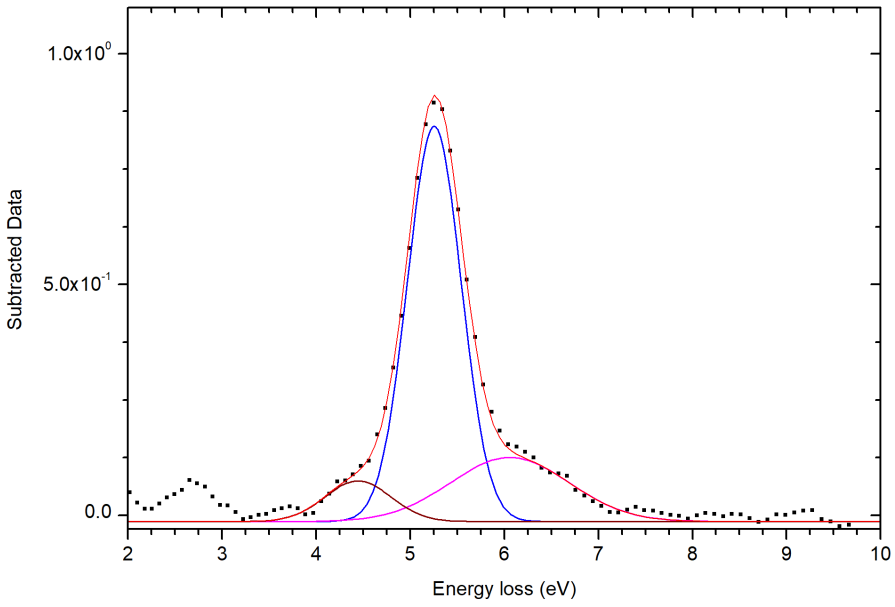

Fitting Results

Peak Index	Peak Type	Area Intg	FWHM	Max Height	Center Grvty	Area IntgP
1.	Gaussian	0.61438	0.67406	0.85626	5.25482	67.39905
2.	Gaussian	0.21968	1.48588	0.13889	6.05818	24.09906
3.	Gaussian	0.0775	0.82691	0.08805	4.44452	8.50189

Figure A.1: Fitting results for energy loss spectrum obtained at 61 eV c.m. collision energy.

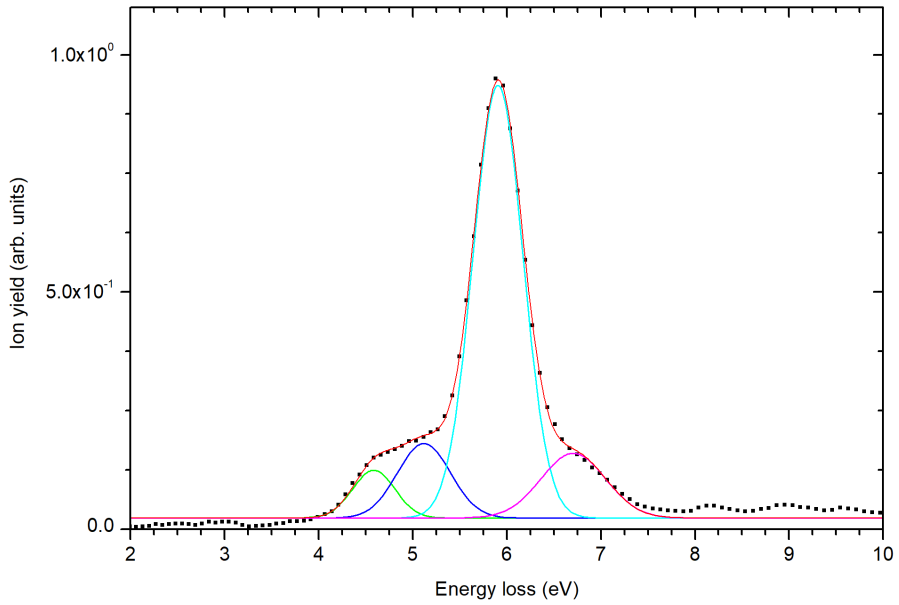

Fitting Results

Peak Index	Peak Type	Area Intg	FWHM	Max Height	Center Grvty	Area IntgP
1.	Gaussian	0.05673	0.53001	0.10055	4.58562	6.36946
2.	Gaussian	0.11101	0.66505	0.15681	5.11899	12.46446
3.	Gaussian	0.6054	0.62421	0.91112	5.90554	67.97717
4.	Gaussian	0.11746	0.81	0.13623	6.70653	13.1889

Figure A.2: Fitting results for energy loss spectrum obtained at 73 eV c.m. collision energy.

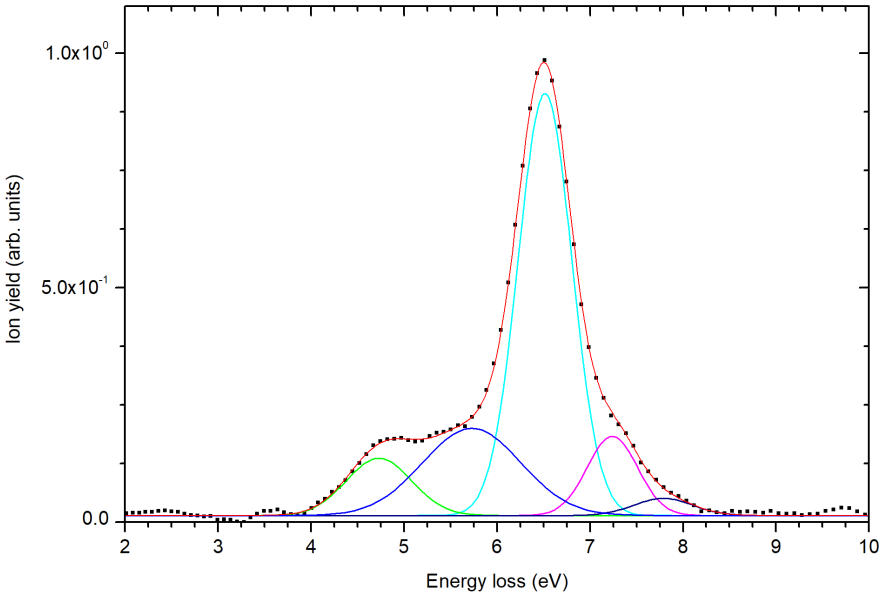

Fitting Results

Peak Index	Peak Type	Area Intg	FWHM	Max Height	Center Grvty	Area IntgP
1.	Gaussian	0.65237	0.68135	0.89947	6.51554	56.72092
2.	Gaussian	0.10796	0.83054	0.12212	4.73135	9.38716
3.	Gaussian	0.11487	0.64005	0.1686	7.23926	9.98728
4.	Gaussian	0.02888	0.7419	0.03657	7.7888	2.51087
5.	Gaussian	0.24606	1.24429	0.18577	5.7289	21.39377

Figure A.3: Fitting results for energy loss spectrum obtained at 84 eV c.m. collision energy.

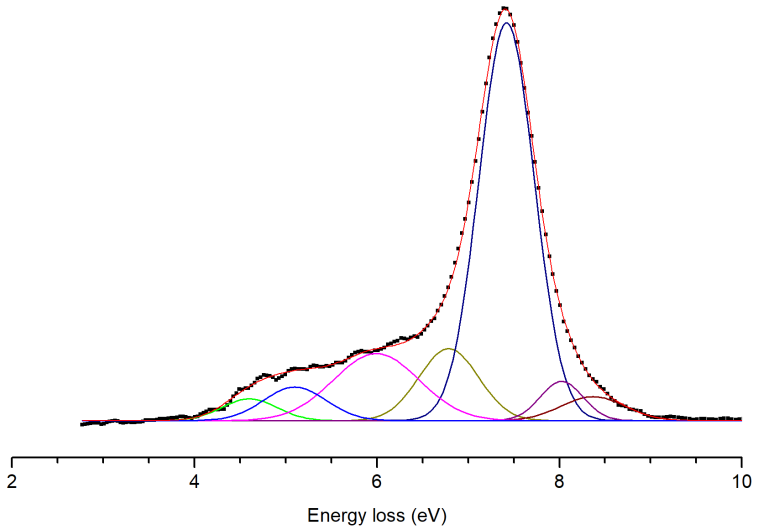

Fitting Results

Peak Index	Peak Type	Area Intg	FWHM	Max Height	Center Grvty	Area IntgP
1.	Gaussian	0.03914	0.70875	0.05188	4.60229	3.0993
2.	Gaussian	0.14005	0.76837	0.17123	6.78643	11.09071
3.	Gaussian	0.72155	0.71638	0.94621	7.4207	57.1396
4.	Gaussian	0.05004	0.82395	0.05705	8.36873	3.96232
5.	Gaussian	0.05485	0.55155	0.09342	8.02415	4.34341
6.	Gaussian	0.18833	1.10802	0.15967	5.99301	14.91363
7.	Gaussian	0.06883	0.81	0.07983	5.1	5.45102

Figure A.4: Fitting results for energy loss spectrum obtained at 111 eV c.m. collision energy.

Appendix B

Analyser specs

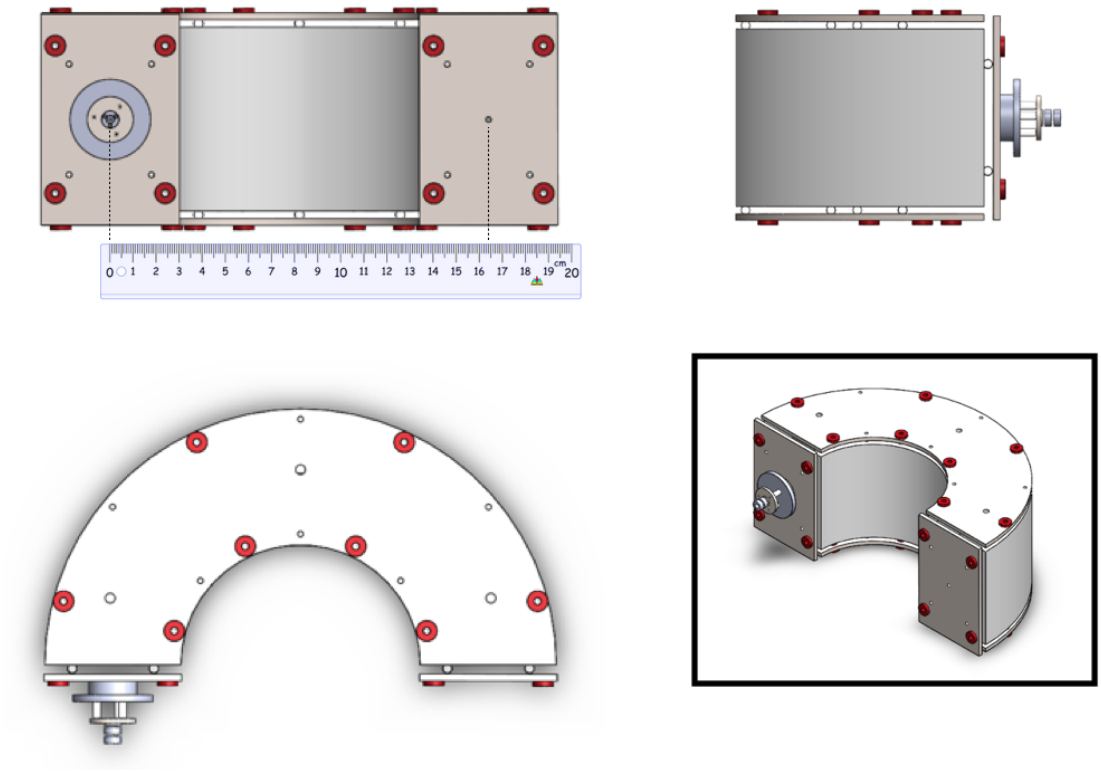

Figure B.1: Schematic representation of the hemispherical analyser. Drawings performed in Solidworks.

Appendix C

Energy loss interfaces

```
/******************Energy Loss version 4.0 ***********************
 *
 * Developper: Tiago Cunha (PhD research Fellow, CEFITEC, 2017)
 *
 * Obs: The following is the code required to run on arduino to
 * enable control of the hemispherical analyser located in the
 * crossed molecular beam setup. It can be used with a labview
 * interface or just turn the Serial monitor on from the IDE.
 *
 * Functions:
 * - Energy loss
 * - Voltage calibration as a function of the channel range
 *
 *
 ****************************************************************/
#define Power 256 // necessary for low pass filter running average

#include <Wire.h>
#include <SPI.h>
#include <LiquidCrystal_I2C.h>
#include <stdlib.h>


// Edit the acquisition parameters here:
int timeBin = 1000; // in millisecond
```

```
int initial_ch = 0;// Initial channel
int final_ch = 510; // Final channel
float calFactor = 200.0/4.84; // Voltage divisor calibration factor
int cycles = 1;

//Panel LED's
int ledVermelho = 5;
int ledVerde = 6;

//MCP41010 digipot
int CS = 10; // assigned to pin 10

//Voltage tuning parameter
int vout = 3;

//relay 4
int relay = 8; // assigned to pin 8

//LCD
LiquidCrystal_I2C lcd(0x3F,2,1,0,4,5,6,7,3,POSITIVE);

//Other Global variables:
volatile int signalIn = 2; // assigned to pin 2
String settings;
float voltage = 0;
int alpha = 15; // changeable from 0-255


//Functions:

// Pulse Counter
// >>> it measures the signal from the channeltron detector

int pulseCounter (int timeBin){
  unsigned long initial_time = 0;
  int count = 0;

  initial_time = millis(); //defines initial time.
  while(millis() - initial_time < timeBin){ // limit the time window
    if(digitalRead(signalIn) == LOW){
      if(digitalRead(signalIn) == HIGH){
```

```
        count++; // It increments every time it detects a pulse
      }
    }
  }
  return count;
}

// digiPotWrite function
// It transfers data to MCP41010 digital pot trough SPI communication
//Notes:
// - 0x80: mid point
// - 0x00: highest resistance
// - 0xFF: lowest resistance

void digiPotWrite (byte value){
  digitalWrite(CS,LOW);
  SPI.transfer(B00010001);// in binary notation
  SPI.transfer(value);
  digitalWrite(CS,HIGH);
}

//Update Settings

void updateSettings(){
  String instringT, instringC , instringI , instringF;
  int i, n;
  do{
        if(settings[i]=='C'){
          for(n=i+1;settings[n]!='T';n++){
            if(isDigit(settings[n])) instringC += (char)settings[n];
            i=n;
          }
          cycles = instringC.toInt();

        }
        if(settings[i]=='T'){
          for(n=i+1;settings[n]!='I';n++){
            if(isDigit(settings[n])) instringT += (char)settings[n];
            i=n;
          }
          timeBin = instringT.toInt();
```

```
        }
        if(settings[i]=='I'){
          for(n=i+1;settings[n]!='F';n++){
            if(isDigit(settings[n])) instringI += (char)settings[n];
            i=n;
          }
          initial_ch = instringI.toInt();
        }
        if(settings[i]=='F'){
          for(n=i+1;settings[n]!='\0';n++){
            if(isDigit(settings[n])) instringF += (char)settings[n];
            i=n;
          }
          final_ch = instringF.toInt();
        }

        i++;
      }while(i<settings.length());
}

void Measuring (int *flag){
  lcd.setCursor(0,1);
  lcd.print("Measuring");
    if (*flag == 0){
      lcd.print(".");
      lcd.print("    ");
      *flag = 1;
    }
    else if(*flag == 1){
      lcd.print("..");
      lcd.print("    ");
      *flag = 2;
    }
    else if(*flag == 2){
      lcd.print("...");
      lcd.print("    ");
      *flag = 3;
    }
    else{
      lcd.print("    ");
      *flag = 0;
```

```
    }
}


// Proress bar widths
byte p1[8]={0x10,0x10,0x10,0x10,0x10,0x10,0x10,0x10};
byte p2[8]={0x18,0x18,0x18,0x18,0x18,0x18,0x18,0x18};
byte p3[8]={0x1C,0x1C,0x1C,0x1C,0x1C,0x1C,0x1C,0x1C};
byte p4[8]={0x1E,0x1E,0x1E,0x1E,0x1E,0x1E,0x1E,0x1E};
byte p5[8]={0x1F,0x1F,0x1F,0x1F,0x1F,0x1F,0x1F,0x1F};


//Initialization: runs once
void setup() {
  pinMode(signalIn,INPUT);
  pinMode(CS, OUTPUT);
  pinMode(ledVermelho,OUTPUT);
  pinMode(ledVerde,OUTPUT);
  pinMode(relay,OUTPUT);
  pinMode(vout,OUTPUT);

  //characters creation
  lcd.createChar(0, p1);
  lcd.createChar(1, p2);
  lcd.createChar(2, p3);
  lcd.createChar(3, p4);
  lcd.createChar(4, p5);

  Serial.begin(9600);
  SPI.begin();
  lcd.begin(16,2);

  digitalWrite(ledVerde,HIGH);
  digitalWrite(ledVermelho,HIGH);


  //initialize LCD

  lcd.setCursor(0,0);
  lcd.print("Alkali ELoss v4");
  delay(200);
```

```
}


//Working routine: runs repeatedly
void loop() {
  int counts;
  String cmd;
  int outputLen = 0;
  char Buffer[30];
  int v = 0;
  float FiltValue = 0;
  //Scanning variables
  int level, initial_level, final_level;
  int flag = -1;

  //Starting
  delay(1000);
  FiltValue=0;

  digitalWrite(ledVermelho,LOW);
  lcd.setCursor(0,0);
  lcd.print("Alkali ELoss v4");
  lcd.print("    ");

  while(Serial.available() == 0){
    //rotina que defina o digipot no maximo
    //e que leia a tensao e contagens no lcd.Standby mode
    digitalWrite(relay,LOW);
    delay(100);
    digiPotWrite(255);

    //Acquire voltage
    v = analogRead(A0);
    voltage = v*(5.0/1024)*calFactor;

    //E.M.A. algorithm
    if(FiltValue == 0){
      FiltValue = voltage;
    }
    else{
```

```
    FiltValue = (alpha*voltage + (Power - alpha)*FiltValue)/Power;
  }

  //Output average value
  Serial.println(FiltValue);

  //visualize voltage in LCD
  lcd.setCursor(0,1);
  lcd.print("V = ");
  lcd.print(FiltValue);
  lcd.print("V");
  lcd.print("    ");
  delay(100);
}
cmd = Serial.readString();

switch(cmd[0]){

  case 'l': // energy loss
    lcd.clear();
    lcd.setCursor(0,0);
    lcd.print("Energy Loss");

    digitalWrite(ledVermelho,HIGH);
    digitalWrite(ledVerde,LOW);

    initial_level = initial_ch - 255;
    final_level = final_ch - 255;

    //digitalWrite(relay,HIGH);

    for(int cycle = 0;cycle<cycles; cycle++){
      for(level=initial_level;level<=final_level;level++){

        //activates the relay and switches from +5V to -5V the voltahe into digipot
        if(level==0){
          digitalWrite(relay,HIGH);
        }
        int Byte = abs(level);
        // Sets digipot position
        digiPotWrite(Byte);
```

```
        delay(500);

        //Acquires signal during timeBin
        counts = pulseCounter(timeBin);

        //Outputs the signal trough Serial port
        outputLen = sprintf(Buffer,"%dF%d\n",level+255,counts);
        for(int k=0; k<outputLen;k++){
          Serial.print(Buffer[k]);
        }

        //Measuring status
        Measuring(&flag);

        //reset the relay to LOW state after 1 sweep
        digitalWrite(relay, LOW);

        //Zero the counter
        signalIn = 0;
        if(Serial.available()>0){
          if(Serial.read() == 's') goto Exit;
        }
      }
    }
    goto Exit;
    break;
  case 'v': // calibration
    lcd.clear();
    lcd.setCursor(0,0);
    lcd.print("Volt calibration");


    digitalWrite(ledVerde,LOW);
    digitalWrite(ledVermelho,HIGH);

    initial_level = initial_ch - 255;
    final_level = final_ch - 255;

    for(level=initial_level;level<=final_level;level++){
```

```
  //Activates relay to switch voltage polarity
  if(level == 0){
    digitalWrite(relay,HIGH);
  }

  // Sets digipot position
  digiPotWrite(abs(level));
  delay(1000);

  //Acquire voltage
  v = analogRead(A0);
  voltage = v*(5.0/1024)*calFactor;

  //Outputs the signal trough Serial port
  char buff[10];
  char sentence[50];

  //E.M.A. algorithm
  if(FiltValue == 0){
    FiltValue = voltage;
  }
  else{
    FiltValue = (alpha*voltage + (Power - alpha)*FiltValue)/Power;
  }

  dtostrf(FiltValue, 4, 3, buff);

  outputLen = sprintf(Buffer,"%dF",level+255);
  outputLen = sprintf(sentence,"%s%s\n",Buffer, buff);

  for(int k=0; k<outputLen;k++){
    Serial.print(sentence[k]);
  }

  //Measuring status
  Measuring(&flag);

  if(Serial.available()>0){
    if(Serial.read() == 's') goto Exit;
  }
}
```

```
      digitalWrite(relay,LOW);
      goto Exit;
      break;
    case 'o': // settings ( 'options')

      settings = cmd; // To avoid changing cmd string
      updateSettings(); // routine to update settings
      break;
    default:
        Exit: // stand by conditions
        digitalWrite(ledVerde,HIGH);
        digitalWrite(ledVermelho,LOW);
        digitalWrite(relay, LOW);
   }

}
```

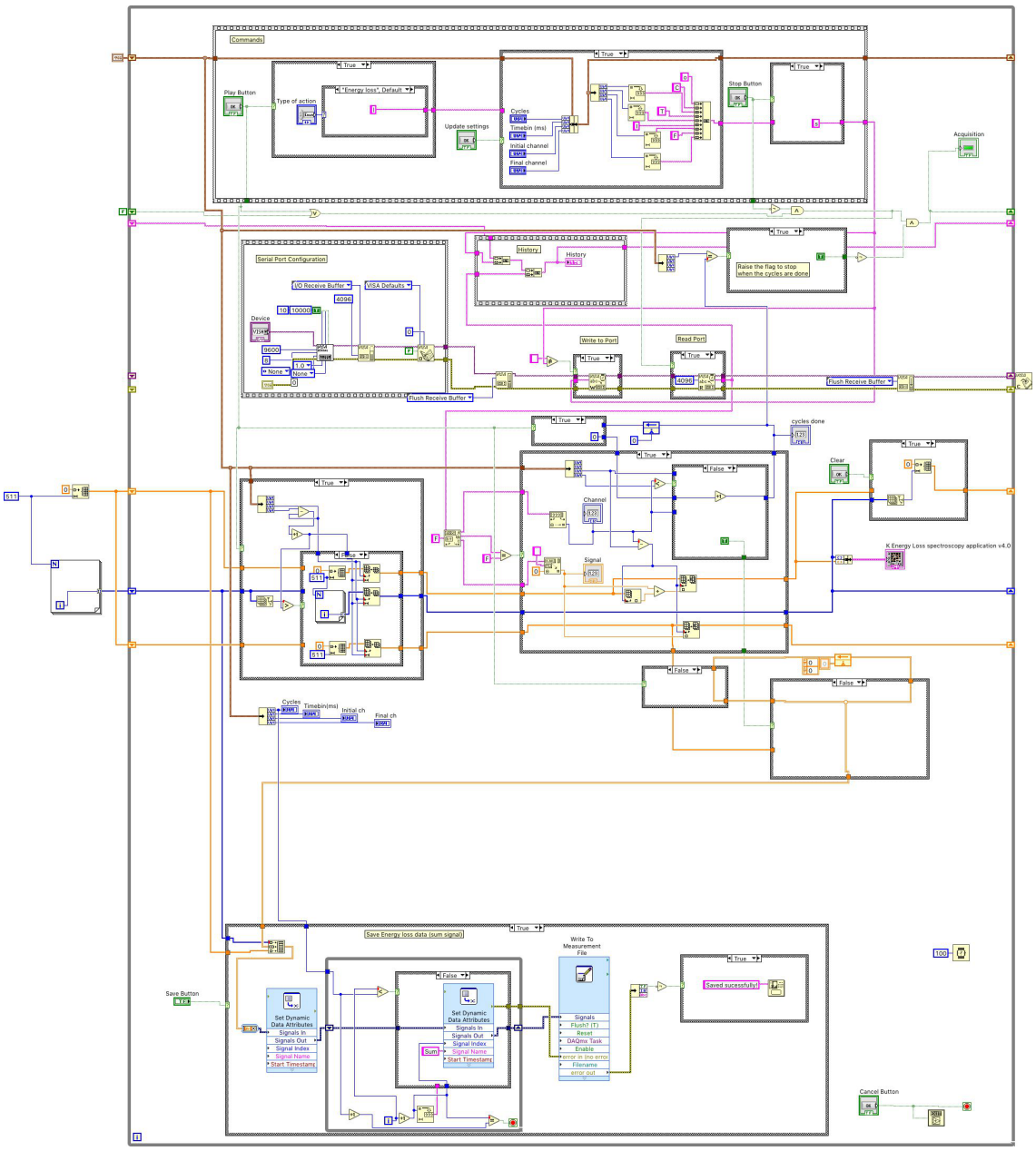

Figure C.1: LabVIEW block diagram of the acquisition interface.

APPENDIX D

K^+ ENERGY PROFILE

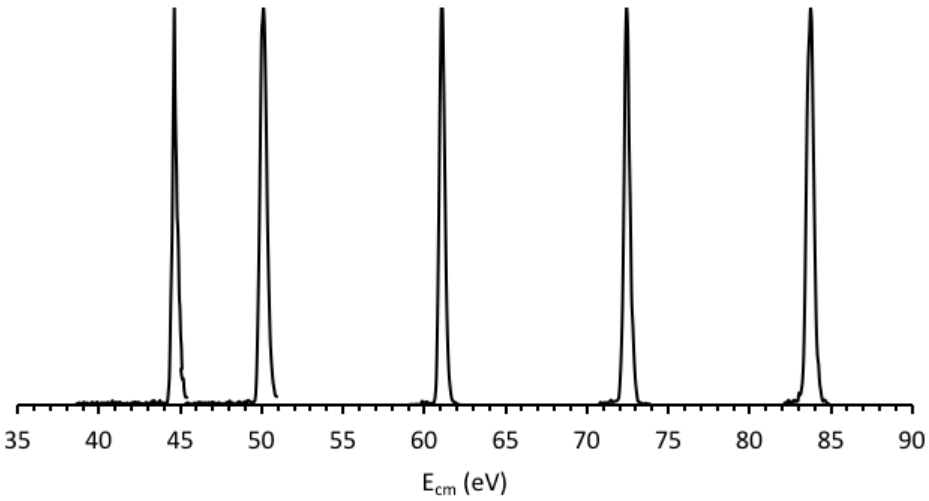

Figure D.1: K^+ beam profiles with normalised intensities to maximum peak, obtained at 82V, 92V, 111V 132, and 152V acceleration voltage corresponding to 45 eV, 50 eV, 61 eV, 73 eV and 84 eV collision energy in the centre-of-mass frame where a FWHM ~0.4 eV in that frame os obtained.

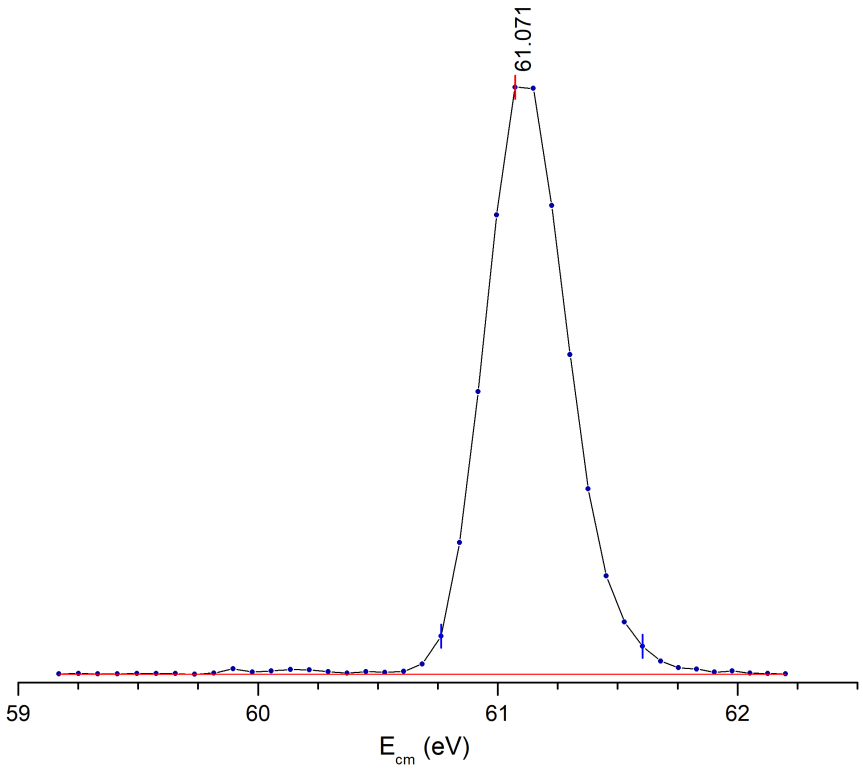

Figure D.2: K^+ beam energy profile at 61 eV c.m. collision energy.

Annex I

Publications

See References [96, 170–175].

Tiago Miguel da Fonseca Cunha

Master of Science in Engineering Physics

Negative Ion Formation in Potassium-Purine Molecules collisions

Thesis submitted in partial fulfillment
of the requirements for the degree of

Doctor of Philosophy in
Radiation Biology and Biophysics
Applied Atomic and Molecular Physics

April, 2018

FACULDADE DE
CIÊNCIAS E TECNOLOGIA
UNIVERSIDADE NOVA DE LISBOA

Tiago Miguel da Fonseca Cunha

Master of Science in Engineering Physics

Negative Ion Formation in Potassium-Purine Molecules collisions

Thesis submitted in partial fulfillment
of the requirements for the degree of

Doctor of Philosophy in
Radiation Biology and Biophysics
Applied Atomic and Molecular Physics

April, 2018

FACULDADE DE
CIÊNCIAS E TECNOLOGIA
UNIVERSIDADE NOVA DE LISBOA

Tiago Cunha
2018
Negative Ion Formation in Potassium-Purine Molecules collisions
2018